return homework
exam Fri — study sheet OK

Week #6 Lecture #1

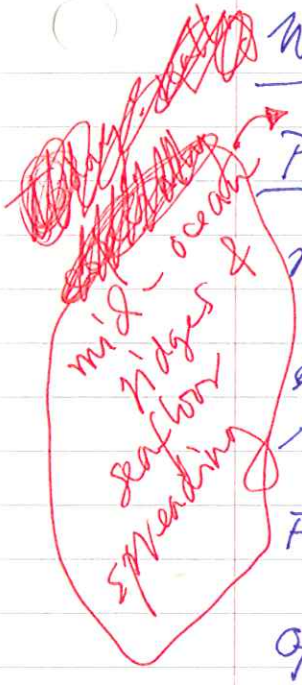

Plate tectonics: Ch. 11 Judson & Richardson

Many early workers noted the jigsaw-puzzle fit of the Atlantic coastlines of the Americas and Europe & Africa

For example, Alexander von Humboldt.

often "explained" as a result of catastrophism, often with biblical overtones (e.g. Moses parting of the Red Sea)

1858 Antonio Snider-Pellegrini (may) postulated idea of drift — again catastrophic — Bullard fit — shelves — 500 fathoms = 927 m.

19th century: catastrophism gradually replaced by uniformitarianism (British geologists James Hutton and Charles Lyell)

Champion of uniformitarian drift was Alfred Wegener, a German meteorologist, astronomer, geophysicist and pioneering balloonist!

Book: The Origin of Continents and Oceans (Die Entstehung der Kontinente und Ozeane) four editions 1915–1928.

Postulated that continents were joined in a single supercontinent Pangaea ("all the earth")

surrounded by proto-Pacific Panthalassa ("all the ocean")

He envisioned the continents as drifting through the oceans

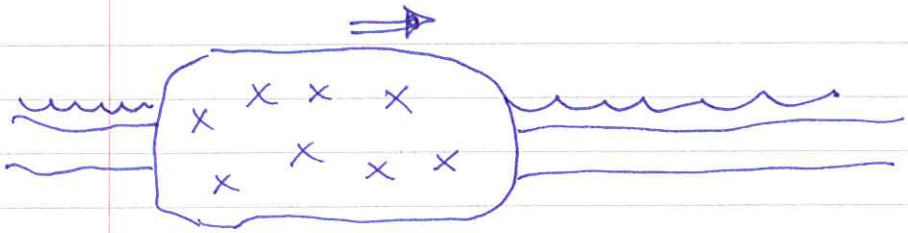

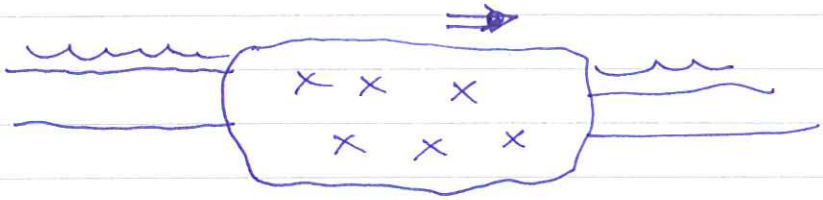

Even had a mechanism — centrifugal force acting on the high-standing continents.

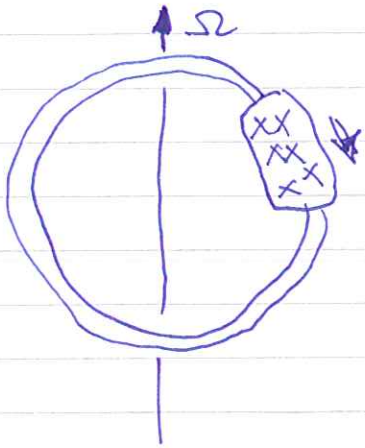

Objections were raised by geophysicists:

(1) force easily shown to be thoroughly negligible

(2) continents not strong enough to "plow" through the seafloor like this.

except by a few geologists, mostly in S. Hemisphere, where evidence for correlations was most pronounced

The idea was generally dismissed. Observational evidence in 1950's from paleomagnetism.

The idea: knowing the vector direction of the Earth's magnetic field at a point on the surface determines the location of the magnetic pole:

William Gilbert 1600 de Magnete physician to Queen Elizabeth — first to demonstrate that ⊕ has a dipole field

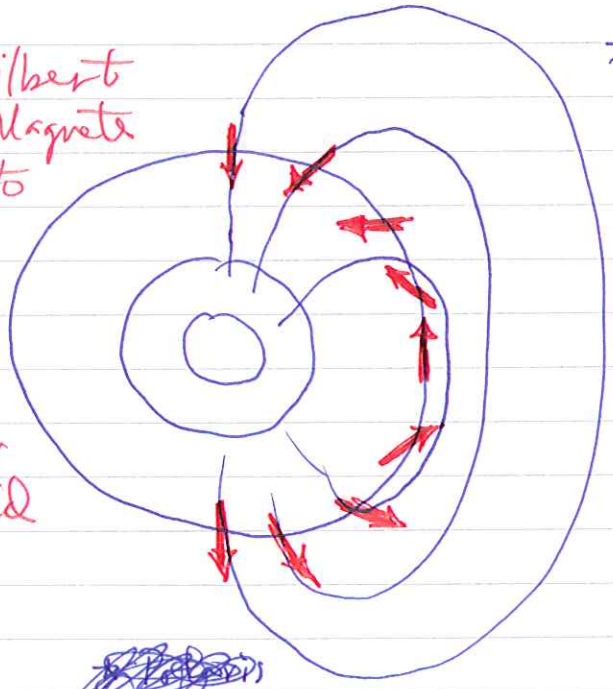

$\vec{B}$: dipole field

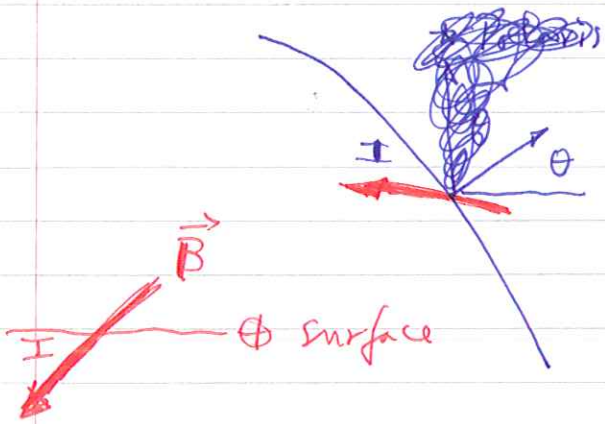

θ: latitude of site

I: magnetic inclination

$$\tan I = 2 \tan \theta$$

paleomagnetic equation

can determine the paleolatitude of a site by measuring inclination I

Igneous rocks — basalts — provide a means of measuring $\vec{B}$ direction in the past.

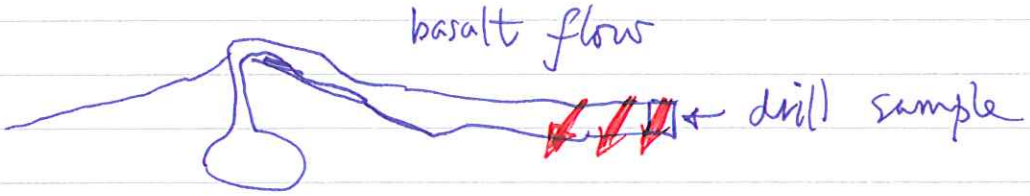

when cooled below a critical (Curie) temperature magnetic minerals are quenched in direction of $\vec{B}$


drill sample

Rocks are very weak magnets — requires a sensitive device to measure their magnetic orientation

One drills a sample, uses a compass or some other means to measure and mark its orientation, brings it back to the lab, and measures the direction.

Conventional to plot the apparent position of the N pole as a function of the rock age — use

Rb–Sr or K–Ar — or simply the stratigraphic age.

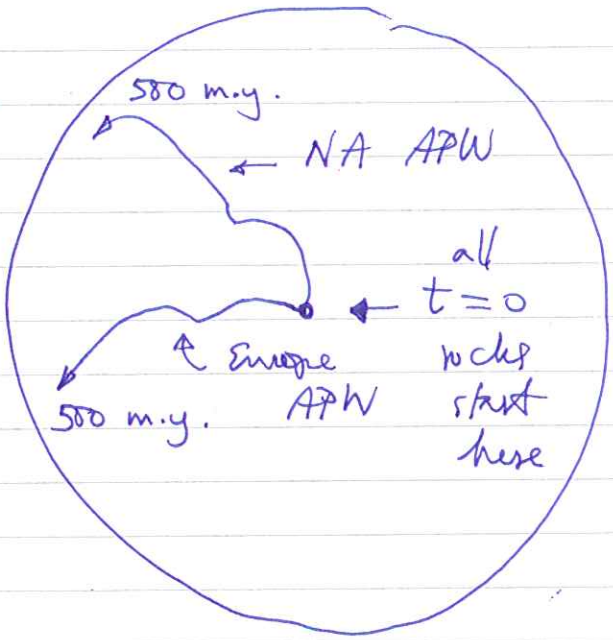

Maybe skip this — takes a long time to explain —

The $\vec{B}$ pole doesn't move — it's tied to the ⊕'s rotation axis.

The continents (or plates) move w.r.t. the pole.

The Europe and NAM APW paths observed to diverge

This evidence convinced many people; others said it depended on the geocentric dipole hypothesis — not necessarily true.

Study of the ocean basins — begun during WW II by Princeton's Harry Hess and others — provided the key evidence in support of plate tectonics in the 1960's.

Hess in particular championed idea of sea-floor spreading.

Continents don't ponderously plow through the oceans as Wegener envisaged, but rather new oceanic crust is created at mid-ocean ridges.

Probably the key insight: Vine-Matthews hypothesis

Explanation for magnetic stripe or anomaly patterns on the seafloor

measure magnetic field (away from steel hull)

Plot versus distance along ship track

anomaly $= |\vec{B}| - |\vec{B}_{dipole}|$

To find the anomaly we subtract the measured strength $|\vec{B}|$ from $|\vec{B}_{dipole}|$

Anomalies due to remanent magnetism of basaltic crust.

Magnetic reversals known to occur $N-S$ poles reverse in a quasi-random way. Last one 700,000 years ago. How determined

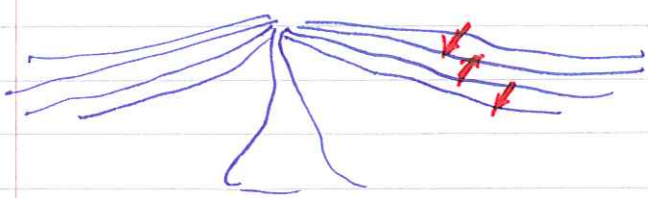

succession of lava flows

K-Ar : early application — applied to 0–5 m.y. old lavas in Sierra Nevada

Magnetic polarity time scale

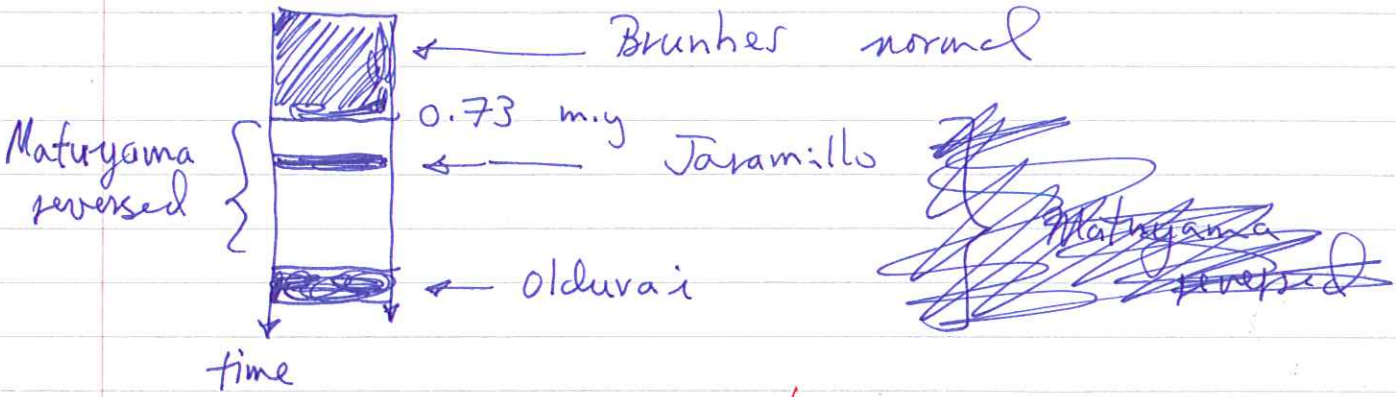

mostly using seafloor anomalies

Now carried back to 170 m.y.

Note long (normal) quiet interval in Cretaceous ~80–120 m.y. ago

Vine-Matthews combined hypothesis of sea-floor spreading with known occurrence of magnetic reversals

Seafloor is a magnetic tape recorder (head at ridge axis)

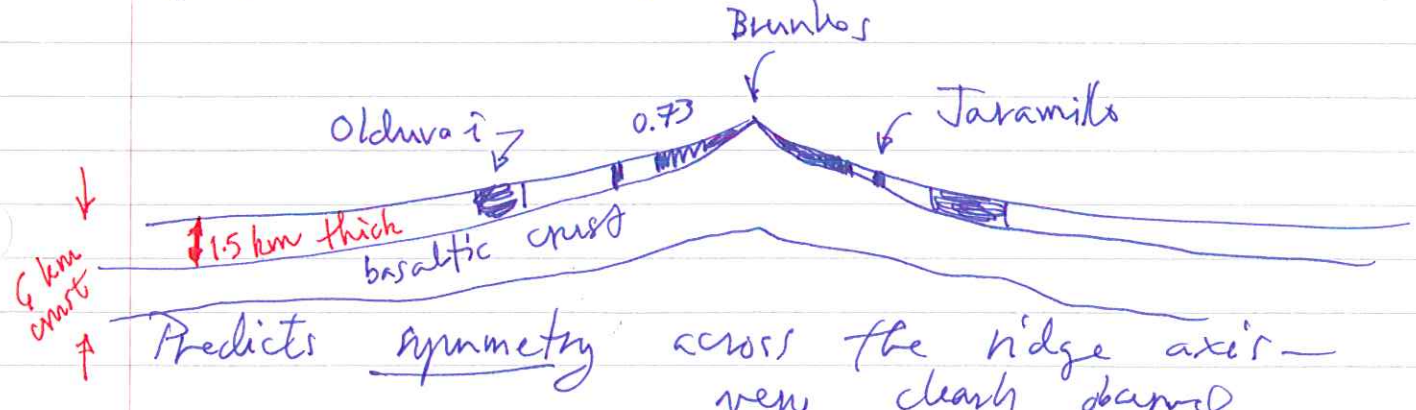

Predicts symmetry across the ridge axis — very clearly observed

Sketch how the anomalies arise

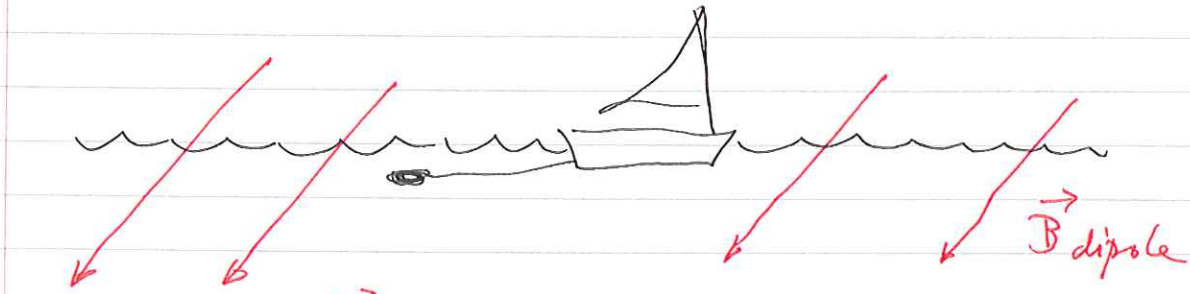

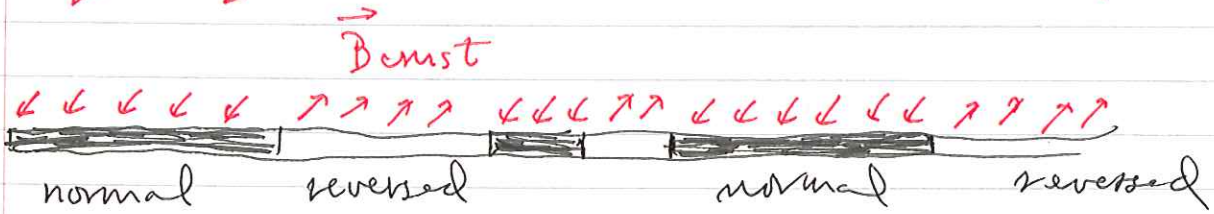

$$\vec{B}_{measured} = \vec{B}_{dipole} + \vec{B}_{crust}$$

$$\vec{B}_{anomaly} = \vec{B}_{crust}$$

One plots the length of the vector

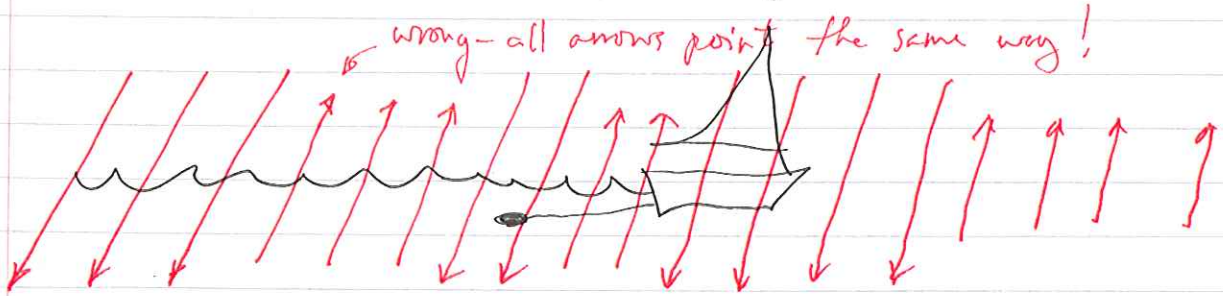

Plot of $|\vec{B}_{crust}| = |\vec{B}_{meas}| - |\vec{B}_{dipole}|$

Maybe even best to explain this in context of a ridge

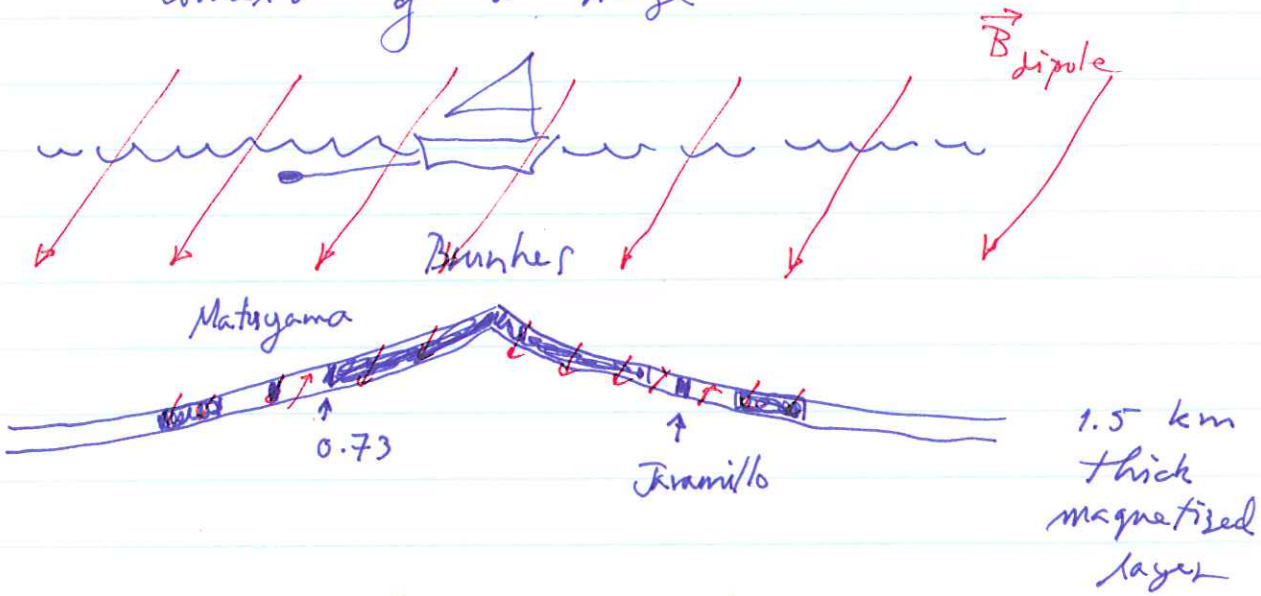

$$\vec{B}_{measured} = \vec{B}_{dipole} + \vec{B}_{magnetized\ ocean\ crust}$$

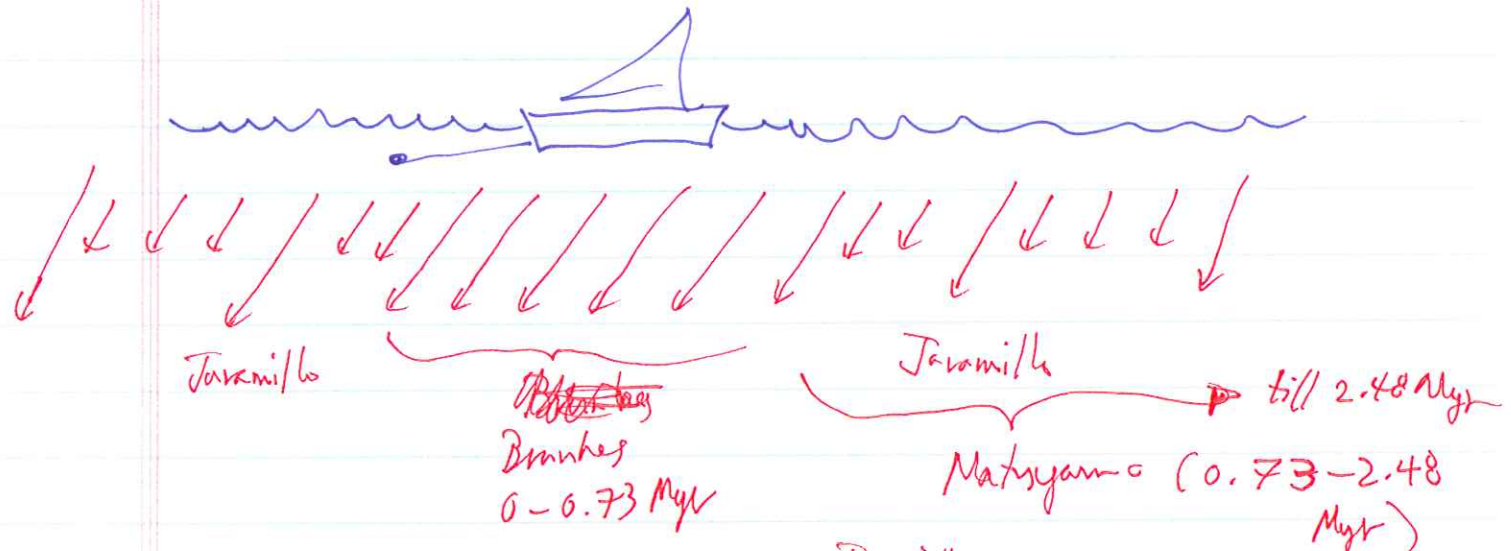

plot of

$$|\vec{B}_{measured} - \vec{B}_{dipole}| \approx |\vec{B}_{crust}|$$

Paleontological confirmation

Deep-sea drilling program — date oldest pelagic sediments just above the basaltic crust

Total length of world's ridges ~ 60,000 km ← map with spreading rates

Rate of creation of new seafloor

$$\frac{dA}{dt} = 2.7 \text{ km}^2/\text{yr}$$

Rate of creation of basaltic crust

(6 km thick) (2.7) = 16 km^3/yr

Average age of seafloor 60 my
Oldest ~ 180 m.y.
Average age at which subducted ~120 m.y. ← twice average age

Average spreading rate / Rate at which fingernails grow.

$$\frac{2.7 \text{ km}^2/\text{yr}}{2 \cdot 60{,}000 \text{ km}} = 22 \text{ mm/yr}$$

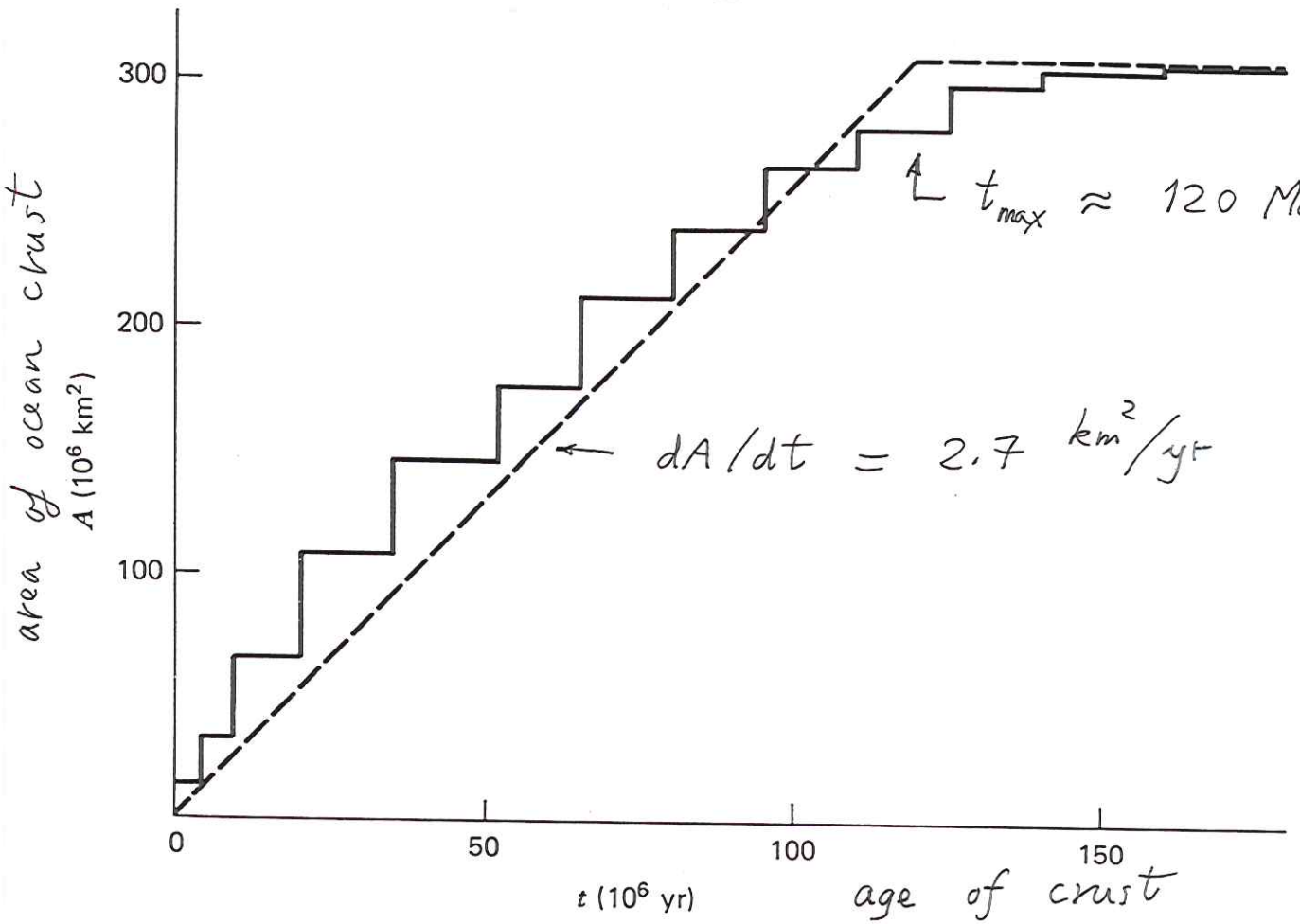

Basalt production at mid-ocean ridges

$(2.7)(6) = \boxed{16 \text{ km}^3/\text{yr}} \gg$ continental volcanoes

Average spreading rate

half-rate → $\dfrac{2.7 \cdot 10^5}{2 \cdot 60{,}000} = \boxed{2.2 \text{ cm/yr}}$ ← rate at which fingernails grow

Σ ridge length

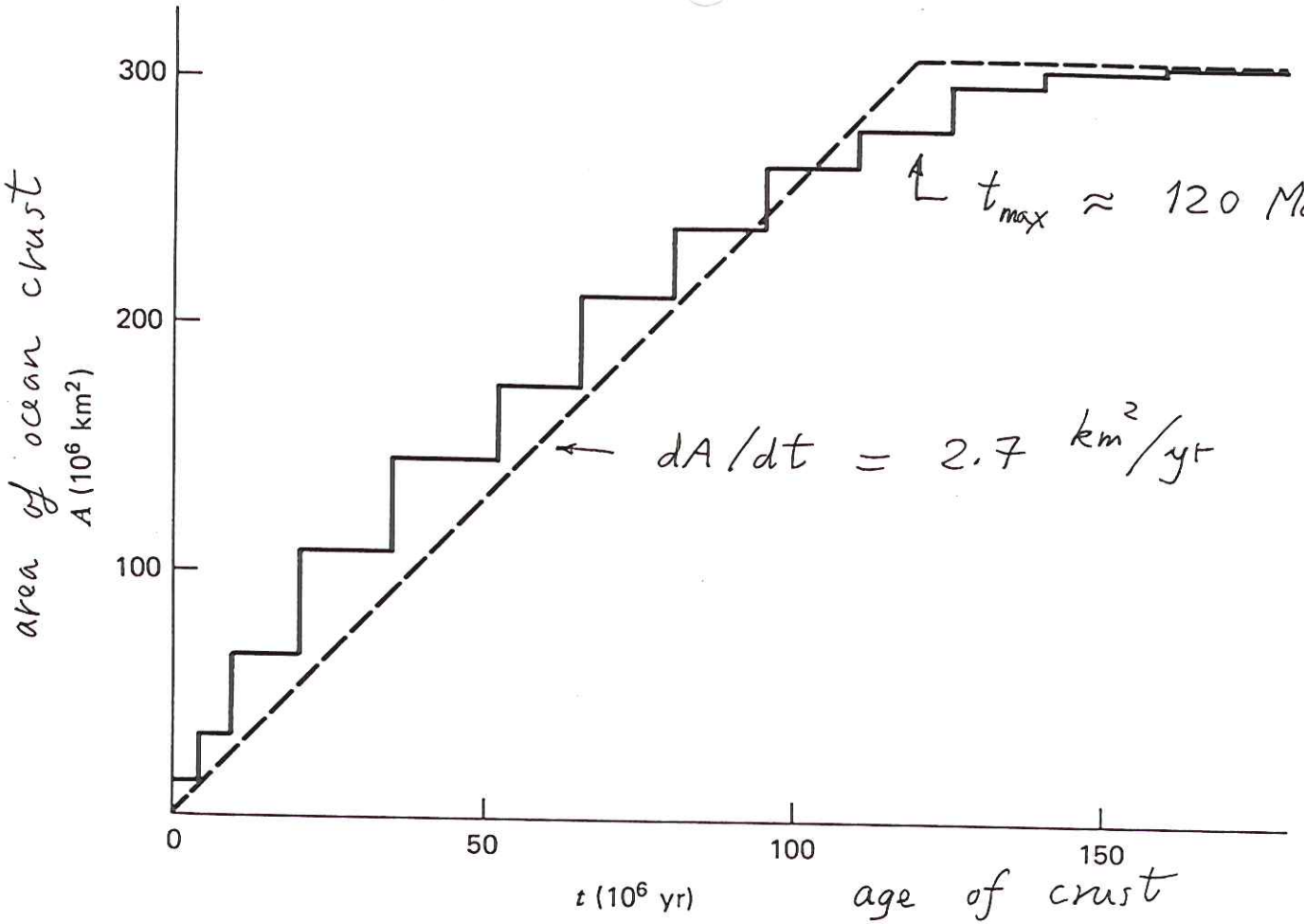

Basalt production at mid-ocean ridges

$(2.7)(6) = \boxed{16 \text{ km}^3/\text{yr}} \gg$ continental volcanoes

Average spreading rate

$$\frac{2.7 \cdot 10^5}{2 \cdot 60{,}000} = \boxed{2.2 \text{ cm/yr}}$$

← rate at which fingernails grow

half-rate → 2 · 60,000 ← ridge length

A new technology has led to new insights about the mid-oceanic ridges — swath mapping

Fast-spreading ridges (thin, hot weak lithosphere) develop overlapping spreading centers

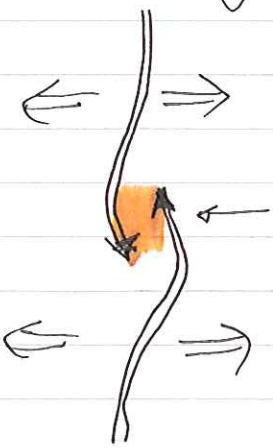

"duelling propagating rifts"

← complex deformed zone (spreading in from both sides)

One eventually wins

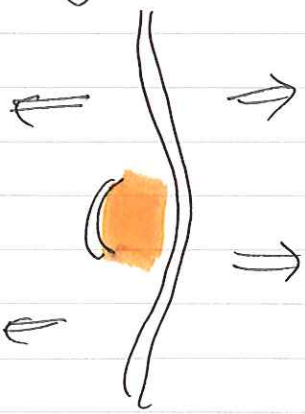

With time (((spreads away:

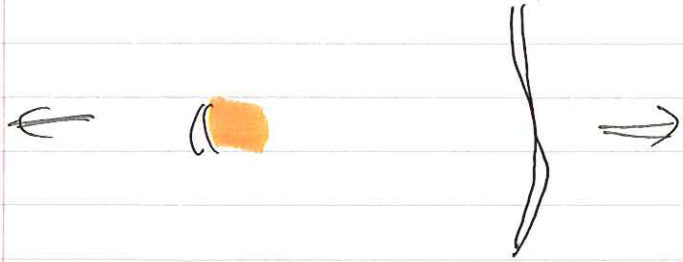

The origin of transform faults:

Concider an initially perpendicularly spreading ridge

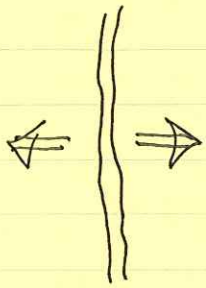

A reorganization of plate motion makes it want to spread obliquely

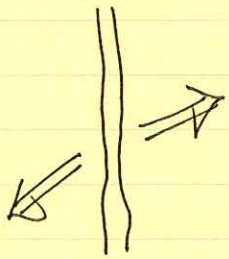

esp. at low spreading rates

Perpendicular spreading is preferred, so a ridge segment – transform system is born

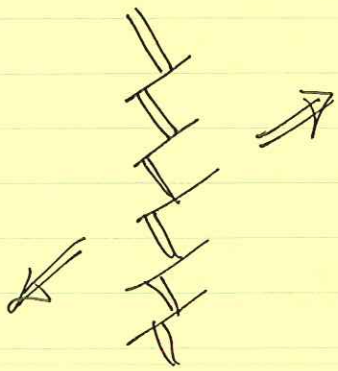

Leaky transform faults also lead to segmented ridges, e.g. Gulf of California

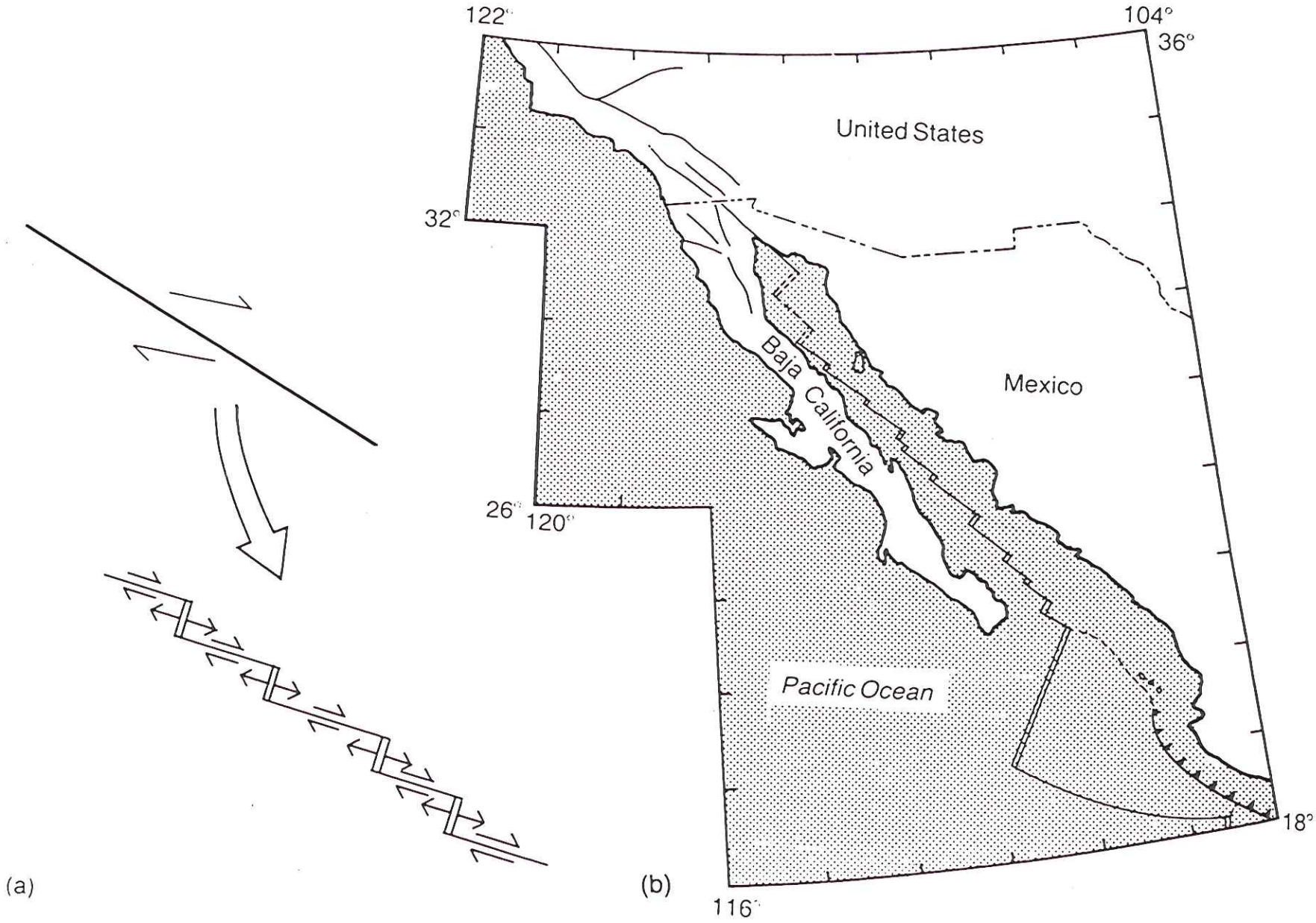

Fig. 7.7 (a) Development of a leaky transform fault because of a change in the pole of rotation. (b) Leaky transform fault in the Gulf of California.

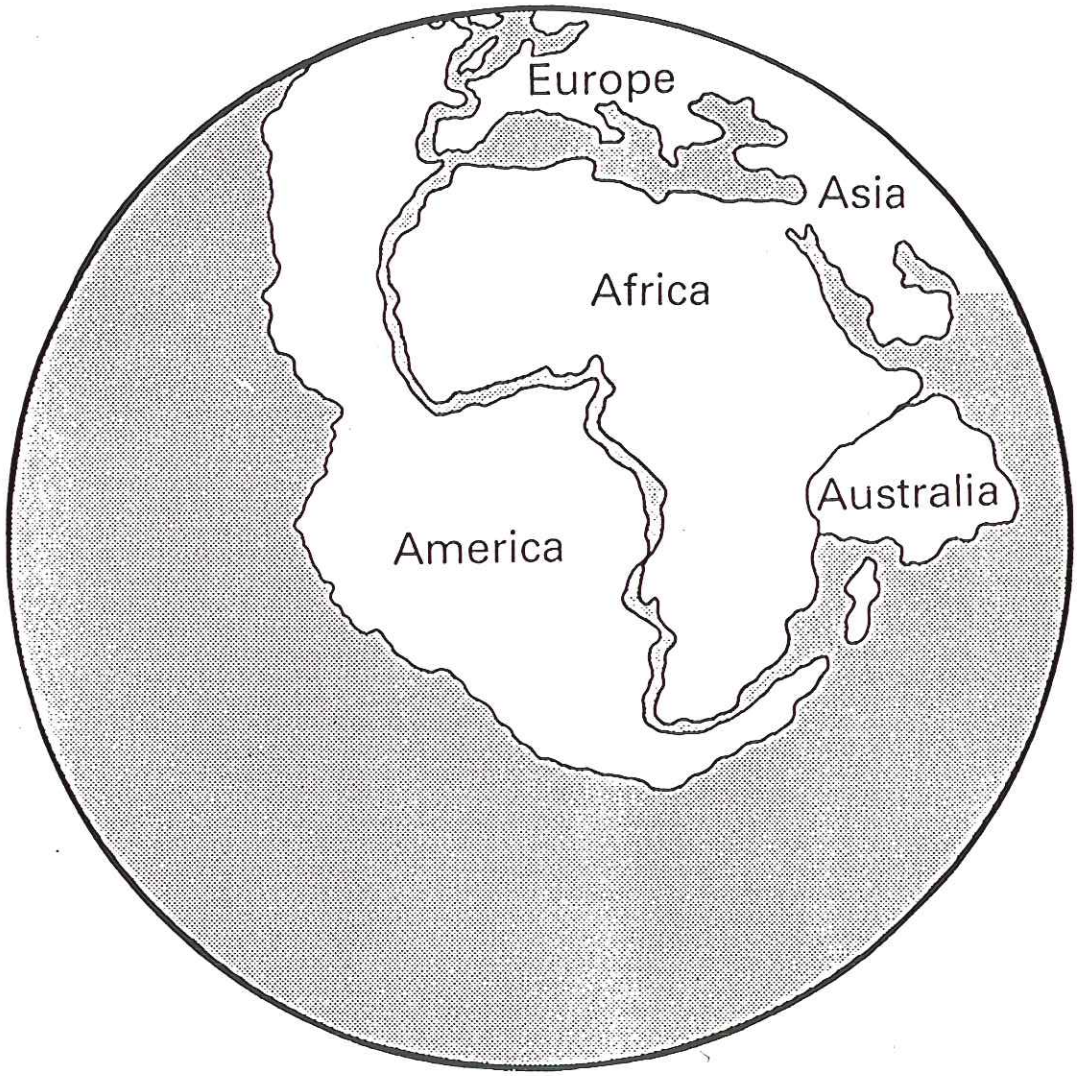

Fig. 1.1 Snider–Pelligrini's reconstruction of 1858.

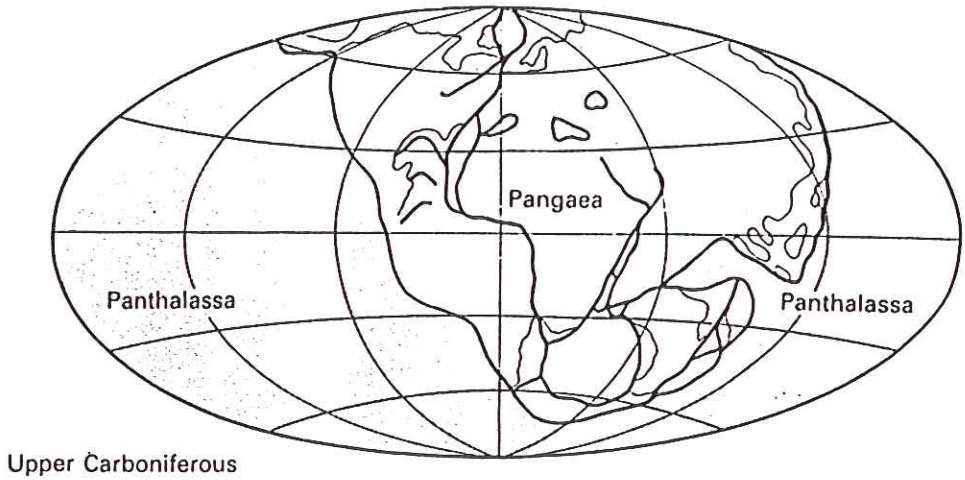

Upper Carboniferous

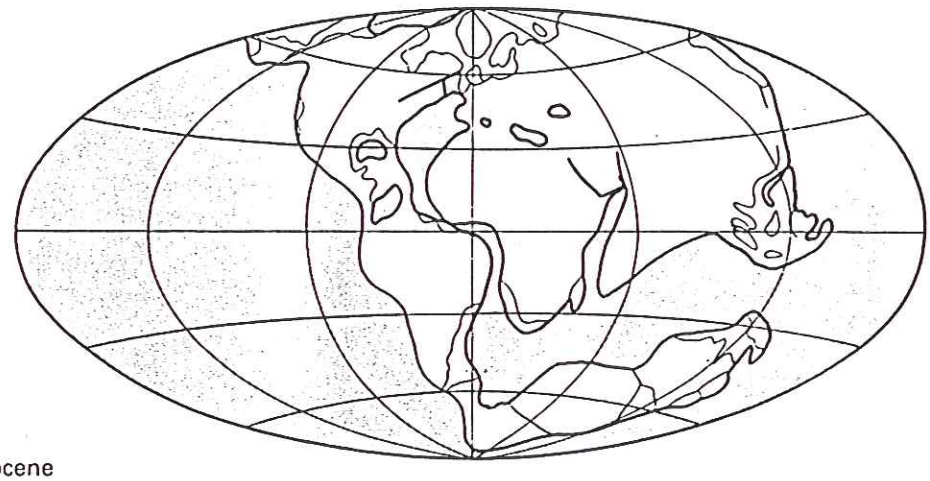

Eocene

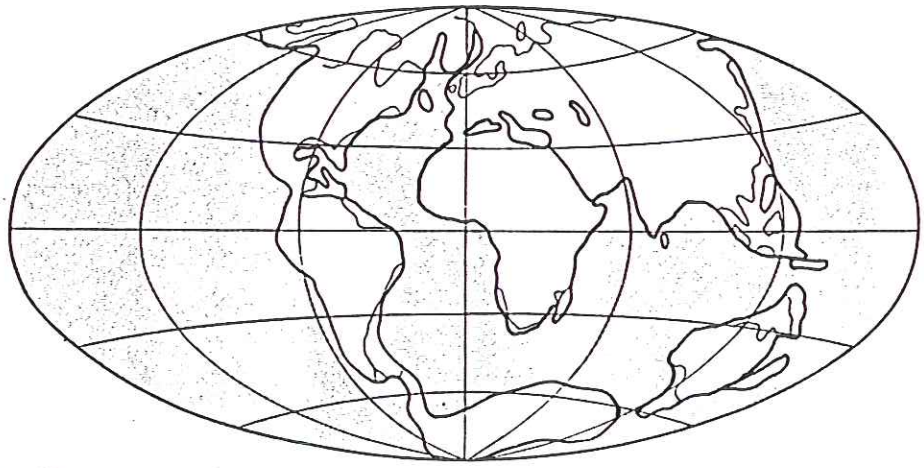

Lower Quaternary

Fig. 1.3 Wegener's reconstruction of the positions of the continents from Carboniferous to Quaternary times.

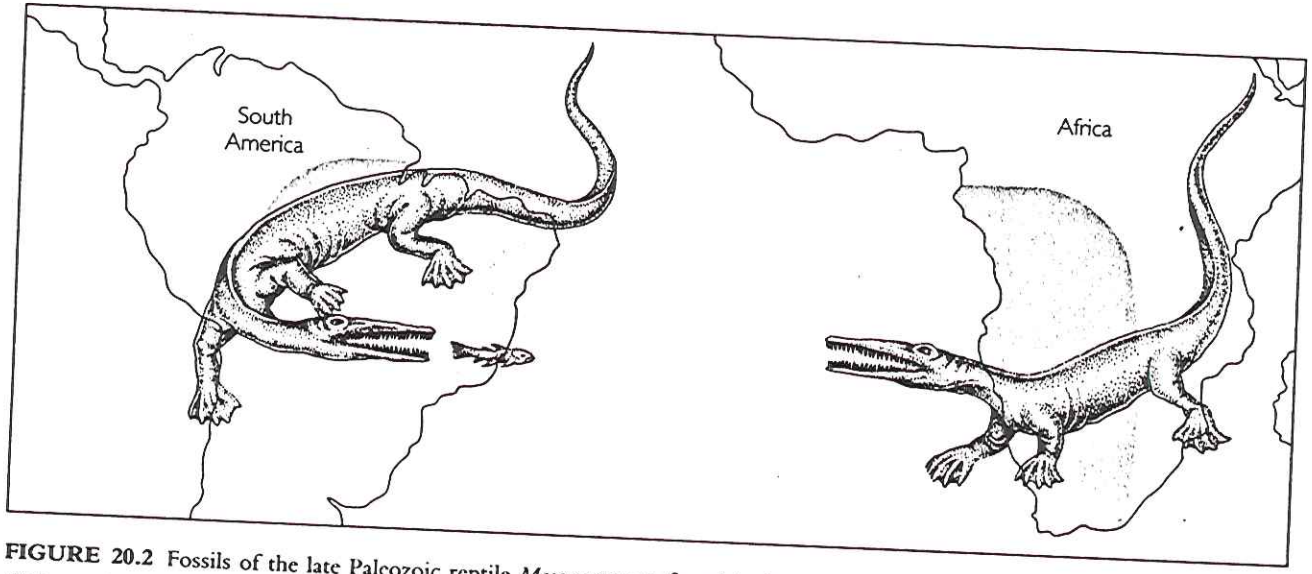

FIGURE 20.2 Fossils of the late Paleozoic reptile *Mesosaurus* are found in South America and Africa and nowhere else in the world. If *Mesosaurus* could swim across the South Atlantic Ocean, it could have crossed other oceans and it should have spread more widely. That it did not suggests that South America and Africa must have been joined at that time. (After A. Hallam, "Continental Drift and the Fossil Record," *Scientific American*, November 1972, pp. 57–66.)

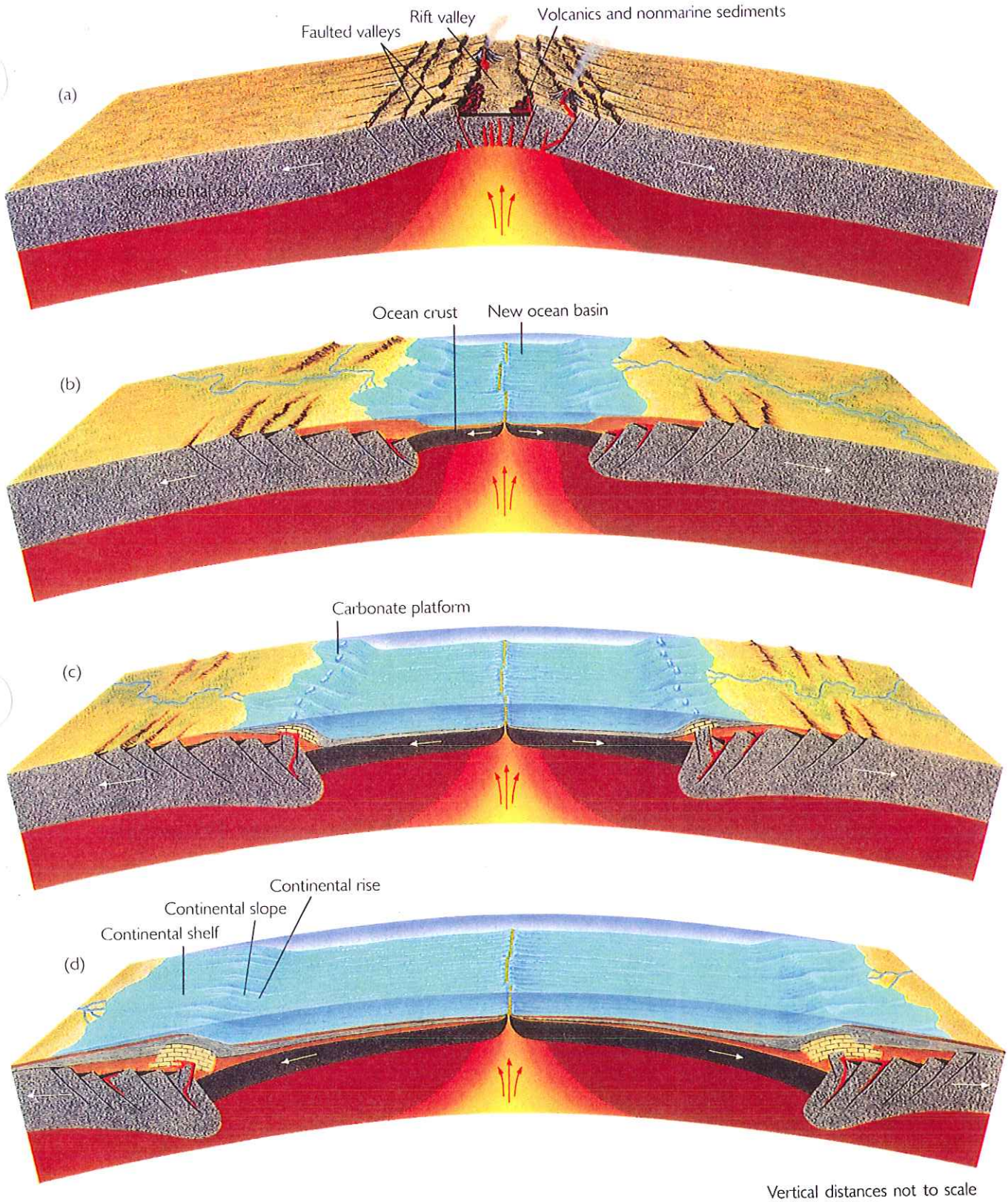

Vertical distances not to scale

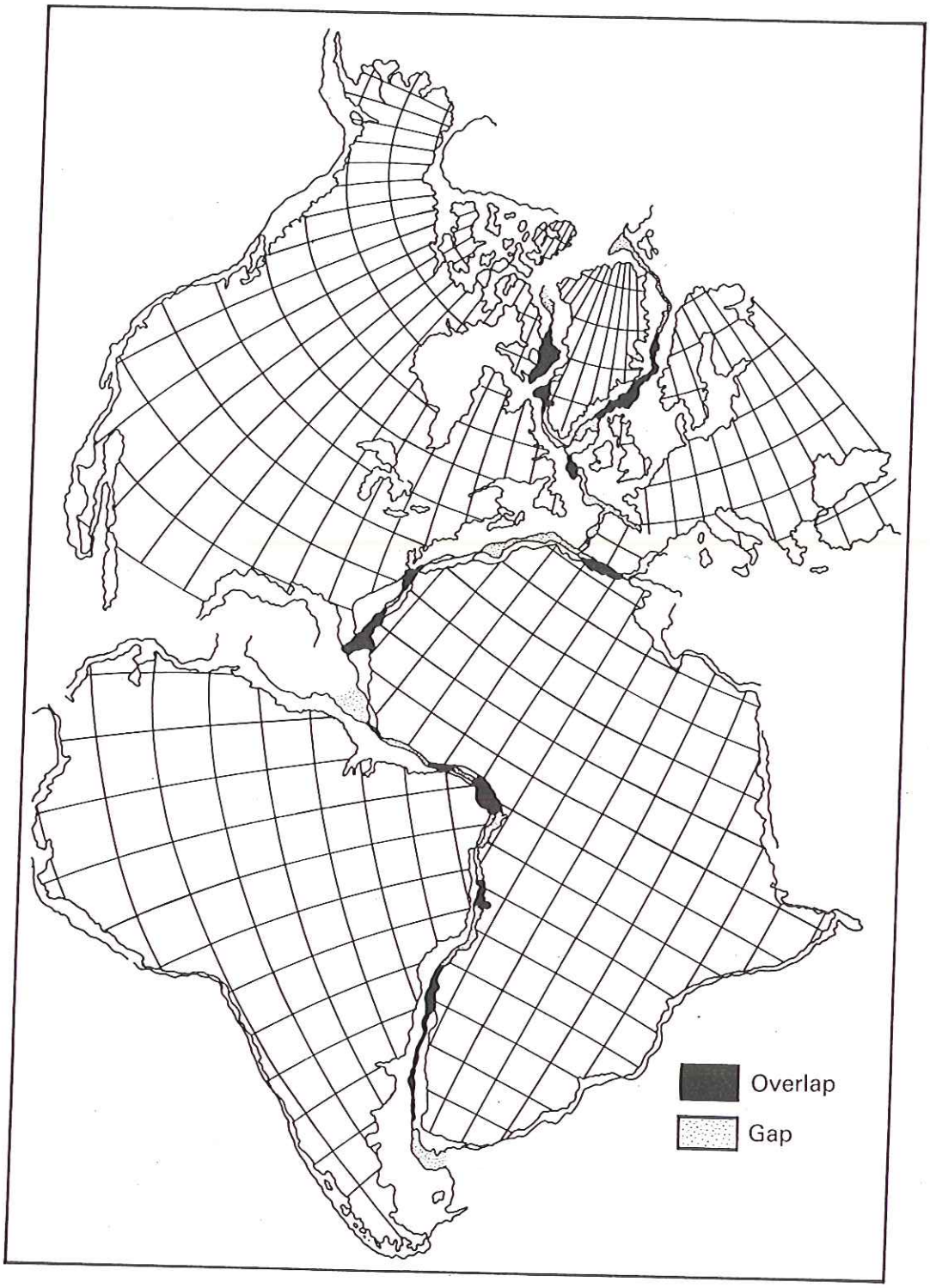

2 Fit of the continents around the Atlantic Ocean, obtained by matching the 500 fathom (927 m) isobath (redrawn Bullard *et al.*, 1965, with permission from the Royal Society).

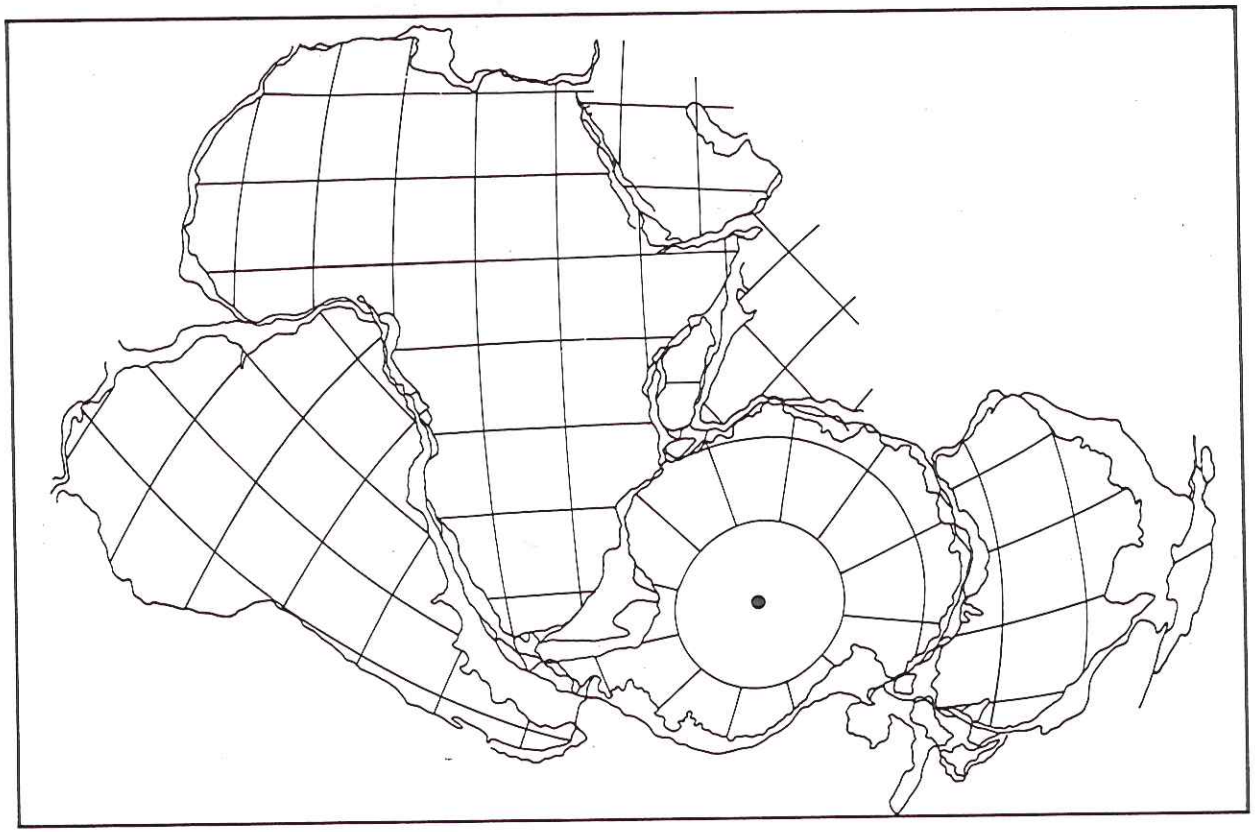

Fig. 3.3 Fit of the southern continents and India (redrawn from Smith & Hallam, 1970, with permission from *Nature*, **225**, 139–44. Copyright © 1970 Macmillan Magazines, Ltd).

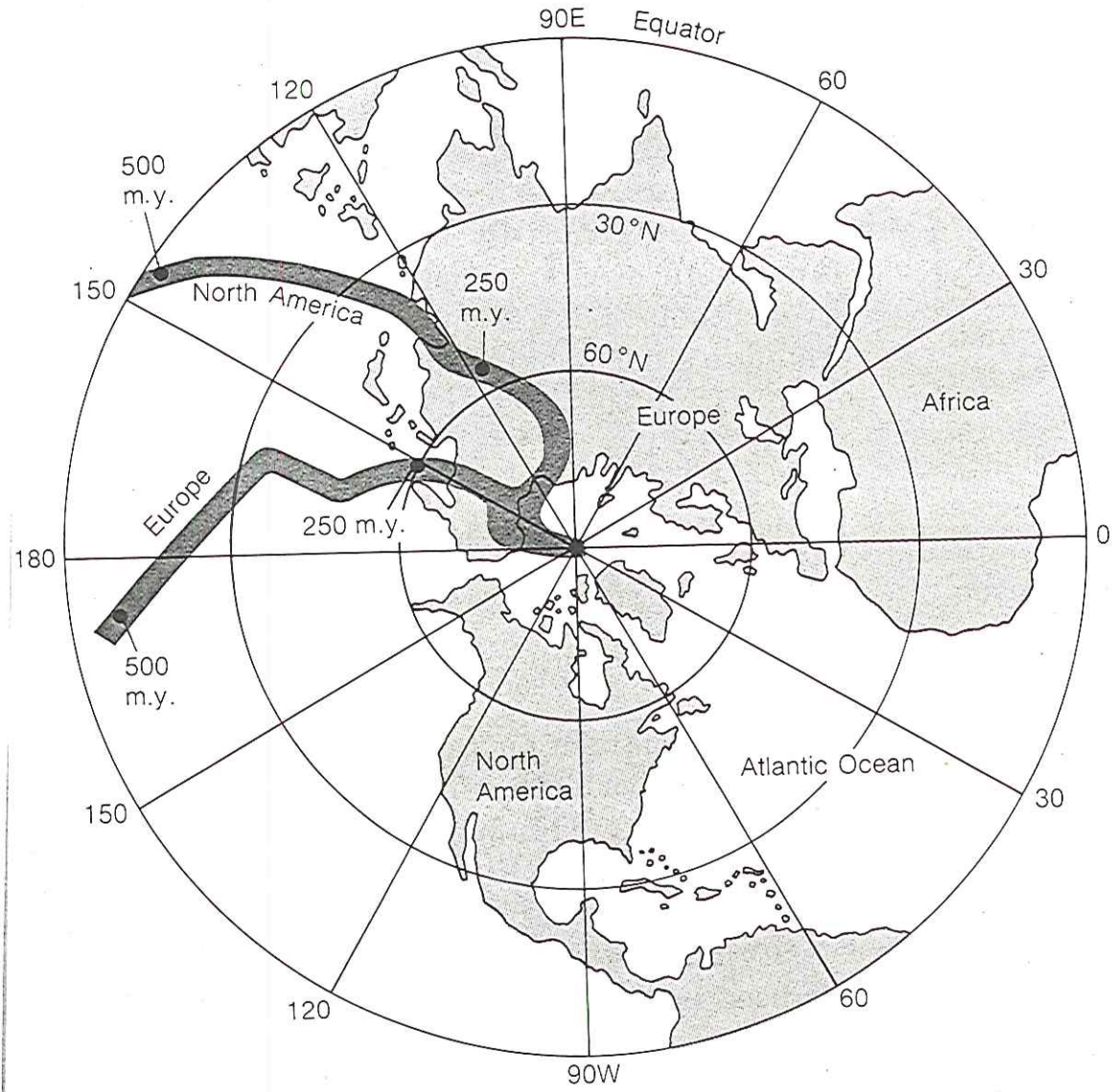

Figure 19-11

Apparent polar-wandering curves based on North American and European paleomagnetic data showing apparent positions of the magnetic pole from the present to 500 million years ago. Most geophysicists believe that the pole didn't actually wander, as the figure implies; it remained fixed, close to the geographic pole, while the "map"—that is, the outer layers of the Earth—drifted over the interior. If the Atlantic had not opened and continental drift had not occurred, the European and North American polar-wandering curves would coincide prior to Triassic time. Thus the polar-wandering curves really indicate the simultaneous northward drift of these continents and the east–west opening of the Atlantic Ocean. The polar-wandering curve, though fictitious, is a convenient way of summarizing paleomagnetic data.

~ half the data are reversed
this corrected for in making
this plot.

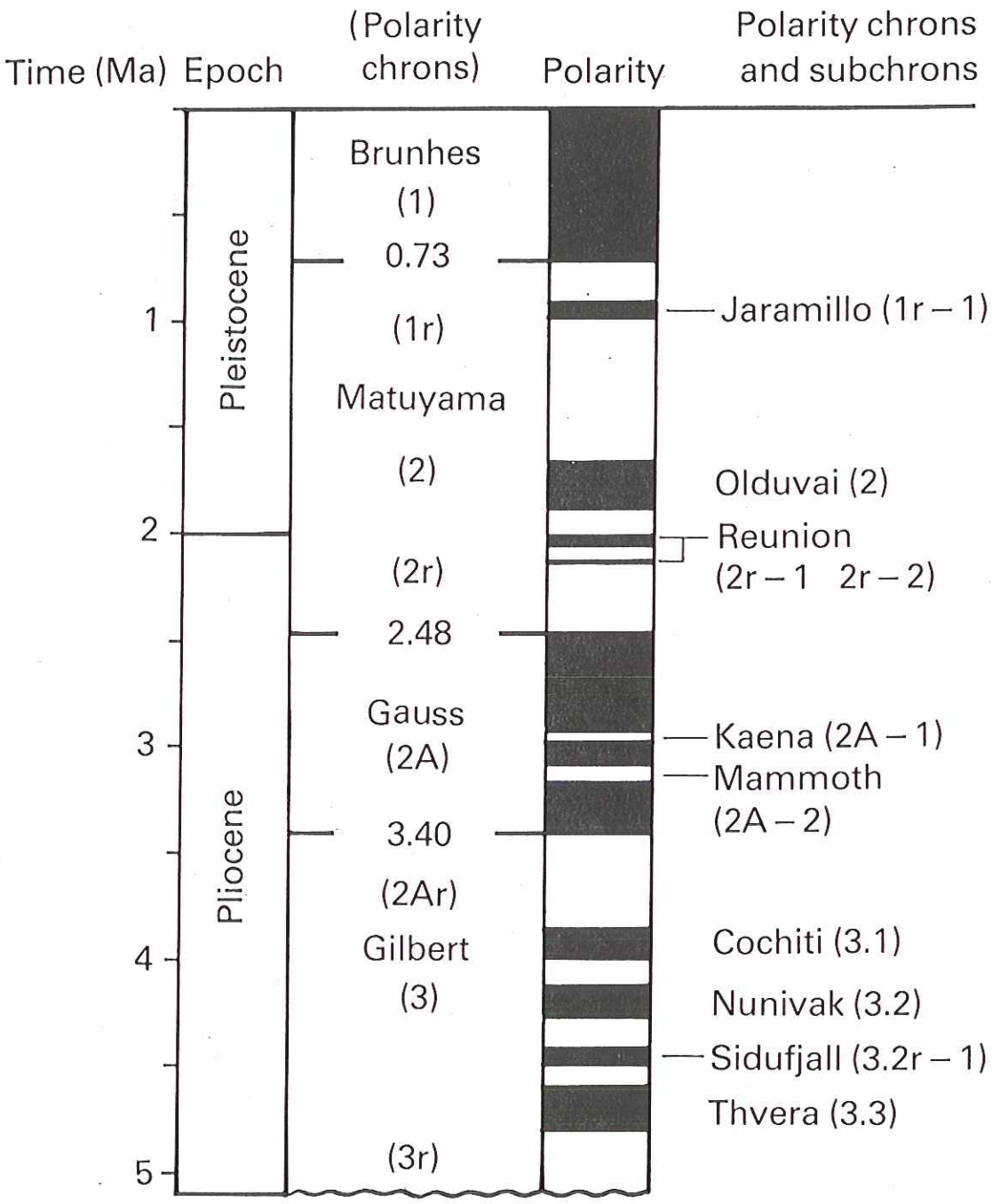

Fig. 4.9 Polarity time scale based on radiometric dating. Alternative numerical designations based on the numbered sequence of marine anomalies are shown in brackets (redrawn from Harland *et al.*, 1982, *A Geological Time Scale*, with permission from Cambridge University Press).

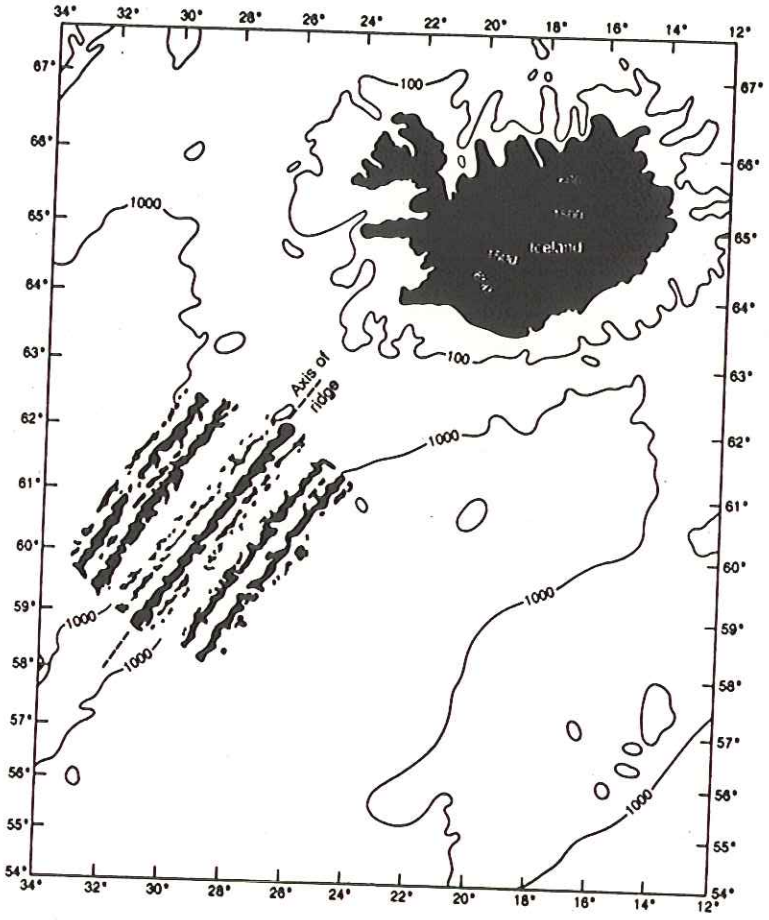

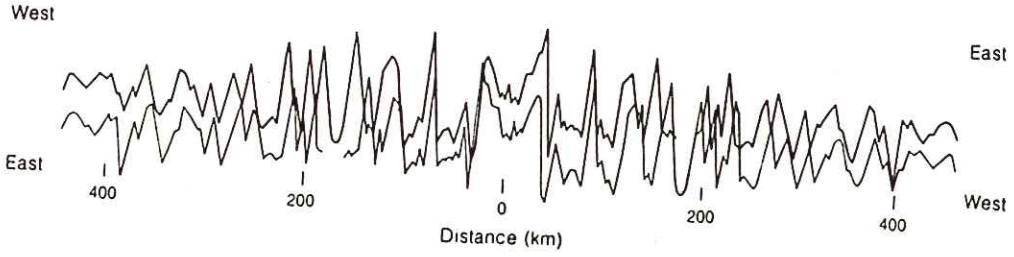

Figure 18-16
Symmetry of the magnetic anomaly of sea-floor rocks on both sides of the ridge axis is demonstrated by reversing a record covering about 900 km of both flanks (brown) and superposing it on the record as ordinarily shown (black). [After "Sea-Floor Spreading" by J. R. Heirtzler.]

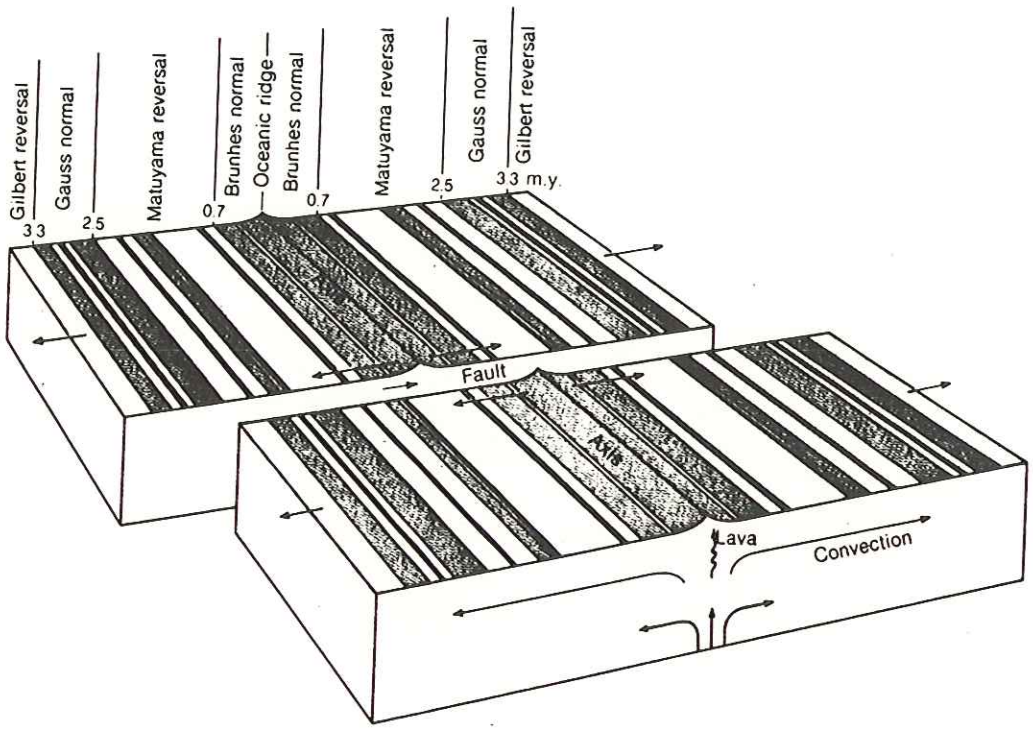

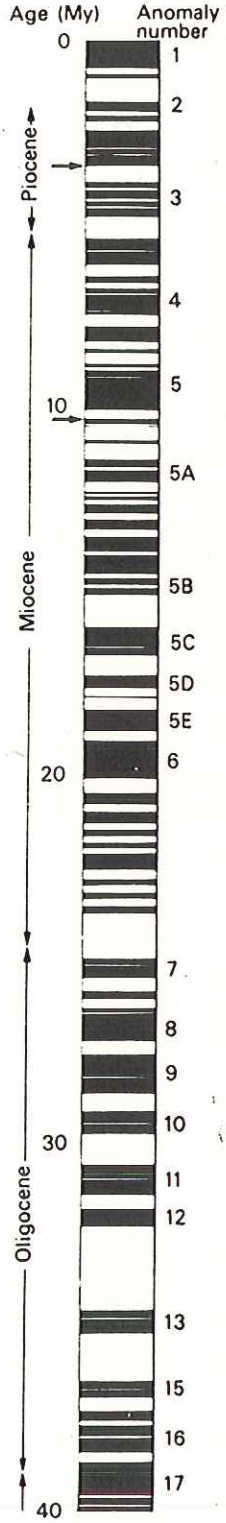

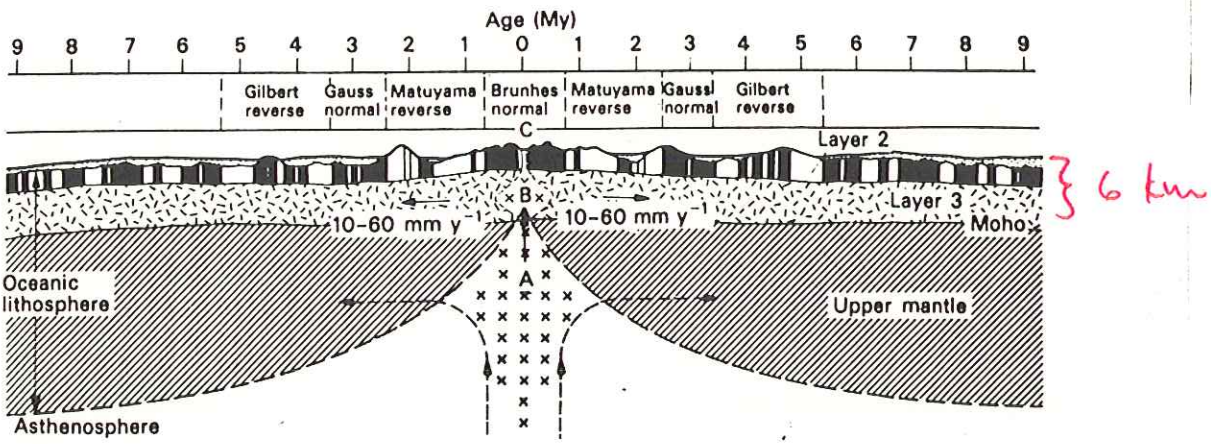

} 6 km

only uppermost basaltic crust is magnetized

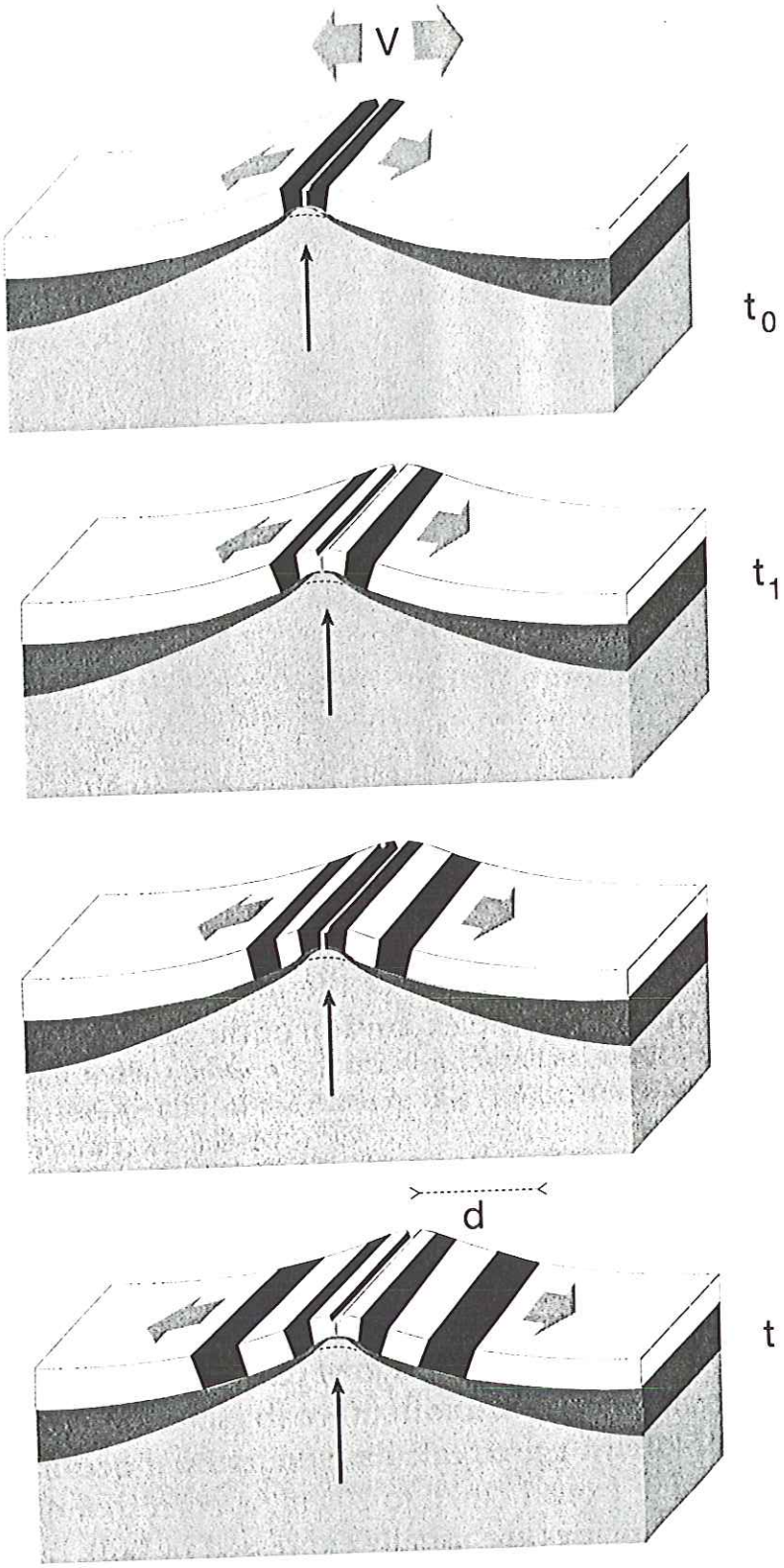

prediction:
symmetry across ridge axis

Figure 1.3
Origin of magnetic anomalies along a ridge. At the present time (t_0), a basaltic lava with normal polarity (*black band*) is extruded on the ridge until a point in time when a magnetic inversion takes place. From this time (t_1) onwards the ridge extrudes basaltic lava of inverted polarity (*white band*) which splits up and pushes to the side the older lava bands of normal polarity. The phenomenon is repeated and thereby leads to the magnetic stripe pattern of the ocean floors. The velocity of opening V is calculated by simply measuring the distance d from the ridge for a certain stripe, the age of which is known. The formula is $V = 2d\ (t\text{-}t_0)$

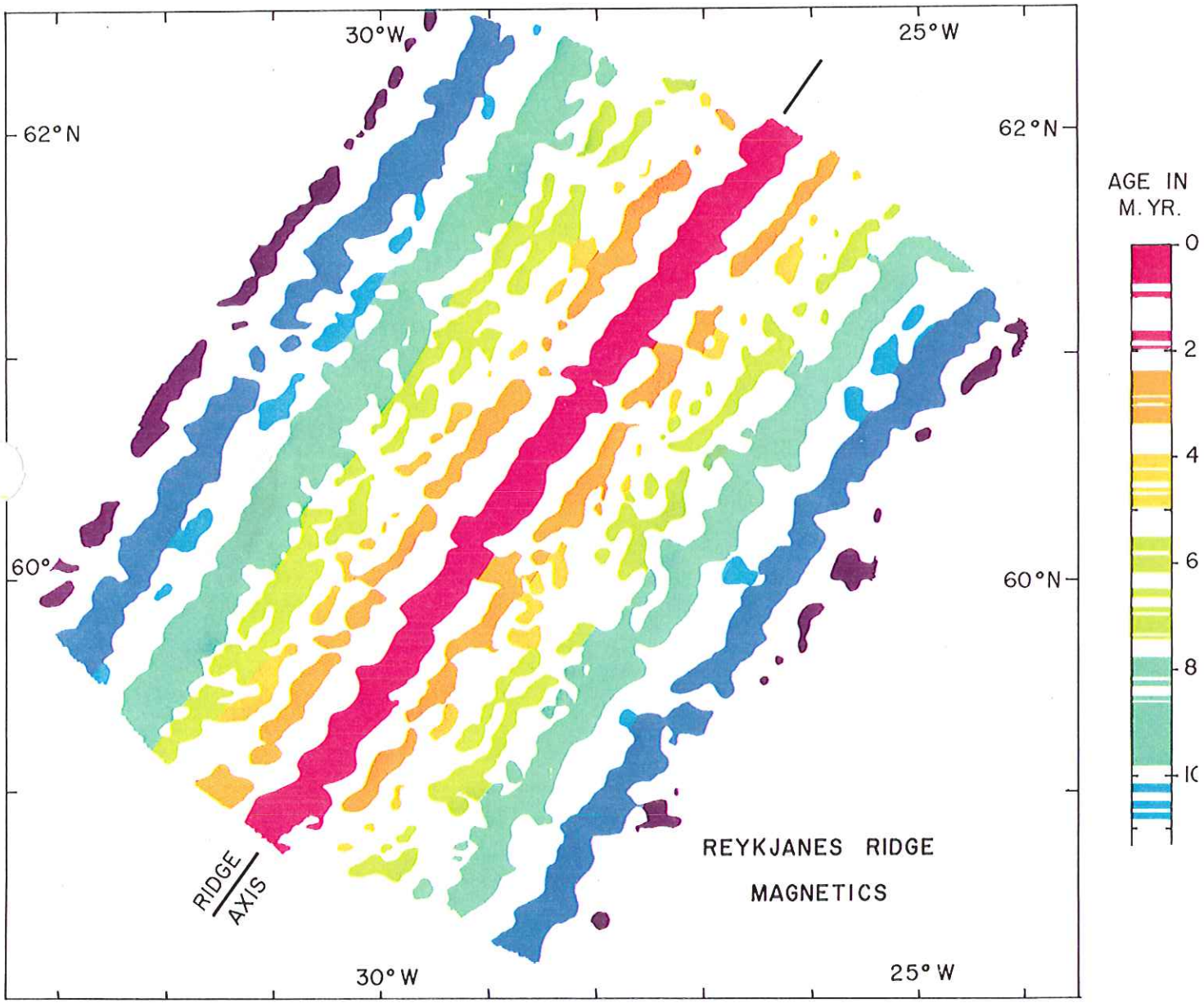
30°W
25°W
62°N
60°
60°N
RIDGE AXIS
REYKJANES RIDGE
MAGNETICS
AGE IN M.YR.
0
2
4
6
8
10

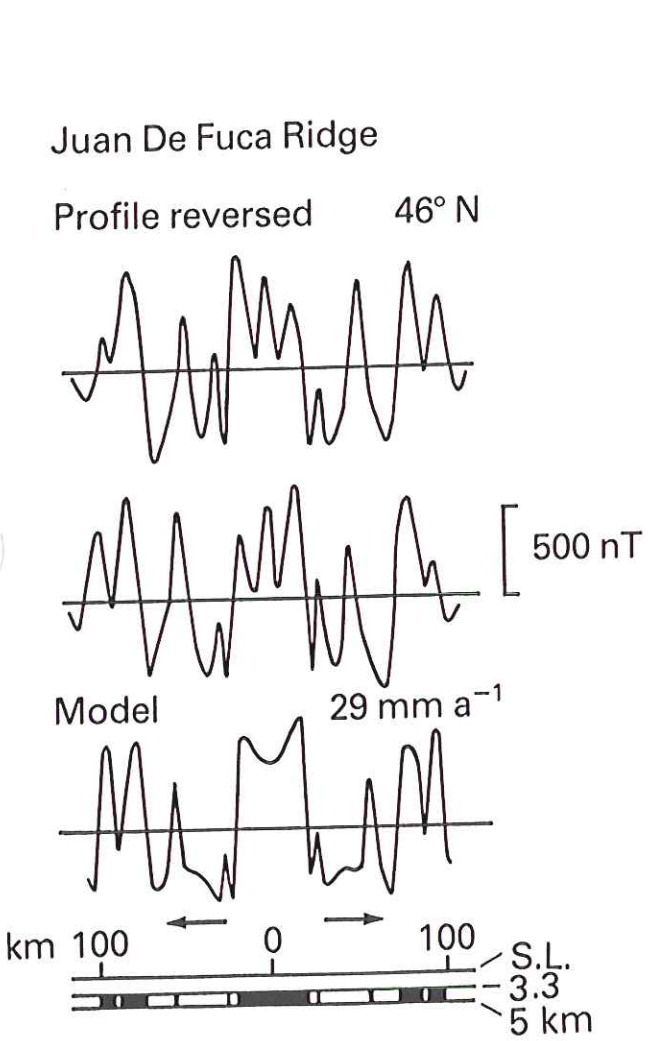

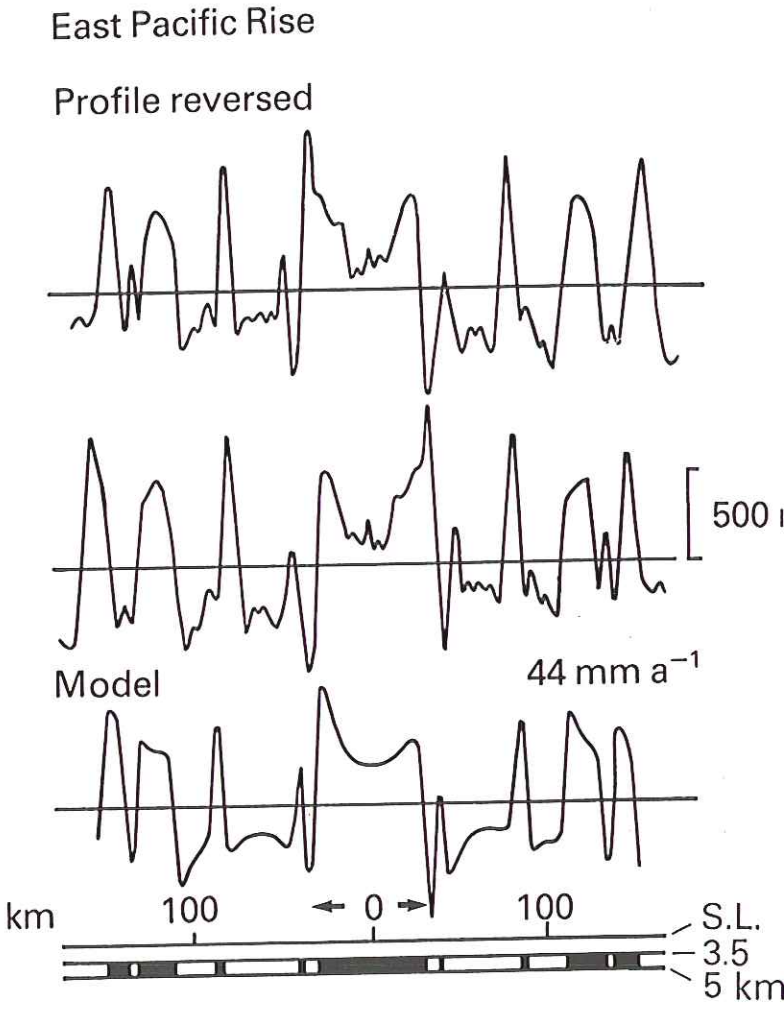

1.5 km thick magnetized layer

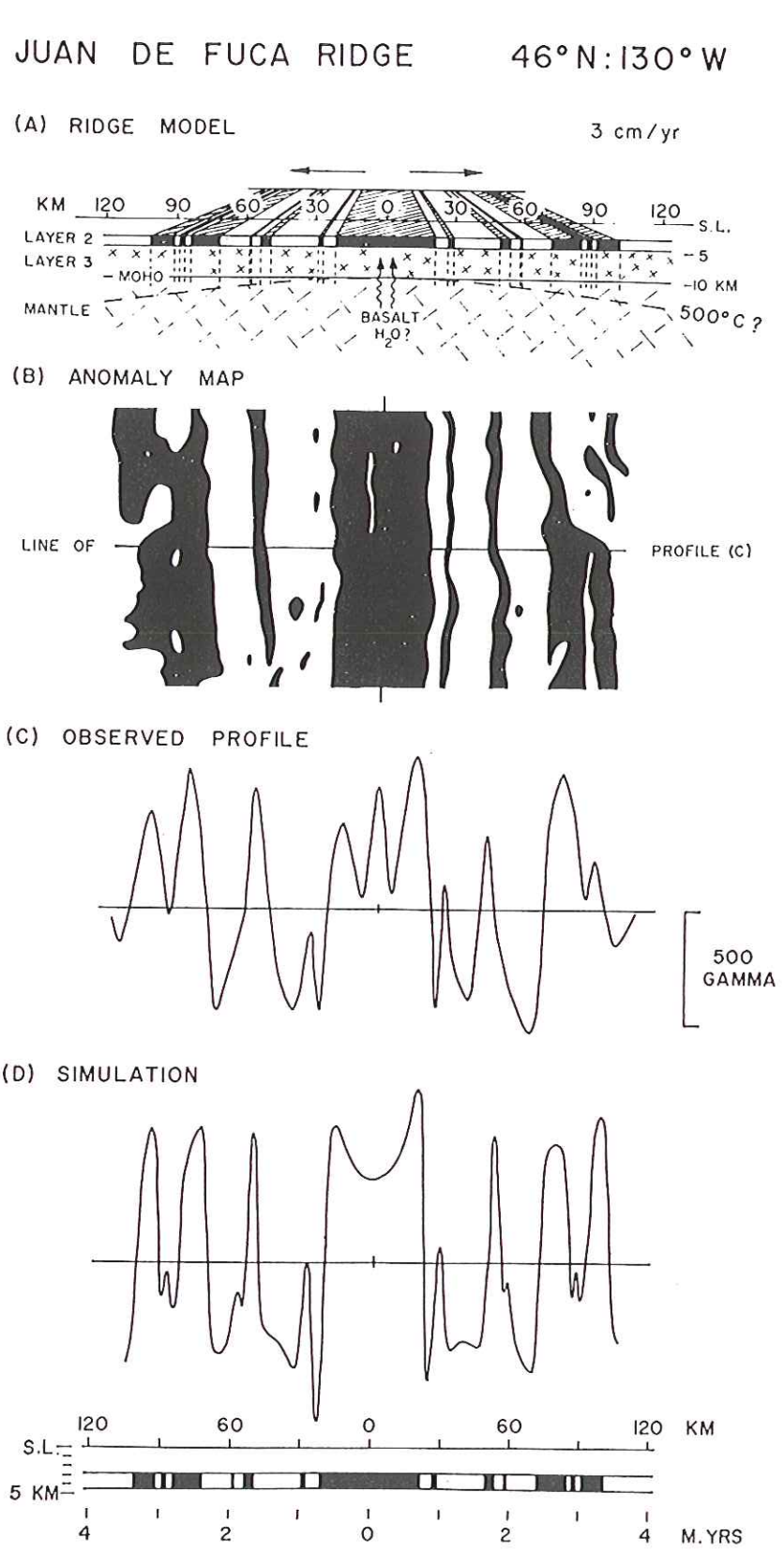

Figure 1. (A) A schematic representation of the crustal model discussed in the text, applied to the Juan de Fuca Ridge, southwest of Vancouver Island (see Fig. 4). Shaded material in layer 2, normally magnetized; unshaded, reversely magnetized.

(B) Part of the summary map of magnetic anomalies recorded over the Juan de Fuca Ridge (Raff and Mason, 1961). Black, areas of positive anomalies; white, areas of negative anomalies.

(C) A total-field magnetic anomaly profile along the line indicated in (B).

(D) A computed profile assuming the model and reversal time scale discussed in the text. Intensity and dip of the earth's magnetic field taken as 54,000 gamma and + 66°; magnetic bearing of profile 087°. (1 gamma = 10^{-5} oersted). (S.L. = sea level.)

Note: Throughout, observed and computed profiles have been drawn in the same proportion: 10 km horizontally is equivalent to 100 gamma vertically. Normal or reverse magnetization is with respect to an axial dipole vector, and the effective susceptibility assumed is ± 0.01 except for the central block at a ridge crest (+ 0.02).

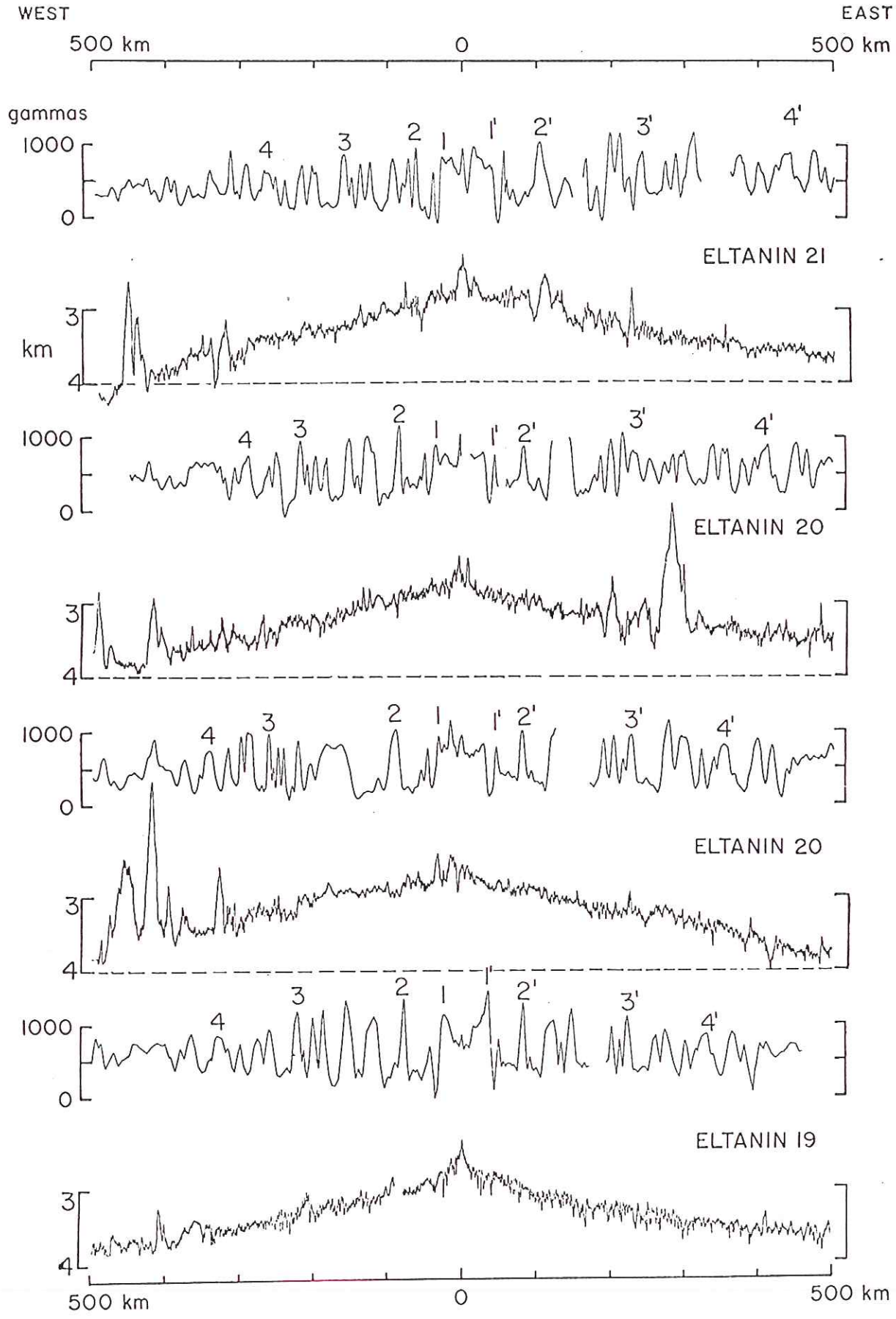

Figure 3. Total magnetic intensity and topographic profiles over the Pacific Antarctic ridge. The numbers 1 and 1′ identify the edges of the axial anomaly here, but number 1 is used to identify the axis in other figures.

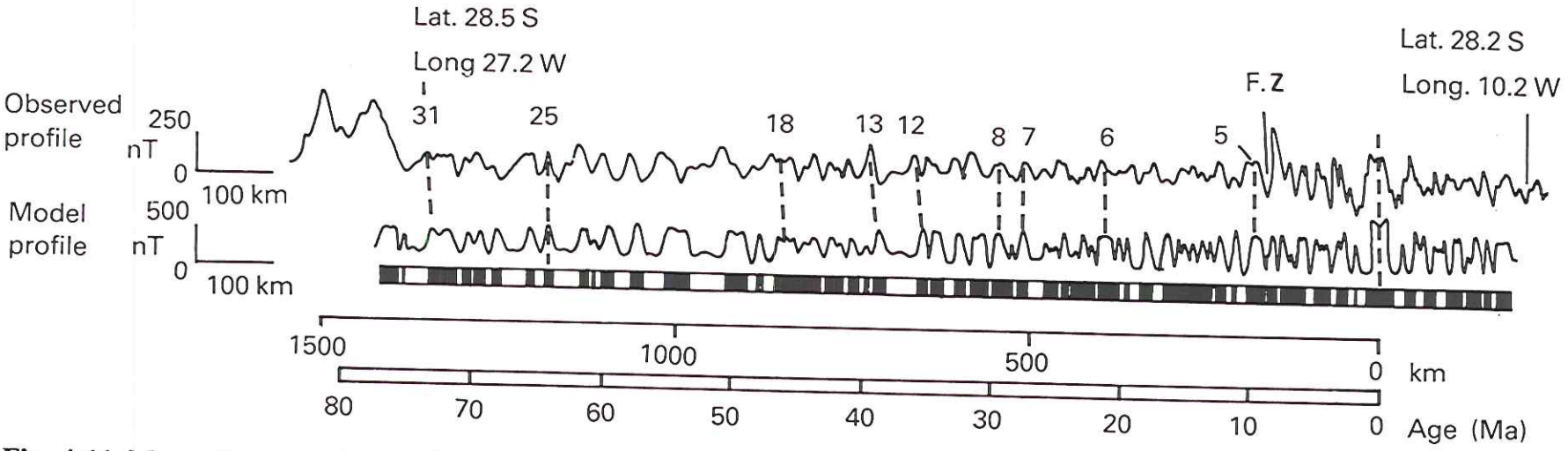

Fig. 4.11 Magnetic anomaly profile and model over the southern mid-Atlantic ridge (redrawn from Heirtzler *et al.*, 1968).

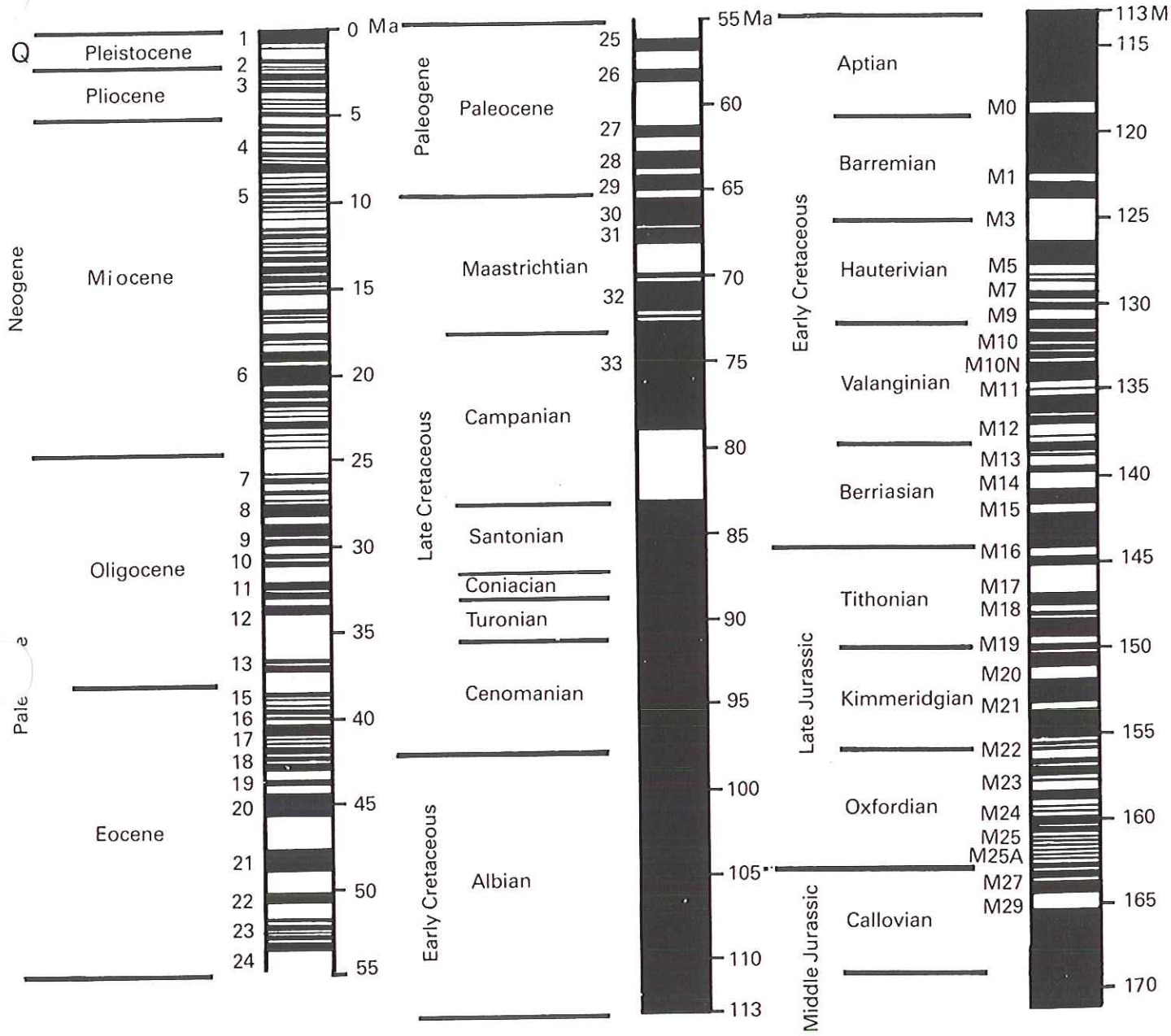

Fig. 4.13 Magnetic reversal time scale from mid-Jurassic times to present (redrawn from Harland *et al.*, 1982, *A Geological Time Scale*, with permission from Cambridge University Press).

note : cretaceous quiet period

83 - 118 Myr

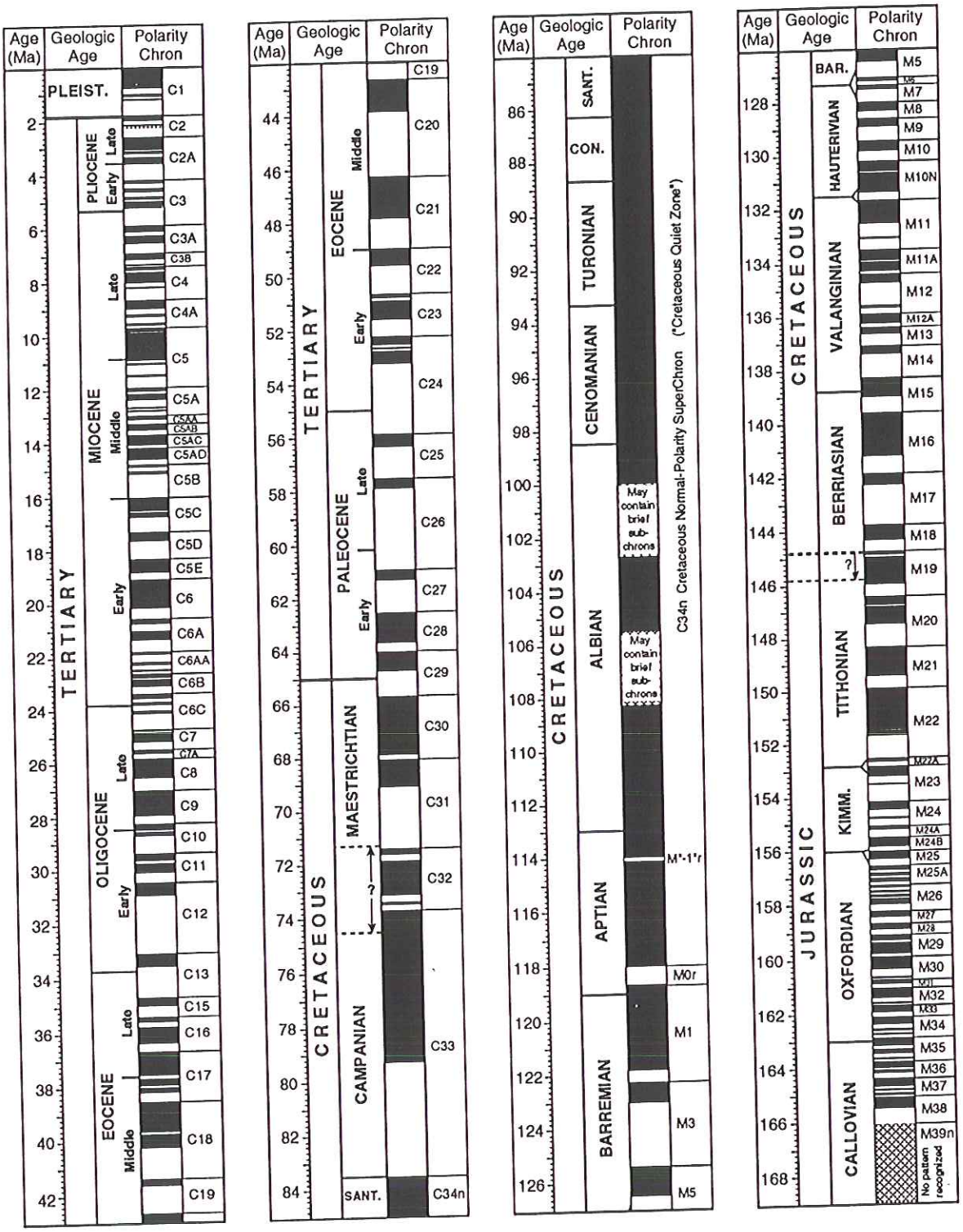

Figure 2. Cenozoic-Late Mesozoic magnetic polarity time scale. Normal-polarity chrons (Table 2) are shown in black, reversed-polarity chrons are white; intervals lacking magnetostratigraphy studies or having uncertain validity are cross-hatchured.

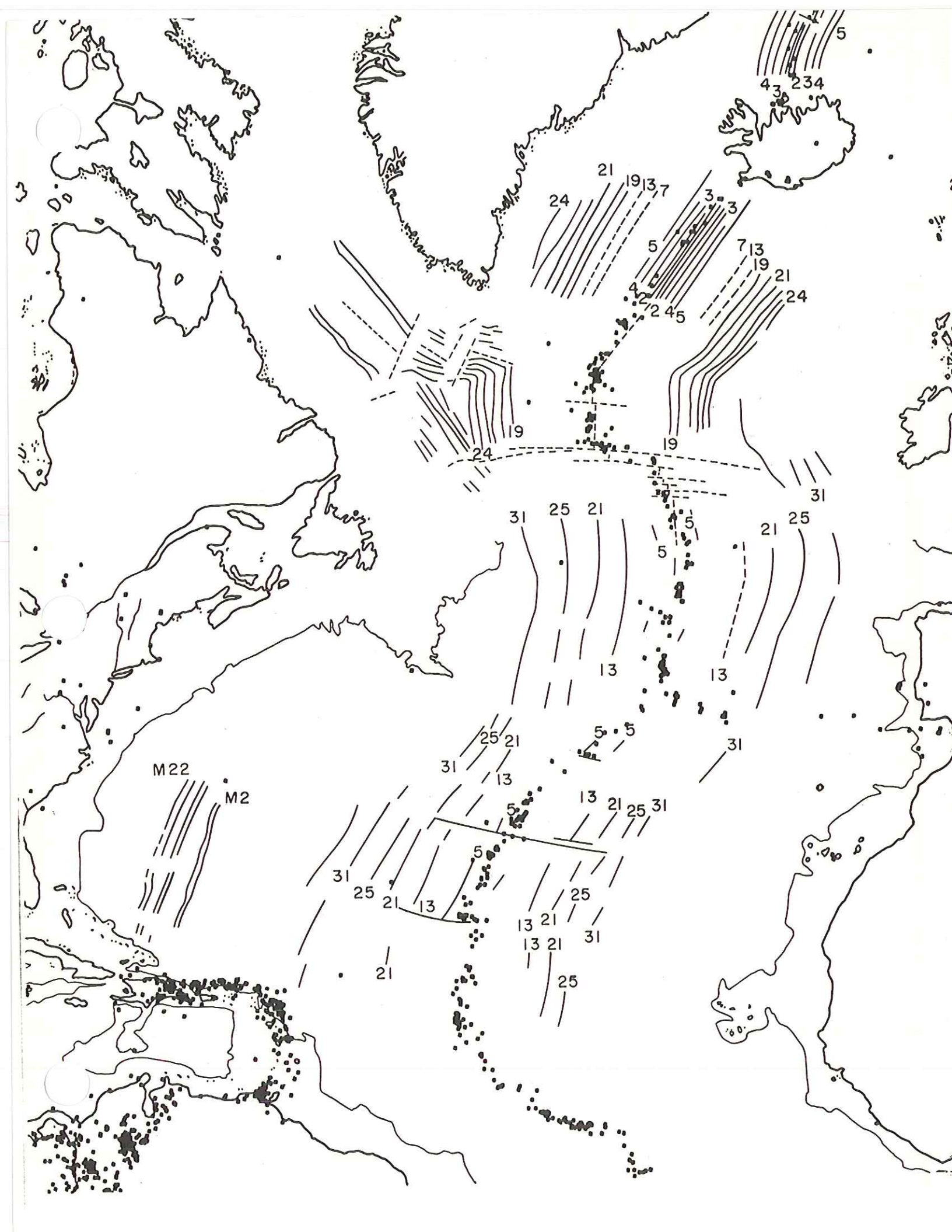
M22
M2

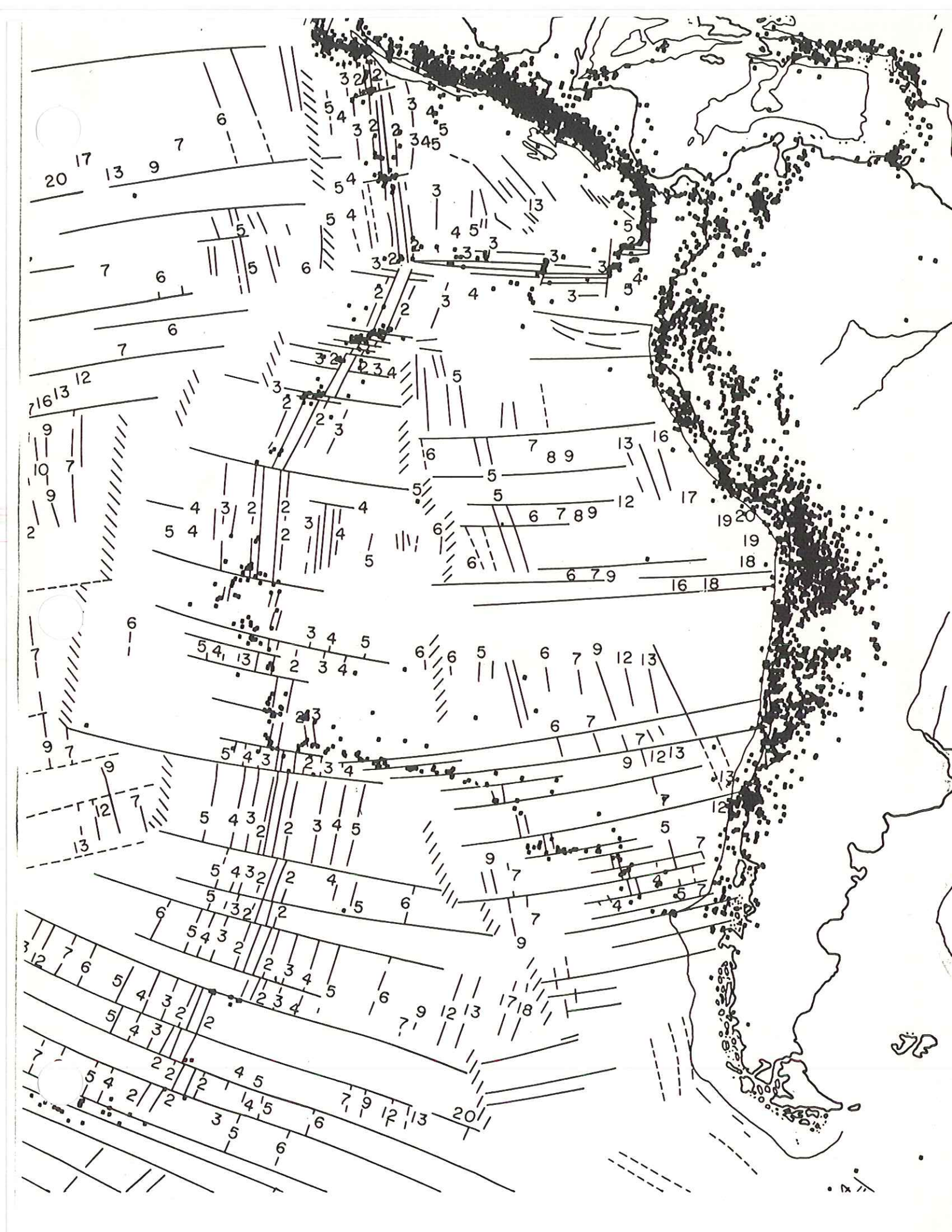

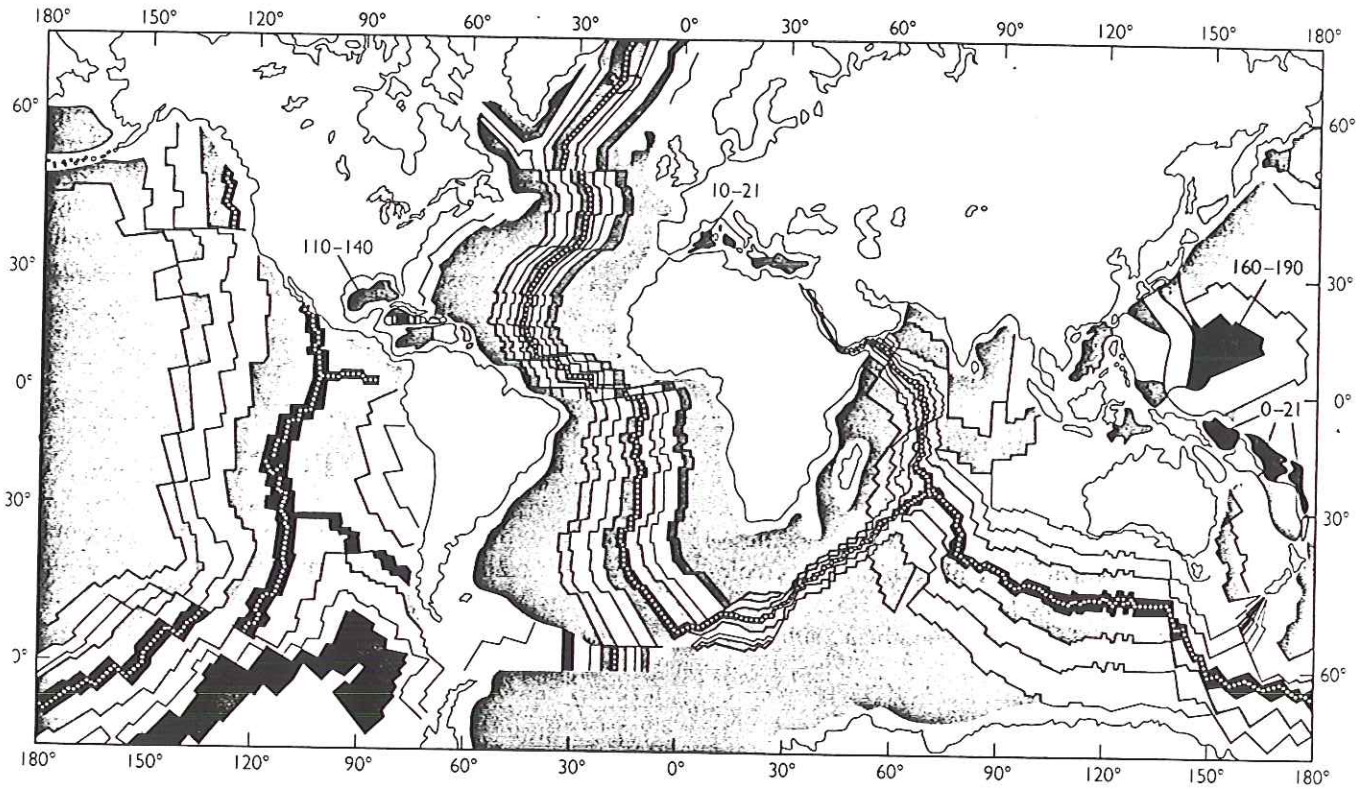

The age of the ocean basins (in millions of years)

0–5	Pleistocene–Pliocene	38–52	Eocene	140–160	Early Jurassic
5–21	Miocene	52–65	Paleocene		
21–38	Oligocene	65–140	Cretaceous		

FIGURE 20.11 The worldwide pattern of seafloor spreading is revealed by the isochrons (contours separating the bands of different colors and textures) that give the age of the seafloor in millions of years since its creation at ridges. Mid-ocean ridges, along which new seafloor is extruded, coincide with the youngest seafloor (red). The Atlantic Ocean is symmetrical about the Mid-Atlantic Ridge. Asymmetry of the pattern in the Pacific is caused partly by subduction in the Aleutian Trench south of Alaska, in the Peru-Chile Trench along the west coast of South America, and in many trenches in the western Pacific. (After map prepared by J. Sclater and L. Meinke.)

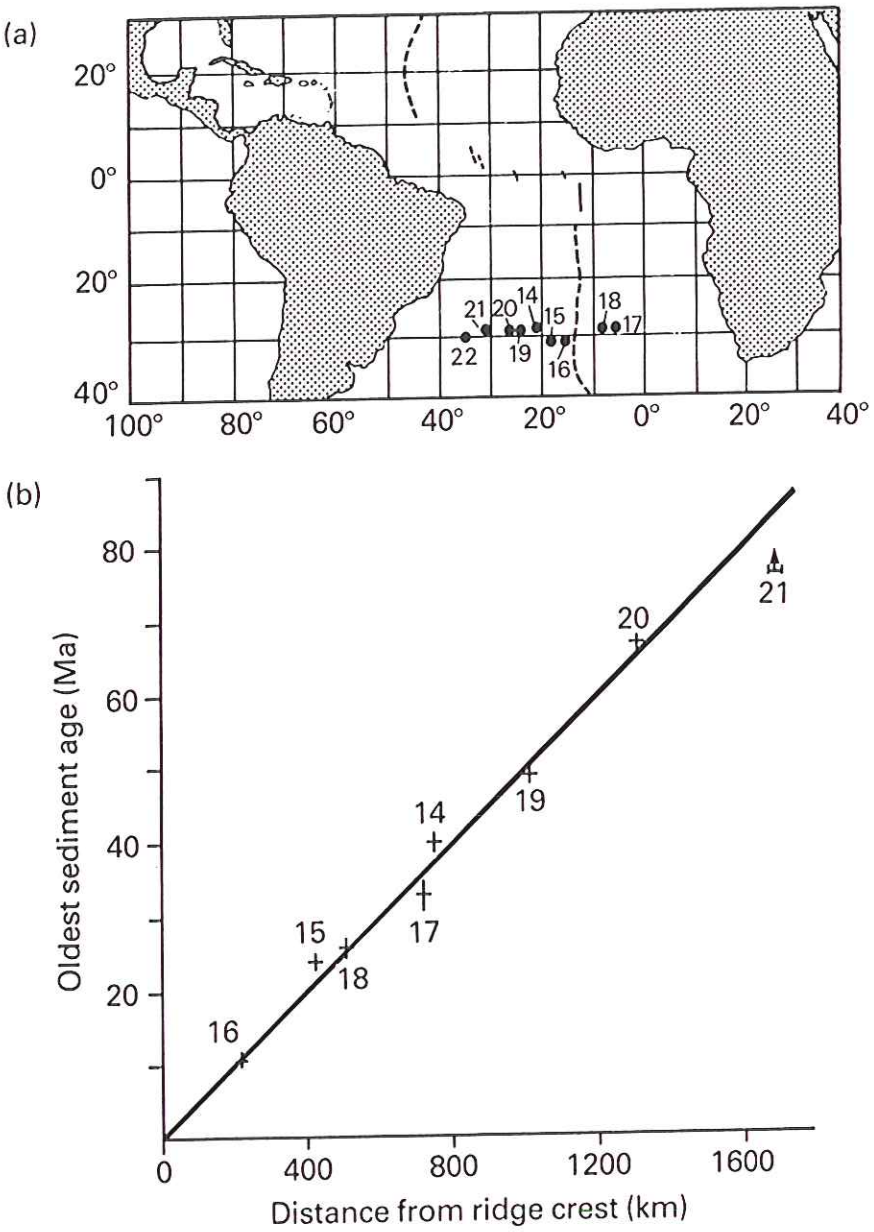

Fig. 4.15 (a) Location map of drilling sites on Leg 3 of the DSDP in the South Atlantic. (b) Relationship between greatest sediment age and distance from the mid-Atlantic ridge crest (after Maxwell *et al.*, 1970, *Science*, **168**, 1041–59, with permission from the AAAS. Copyright © 1970 by the AAAS).

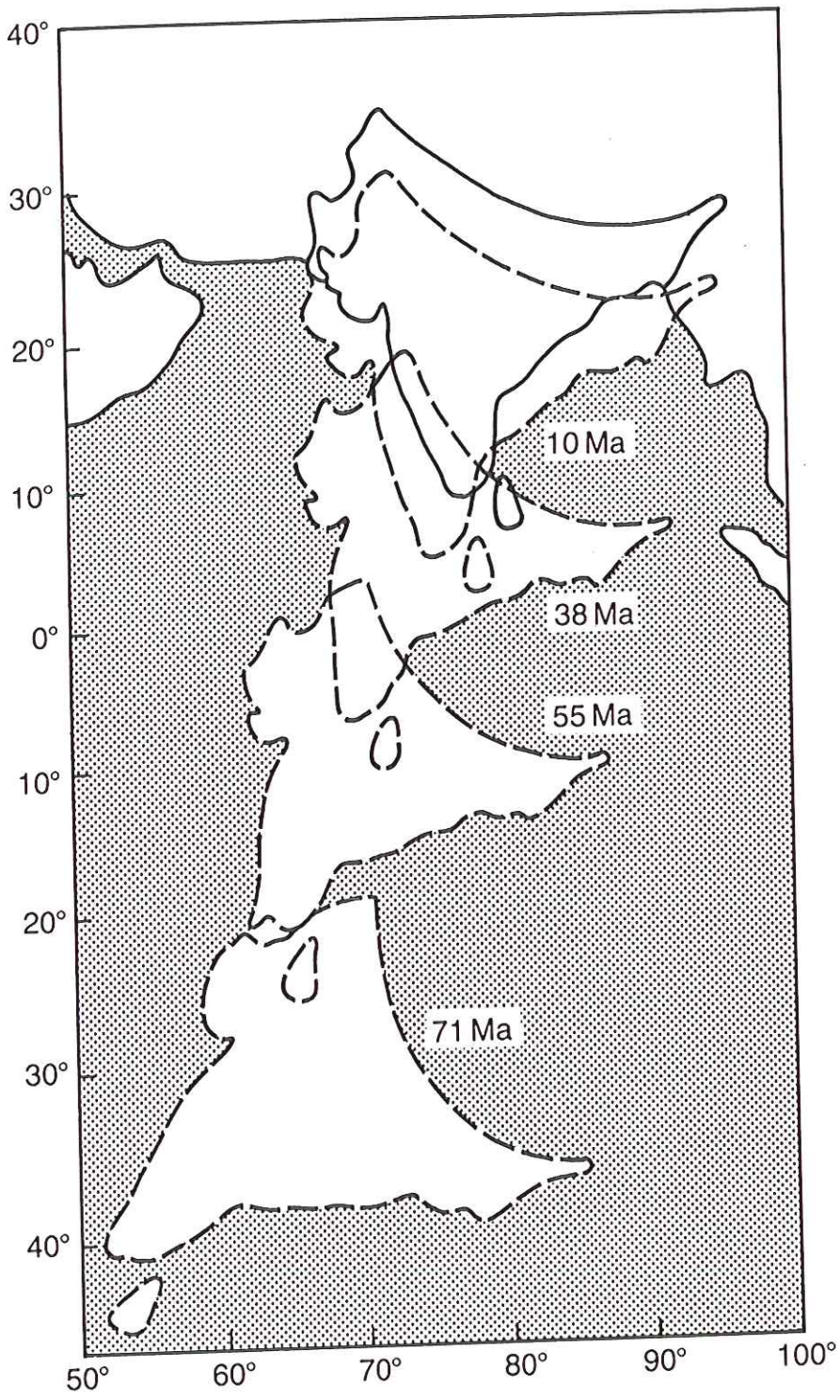

Fig. 9.12 Northward drift of India with respect to Asia for the period 71 Ma to present determined from magnetic lineations in the Indian and Atlantic Oceans (redrawn from Molnar & Tapponnier, 1975, *Science*, **189**, 419–26, with permission from the AAAS. Copyright © 1975 by the AAAS).

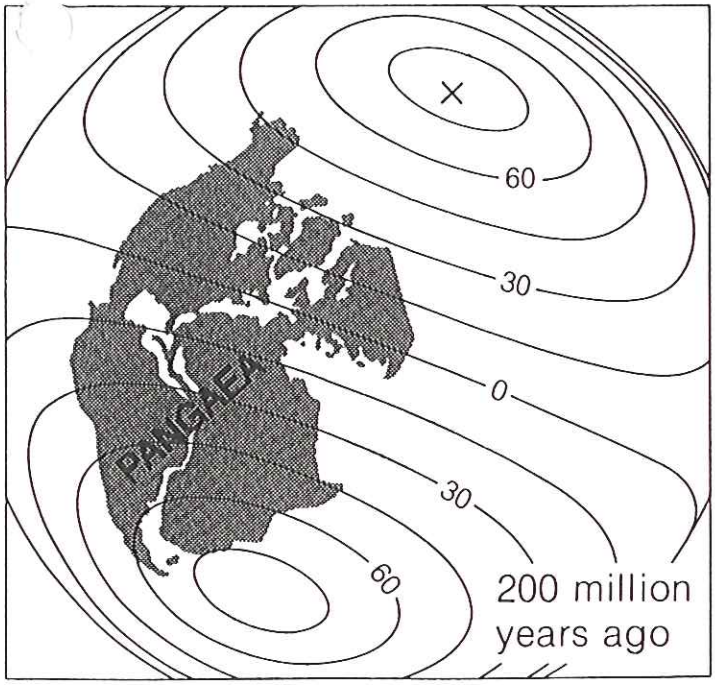

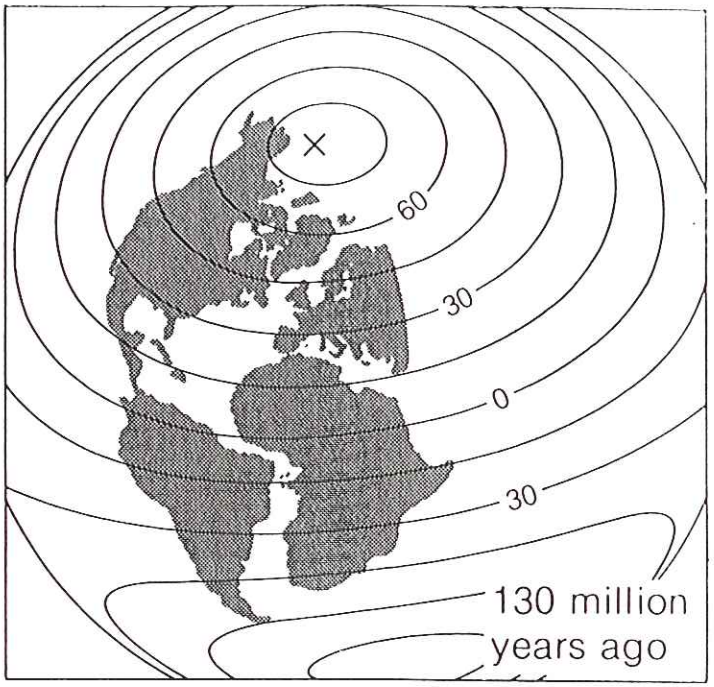

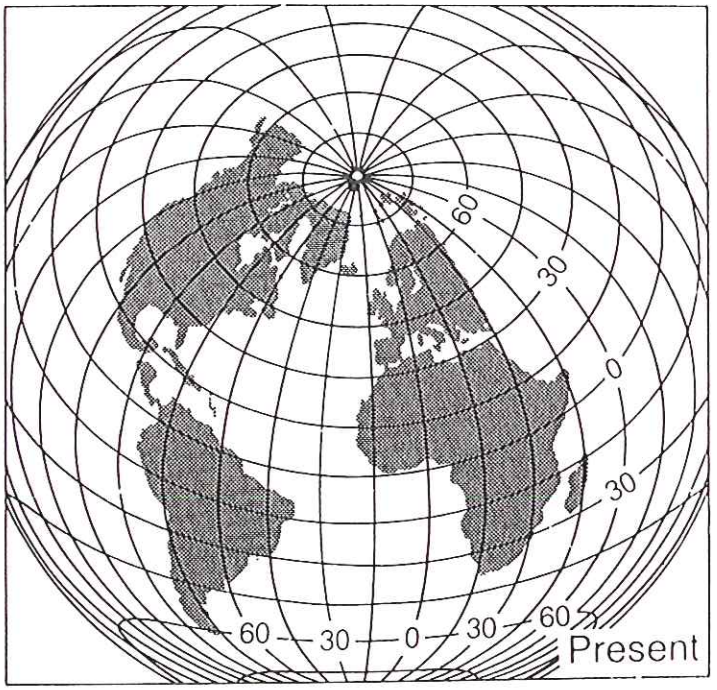

× = Ancient geographic pole

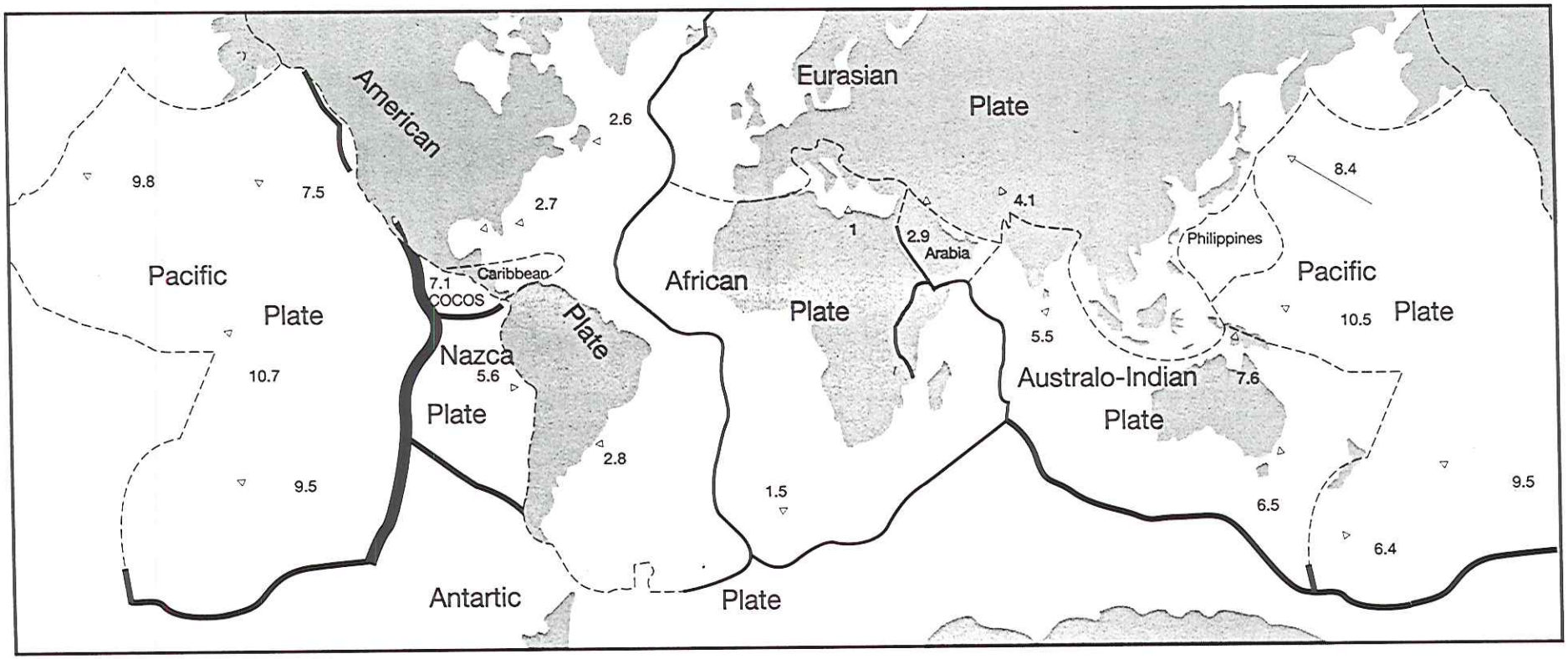
American
Plate
Eurasian
Plate
Pacific
Plate
Caribbean
Plate
Nazca
Plate
African
Plate
Arabia
Philippines
Pacific
Plate
Australo-Indian
Plate
Antartic
Plate
9.8
7.5
10.7
9.5
2.6
2.7
7.1
COCOS
5.6
2.8
1
2.9
4.1
1.5
5.5
7.6
6.5
8.4
10.5
9.5
6.4

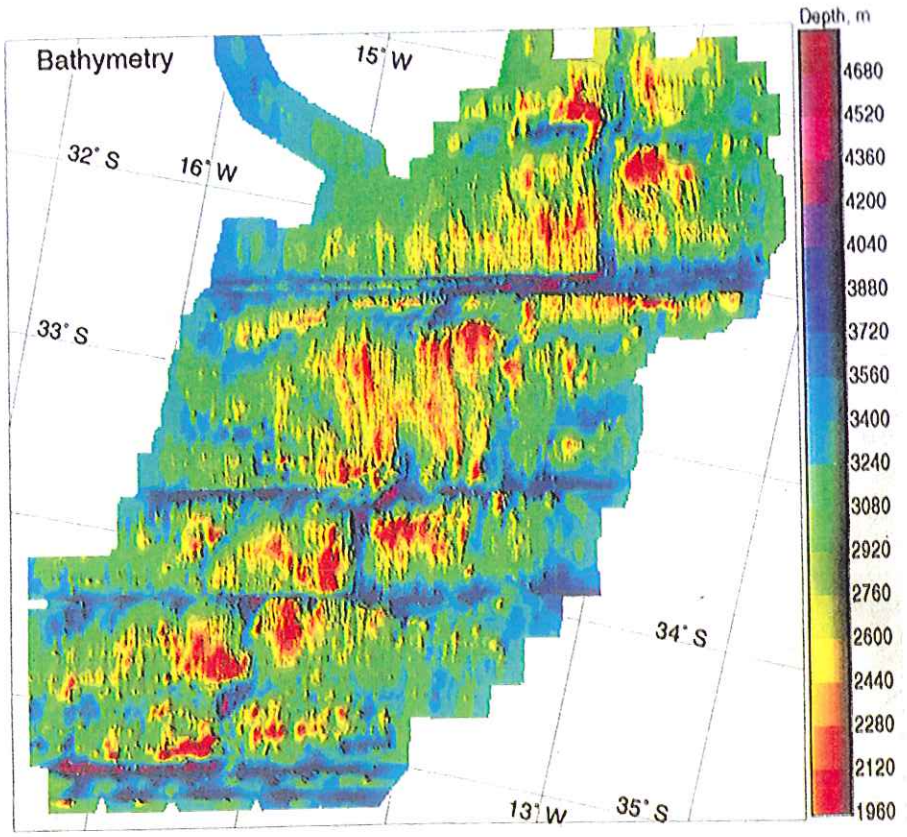
Bathymetry
15° W
16° W
32° S
33° S
34° S
35° S
13° W
Depth, m
4680
4520
4360
4200
4040
3880
3720
3560
3400
3240
3080
2920
2760
2600
2440
2280
2120
1960

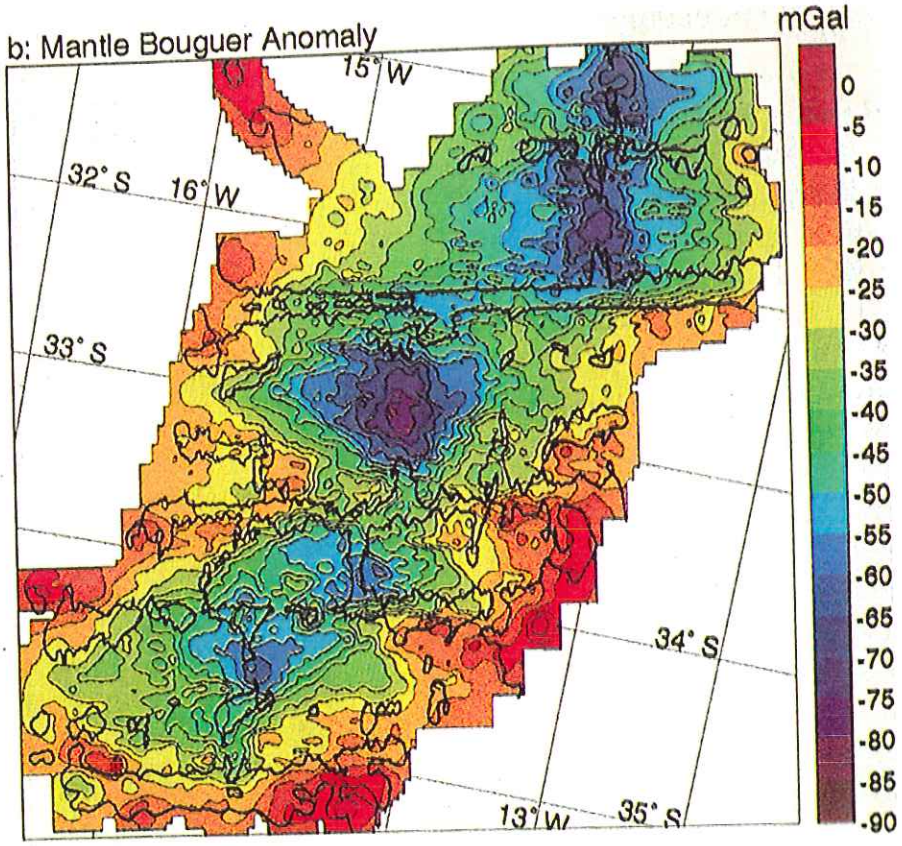
b: Mantle Bouguer Anomaly
15° W
16° W
32° S
33° S
34° S
35° S
13° W
mGal
0
-5
-10
-15
-20
-25
-30
-35
-40
-45
-50
-55
-60
-65
-70
-75
-80
-85
-90

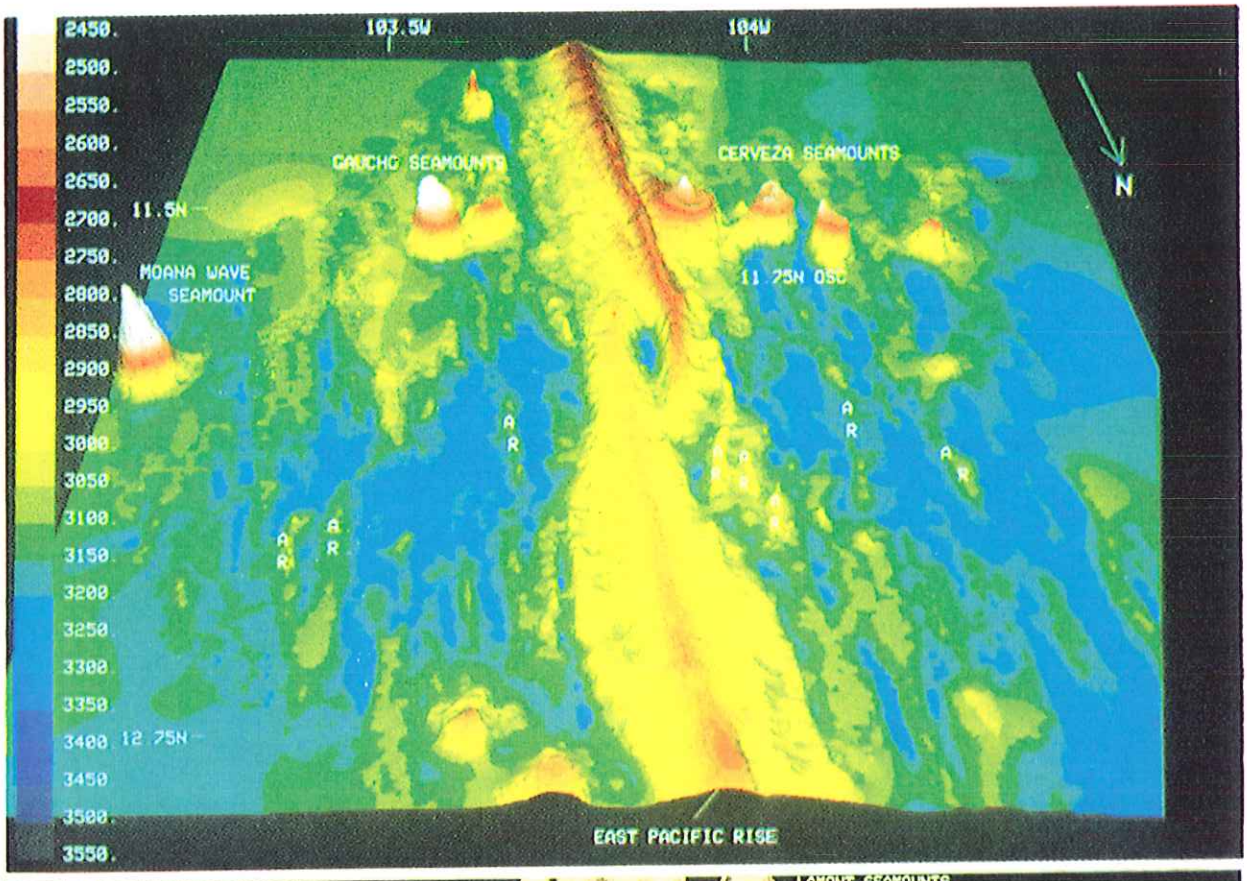
2450.
2500.
2550.
2600.
2650.
2700.
2750.
2800.
2850.
2900.
2950.
3000.
3050.
3100.
3150.
3200.
3250.
3300.
3350.
3400.
3450.
3500.
3550.
103.5W
104W
11.5N
12.25N
CAUCHO SEAMOUNTS
CERVEZA SEAMOUNTS
MOANA WAVE SEAMOUNT
11.25N OSC
N
A
R
EAST PACIFIC RISE

a

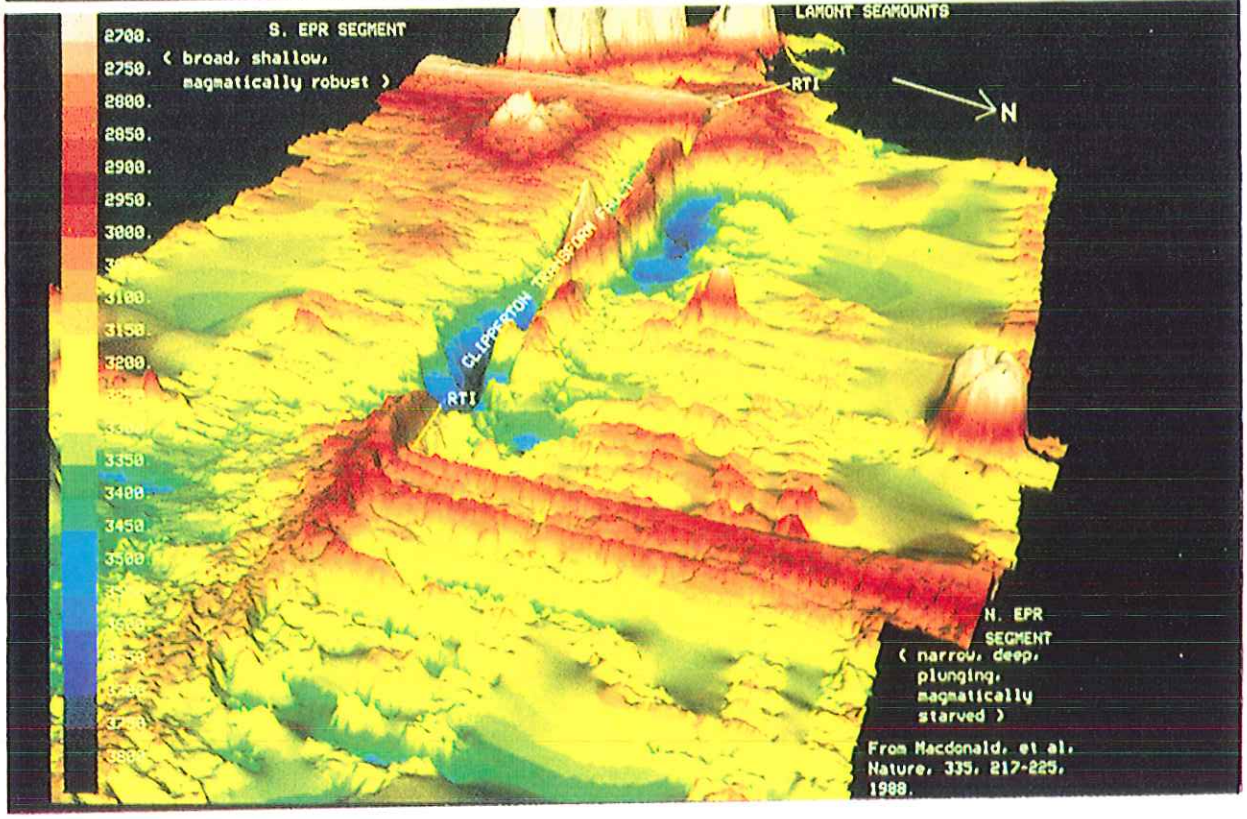
2700.
2750.
2800.
2850.
2900.
2950.
3000.
3100.
3150.
3200.
3350.
3400.
3450.
S. EPR SEGMENT
(broad, shallow, magmatically robust)
LAMONT SEAMOUNTS
RTI
N
CLIPPERTON TRANSFORM FAULT
RTI
N. EPR SEGMENT
(narrow, deep, plunging, magmatically starved)
From Macdonald, et al. Nature, 335, 217-225, 1988.

b

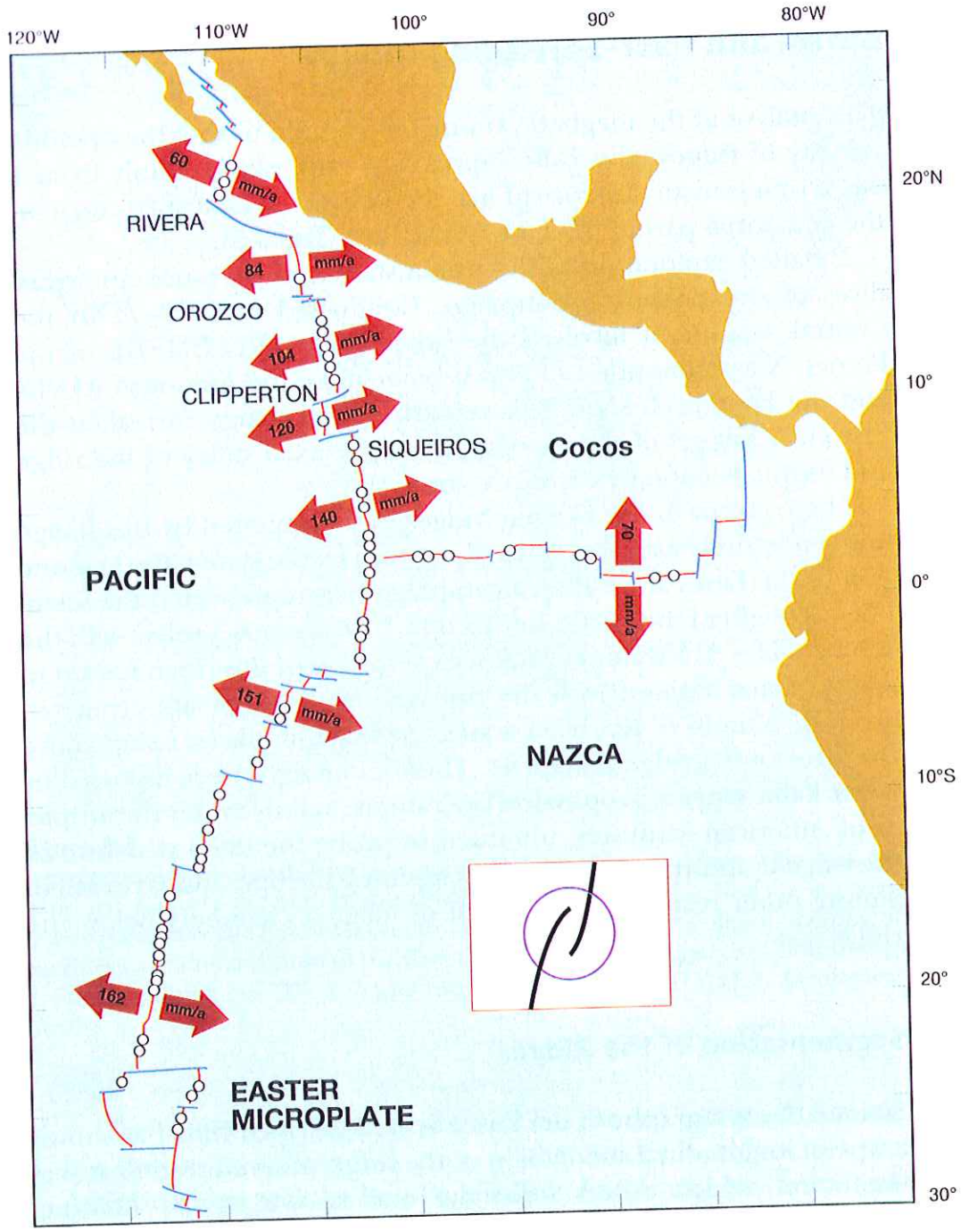

Figure 3.10
The segmentation of the fast-spreading ridges is determined by fracture zones and overlapping spreading centres. (K. C. MacDonald et al. 1986, J. Geophys. Res., 91, 10501–10511)

$$R_{SF} = \frac{-2(W_{SFM})}{W_{SF}} \exp\left(\frac{|\omega| T_w}{2Q_w}\right) \qquad (1)$$

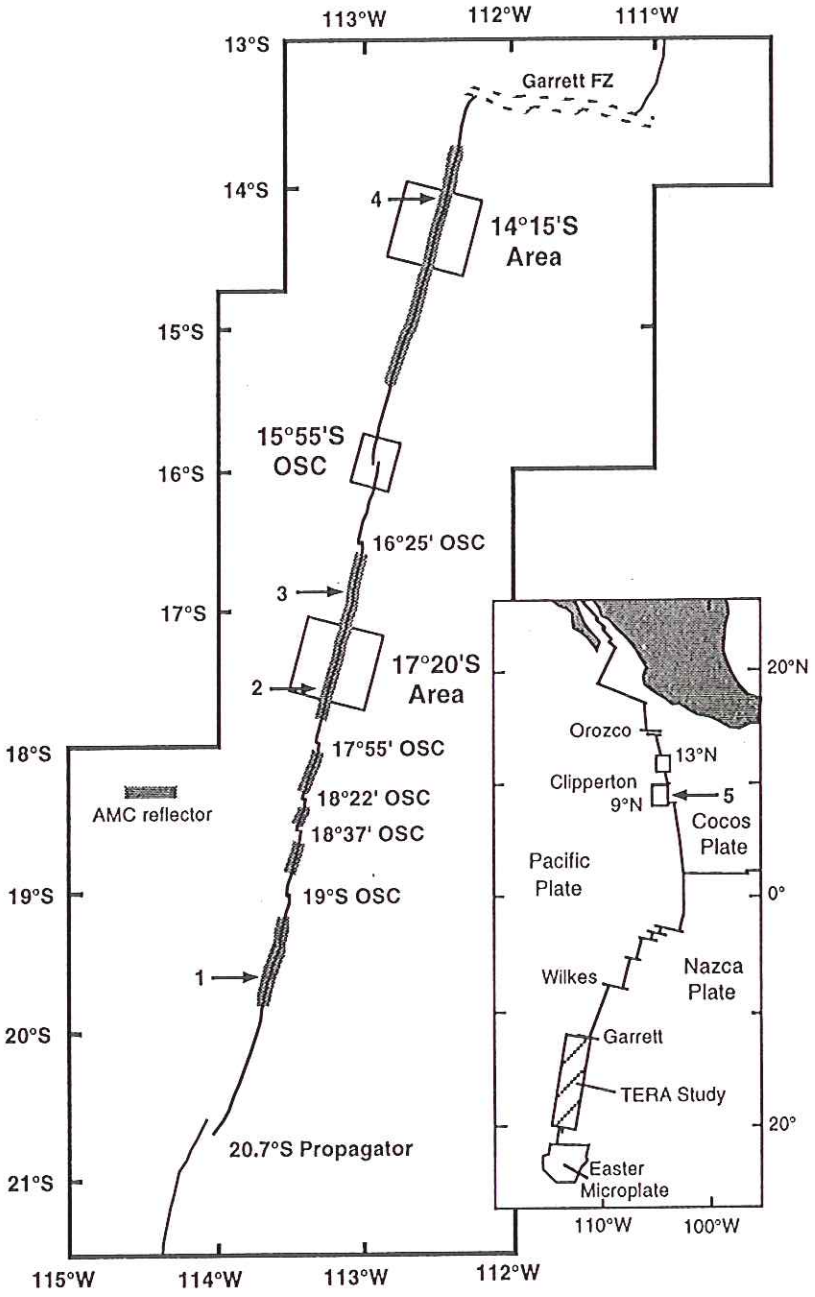

Figure 1. Map of the southern EPR. Major segment bou aries are indicated, and gray bands show those portions ridge which exhibit an AMC reflection in the along-a CDP data. Numbered arrows indicate those points along rise axis from which data were extracted and analyzed in study. Excerpted with permission from *Detrick et al.* [19 Copyright 1993 American Association for the Advancen of Science.

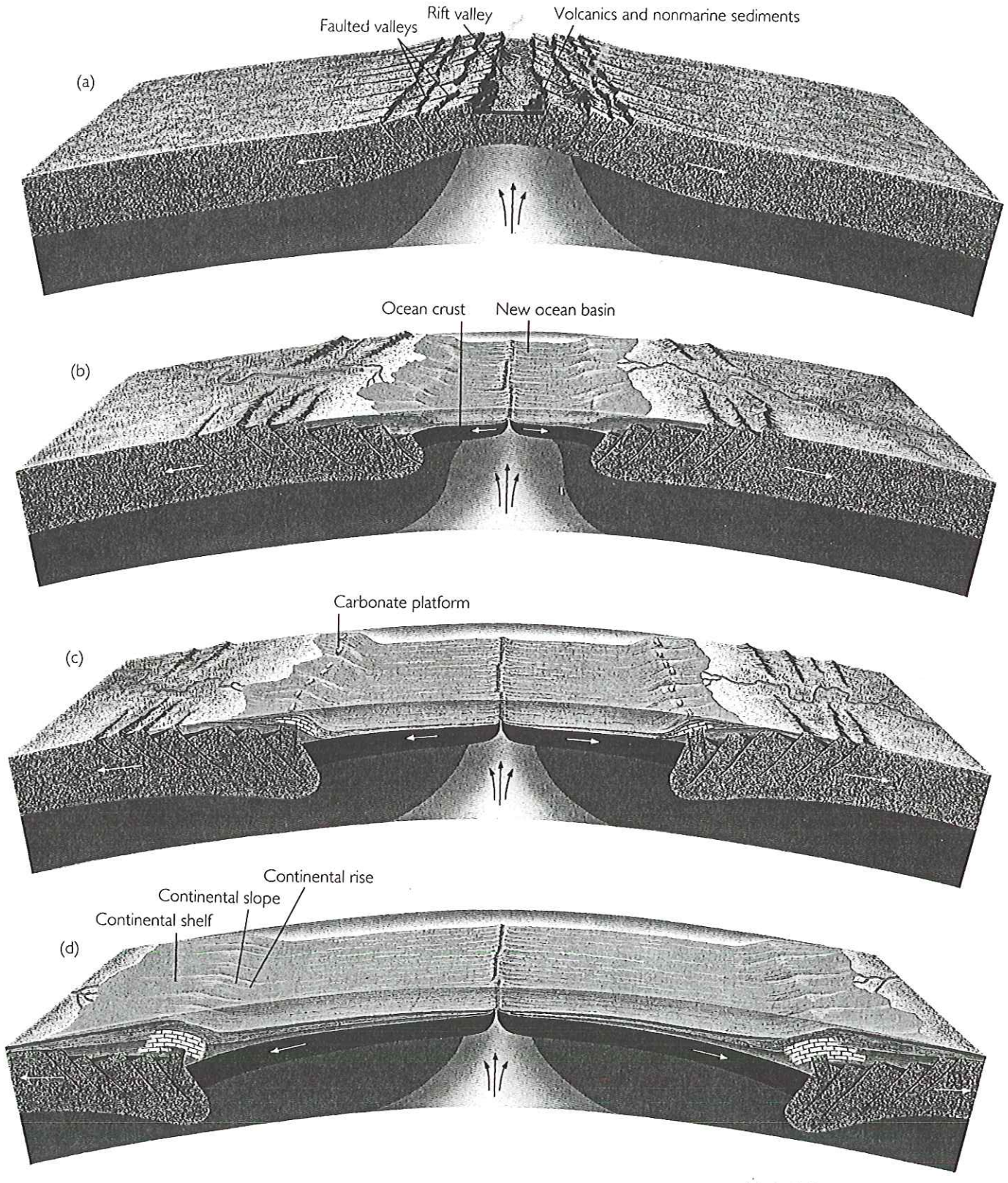

FIGURE 20.17 The development of sedimentary basins on a rifted continental margin. A rift develops in Pangaea as hot mantle materials upwell and the ancient continent stretches and thins. Volcanics and Triassic nonmarine sediments are deposited in the faulted valleys (a). Seafloor spreading begins (b). The lithosphere cools and contracts under the receding continental margins, which subside below sea level. Evaporites, deltaic deposits, and carbonates (c) are deposited and then covered by Jurassic and Cretaceous sediments derived from continental erosion (d). The Atlantic margins of Europe, Africa, and North and South America have histories similar to this.

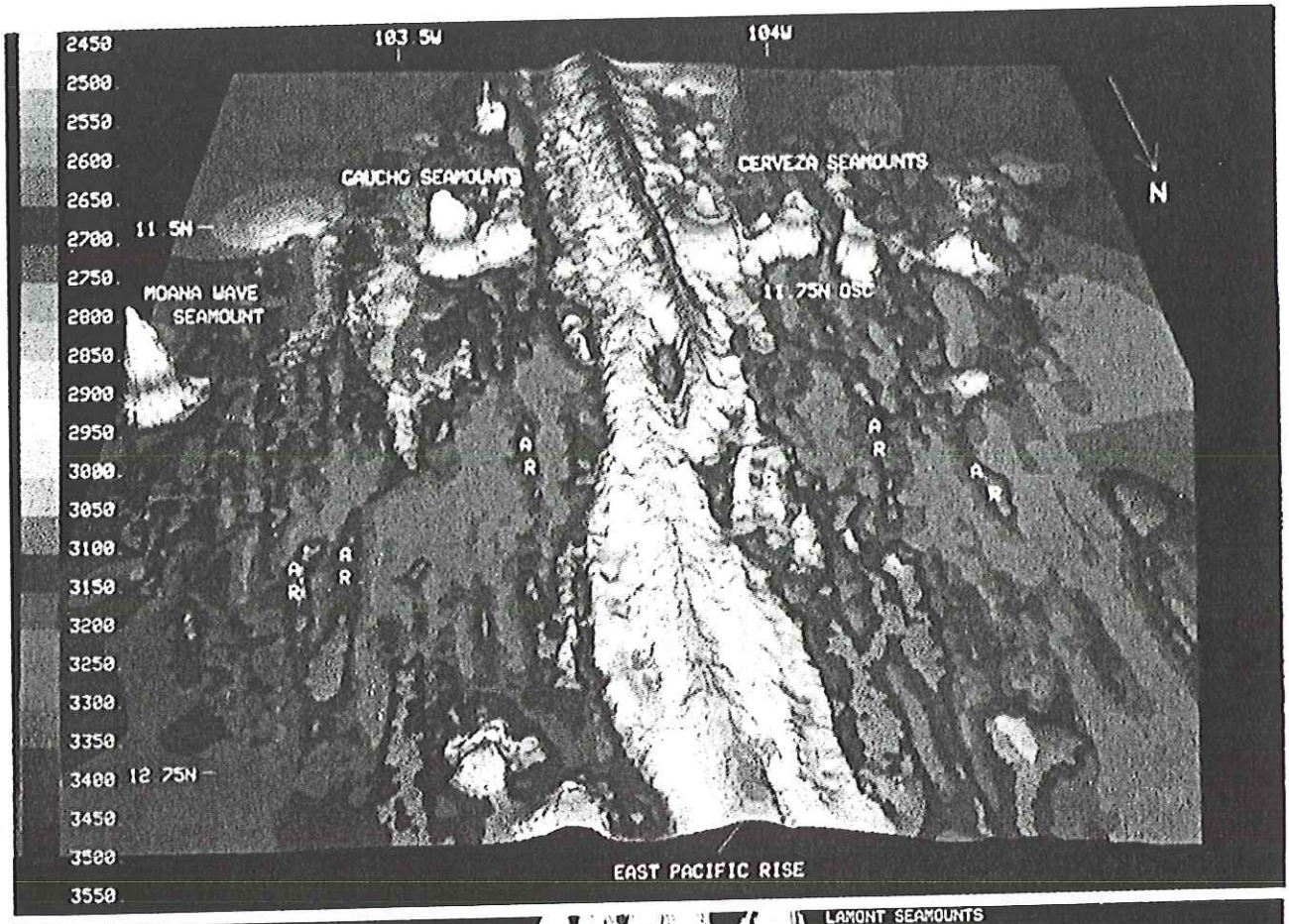
2450
2500
2550
2600
2650
2700
2750
2800
2850
2900
2950
3000
3050
3100
3150
3200
3250
3300
3350
3400
3450
3500
3550
103 5W
104W
11 5N
12 75N
CAUCHO SEAMOUNTS
CERVEZA SEAMOUNTS
MOANA WAVE SEAMOUNT
11 75N OSC
N
A
R
EAST PACIFIC RISE

a

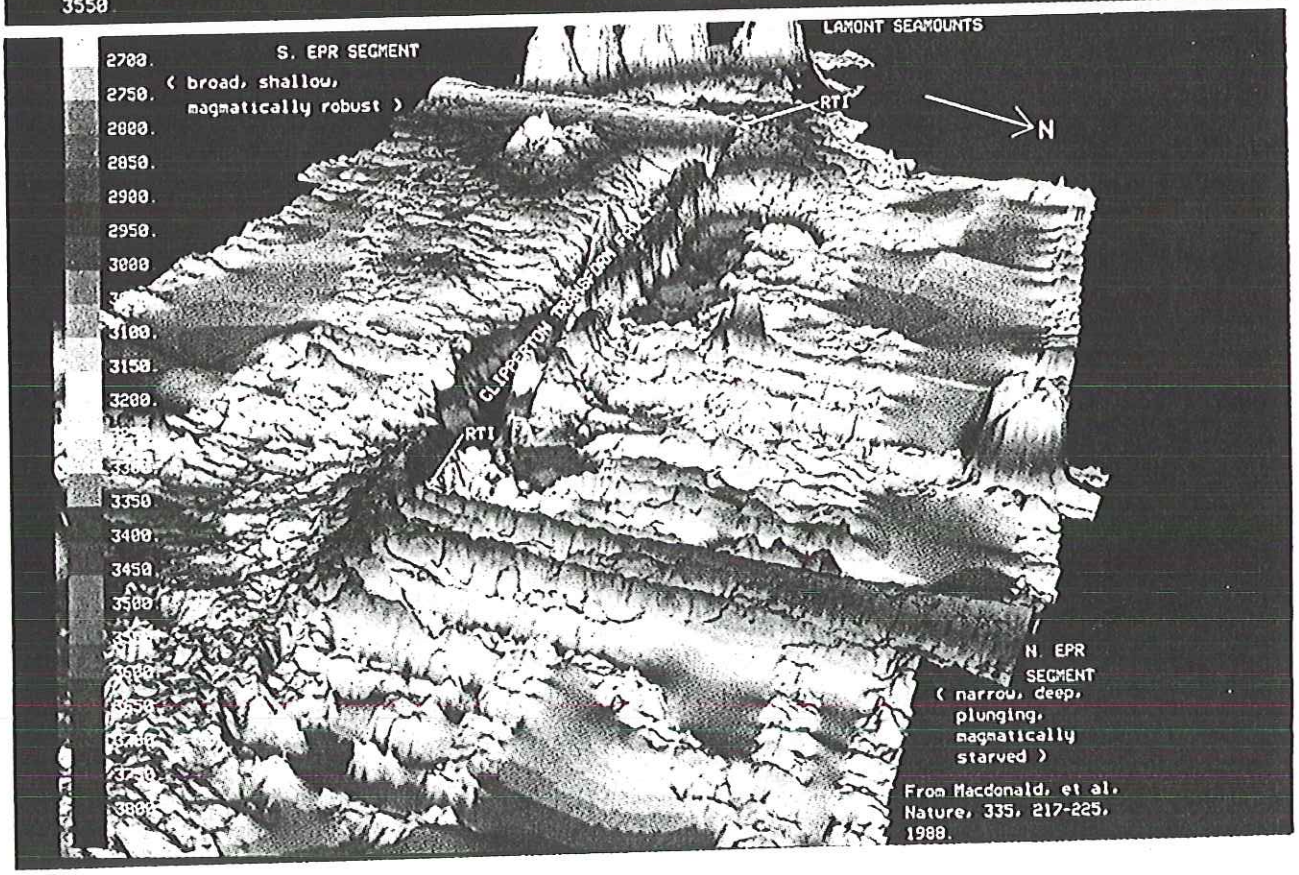
S. EPR SEGMENT
(broad, shallow, magmatically robust)
LAMONT SEAMOUNTS
RTI
N
CLIPPERTON TRANSFORM FAULT
RTI
N. EPR SEGMENT
(narrow, deep, plunging, magmatically starved)
From Macdonald, et al. Nature, 335, 217-225, 1988.

b

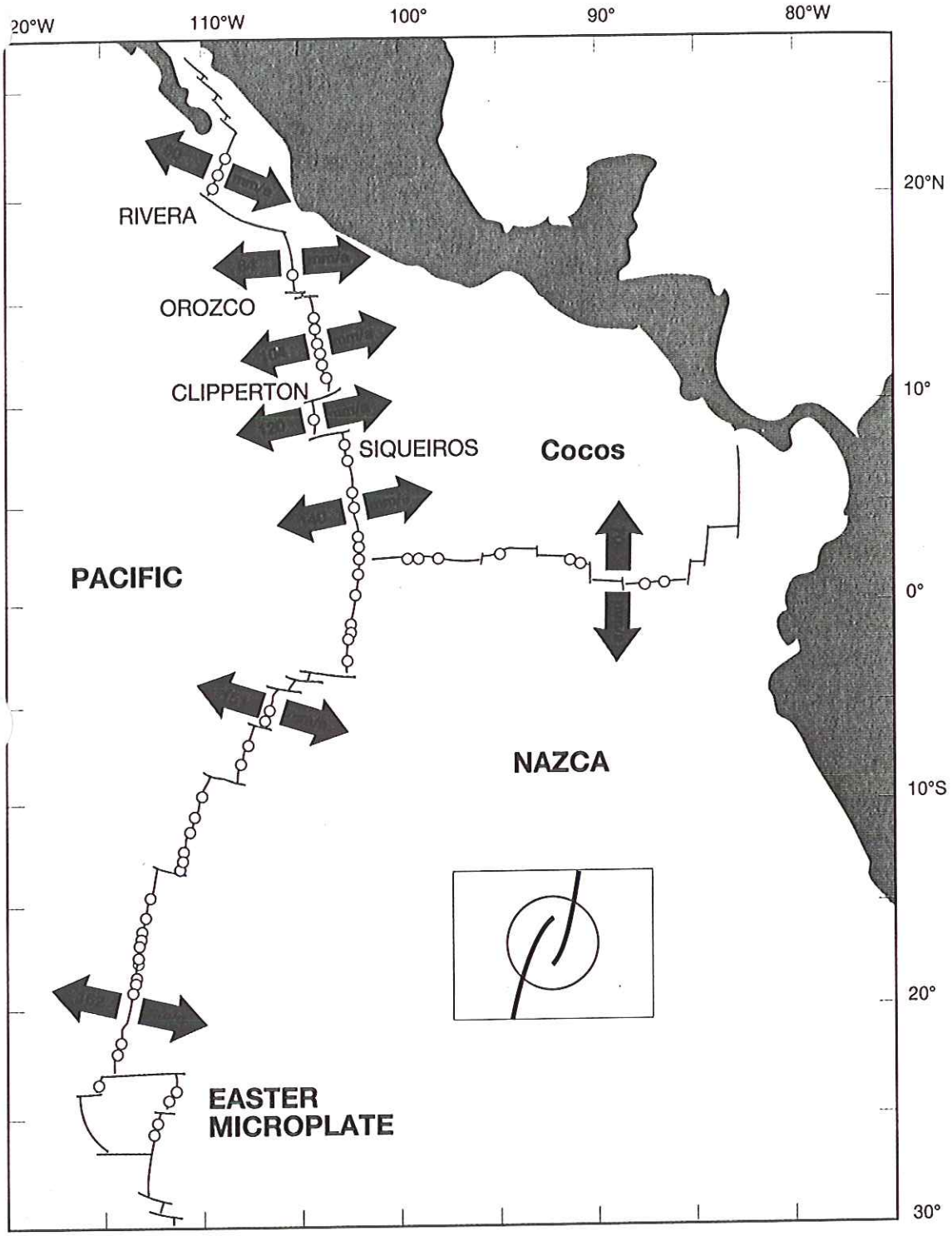

Figure 3.10
The segmentation of the fast-spreading ridges is determined by fracture zones and overlapping spreading centres. (K. C. MacDonald et al. 1986, J. Geophys. Res., 91, 10501–10511)

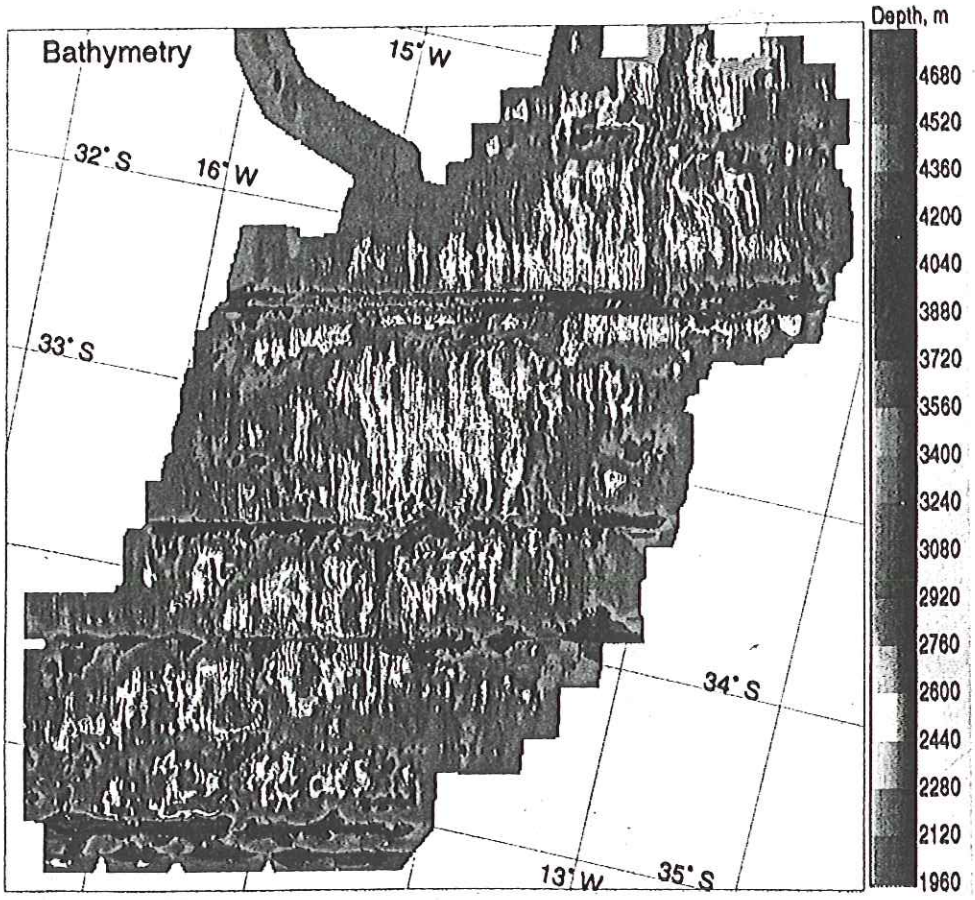
Bathymetry
15° W
32° S
16° W
33° S
34° S
13° W
35° S
Depth, m
4680
4520
4360
4200
4040
3880
3720
3560
3400
3240
3080
2920
2760
2600
2440
2280
2120
1960

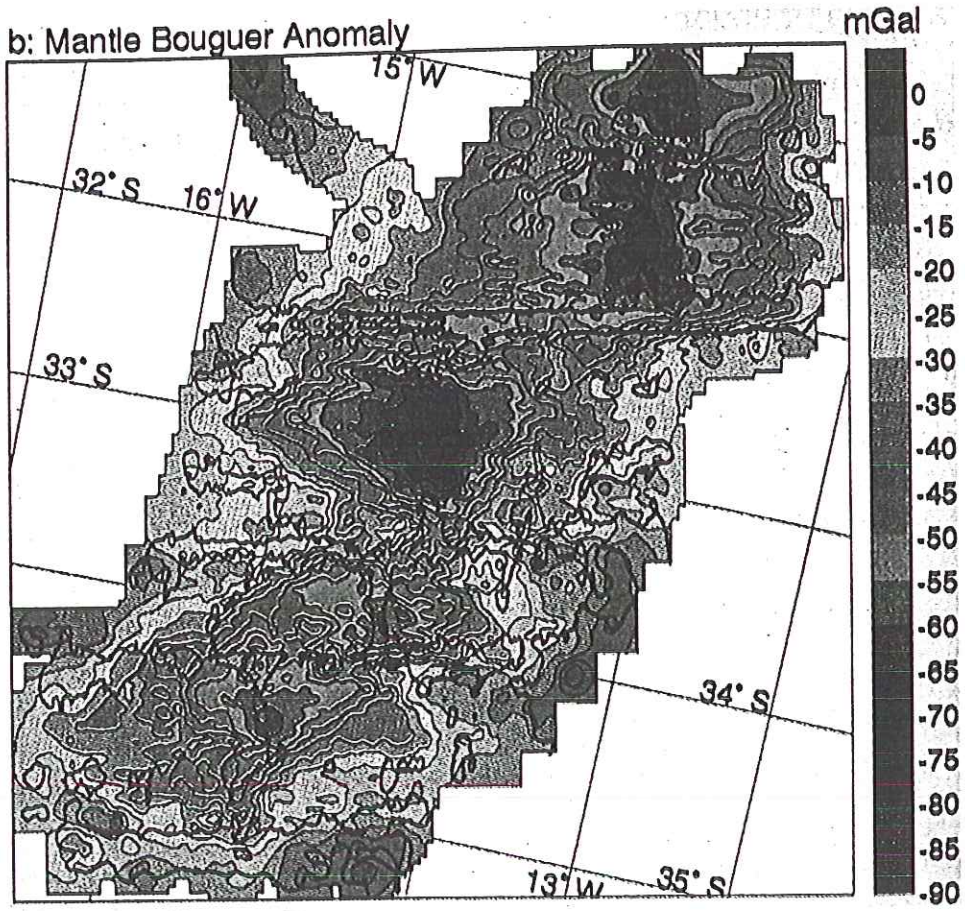
b: Mantle Bouguer Anomaly
mGal
15° W
32° S
16° W
33° S
34° S
13° W
35° S
0
-5
-10
-15
-20
-25
-30
-35
-40
-45
-50
-55
-60
-65
-70
-75
-80
-85
-90

Week 6 — Lecture #2 — last lecture before exam — plate tectonics

1960's time of installation of WWSSN — global seismic network for monitoring nuclear explosions underground

Kennedy — Kruschev LTBT 1963 drove testing underground

First reliable map of global seismicity — outlined the major plates

Plate tectonics synthesized these various threads — developed by D. McKenzie (Cambridge) and Jason Morgan (Princeton)

Earth's surface divided into about a dozen quasi-rigid plates.

Three types of plate boundaries

(1) mid-ocean ridges where seafloor is created

(2) subduction zones where it is destroyed

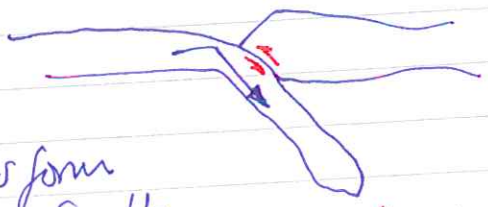

(3) transform faults

frequently offsetting MOR but not always

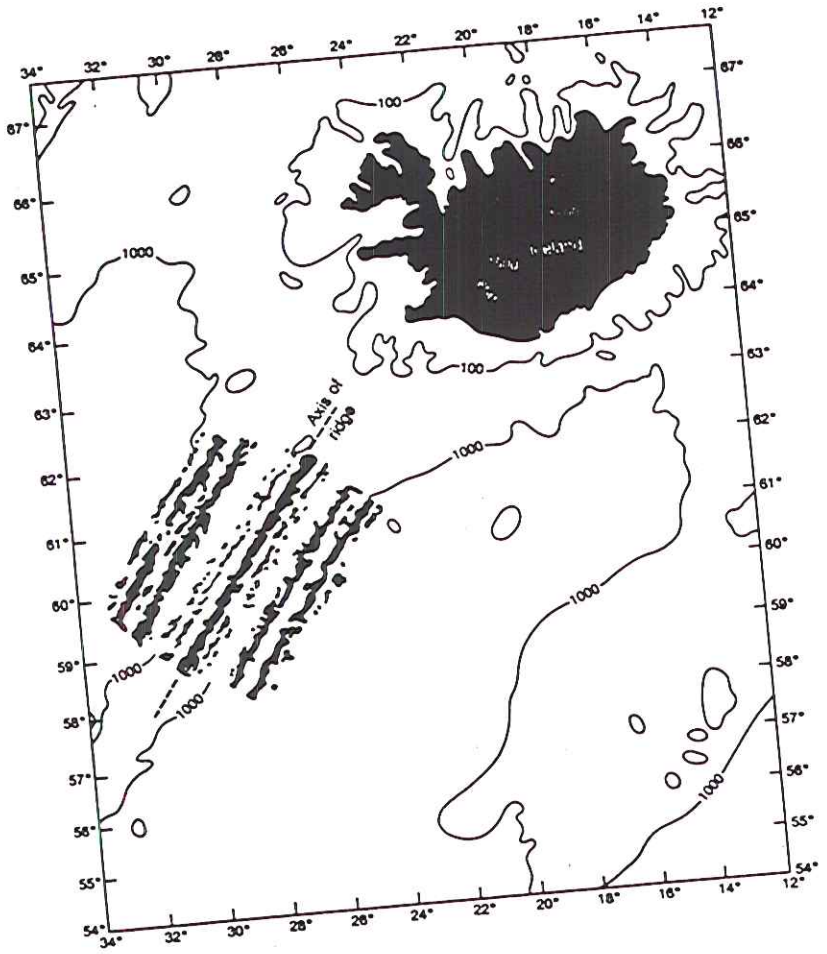

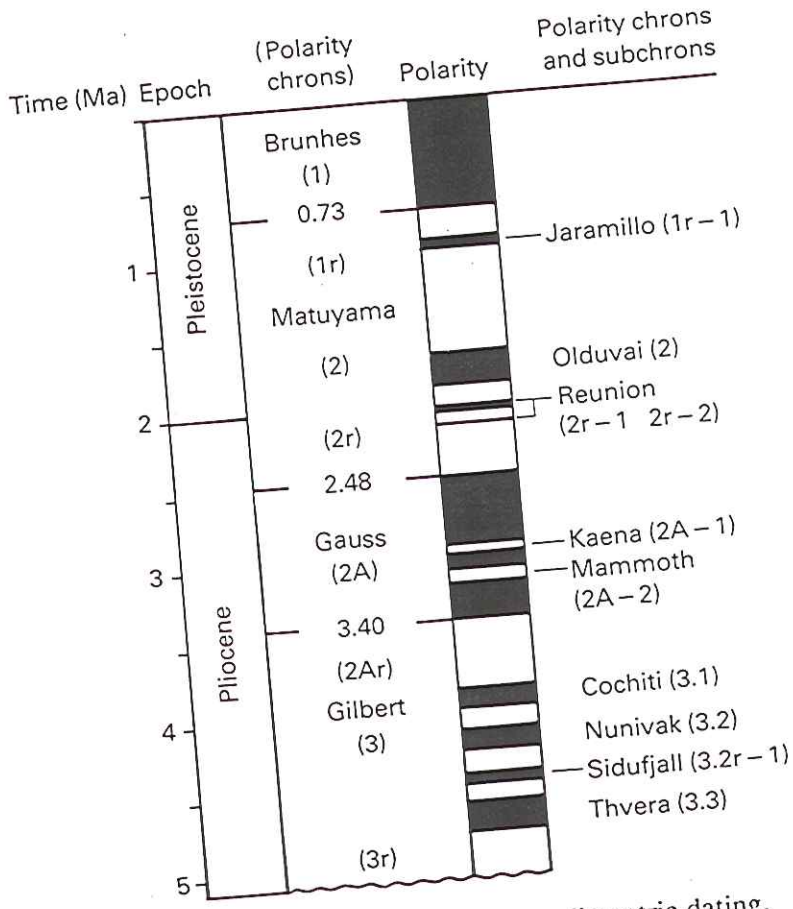

Fig. 4.9 Polarity time scale based on radiometric dating. Alternative numerical designations based on the numbered sequence of marine anomalies are shown in brackets (redrawn from Harland *et al.*, 1982, *A Geological Time Scale*, with permission from Cambridge University Press).

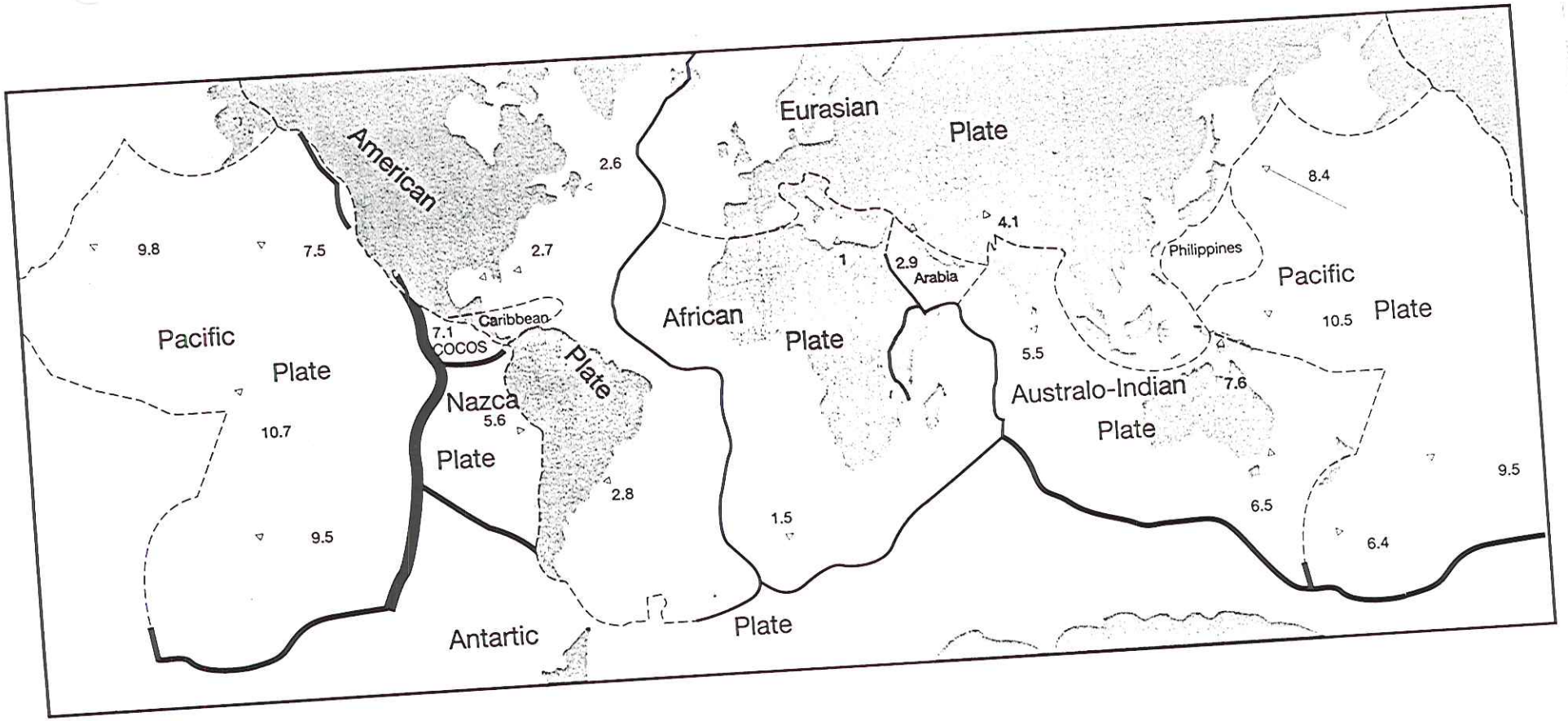
American
Plate
2.6
2.7
9.8
7.5
Pacific
Plate
10.7
9.5
7.1
COCOS
Caribbean
Plate
Nazca
5.6
Plate
2.8
Antartic
Plate
Eurasian
Plate
4.1
1
2.9
Arabia
African
Plate
1.5
Philippines
8.4
Pacific
Plate
10.5
5.5
Australo-Indian
Plate
7.6
6.5
6.4
9.5

Current plate Motions — do this first, then Pacific Margin evolution and motion of India

Rates of plate motion can be measured along ridges.

Directions can be measured by noting the strikes of transform faults

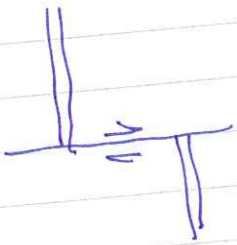

Also by focal mechanisms at subduction zones.

Over 10,000 of these at present time using earthquake

Motions on a sphere : governed by Euler's theorem

Be sure to tak a copy of J. as a prop.

On a flat plane

every rigid motion is a rotation — pole + rate

θ, φ

i.e. 3 variables

rotation

translation ≡ rotation about a pole

(Also true on a sphere : only a rotation is required.

True in 2D, not 3D.

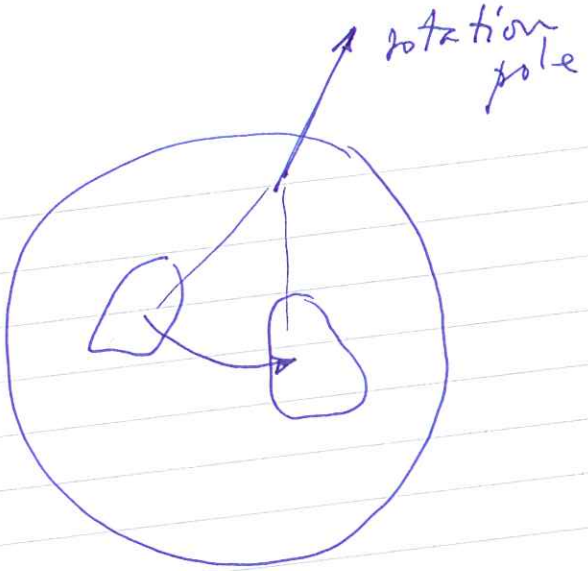

Euler's theorem — every rigid motion of a plate on a sphere can be described by a rotation about a rotation pole

The transform faults between two plates define the rotation pole describing their relative motion

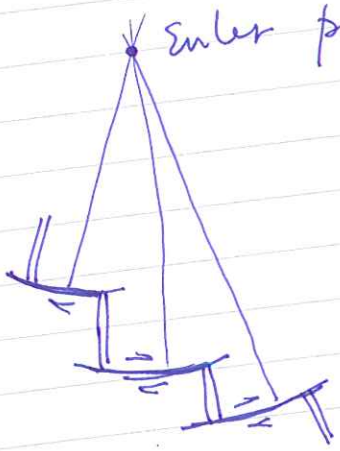

By putting this information together can compile a complete picture of present-day plate motions relat

Discuss present-day (NUVEL-1) fin

then reconstruction of past.

Could also discuss origin of transform faults here

Slight changes in plate motions can cause rearrangements, e.g.

leaky transform fault

This process responsible for rifting of the Gulf of Mexico and the Gulf of Aden, for example.

Fig 12.38 in book

Scenario for evolution of San Andreas Fault:

In the Oligocene (30 m.y. ago) the Pacific Coast of Calif. was a subduction boundary

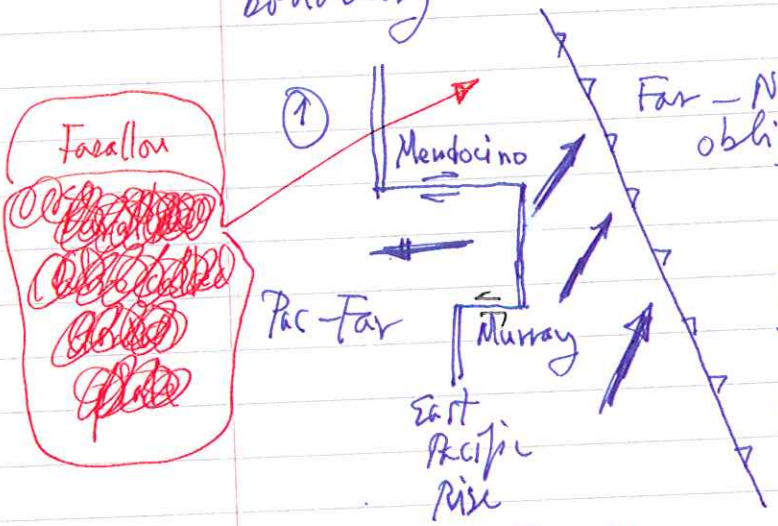

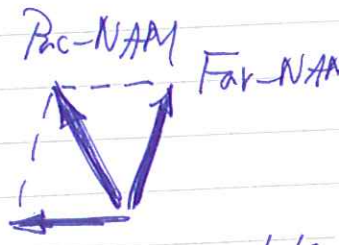

relativ
velocit
triangle
(vector
addition

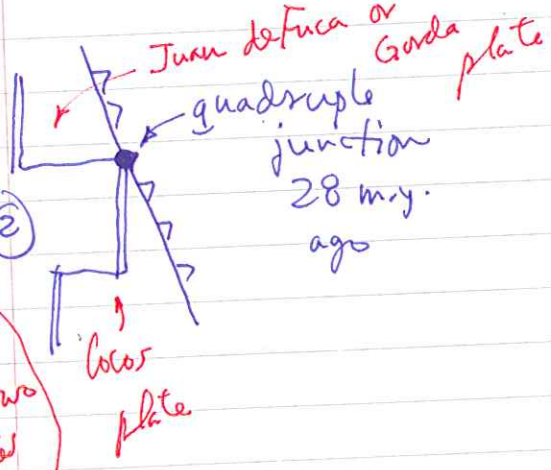

Farallon "splits" into two plates 28 Myr ago

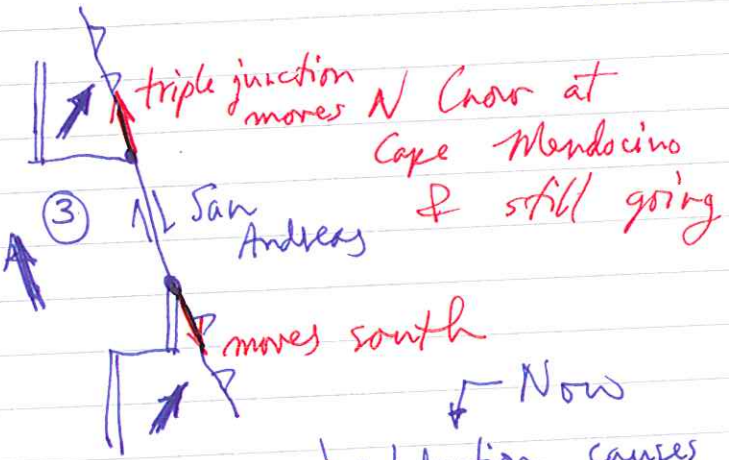

Now

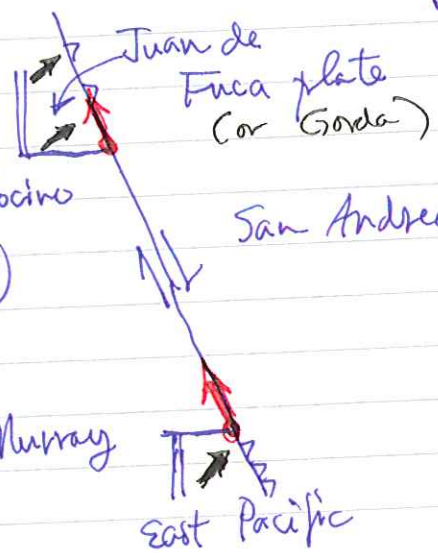

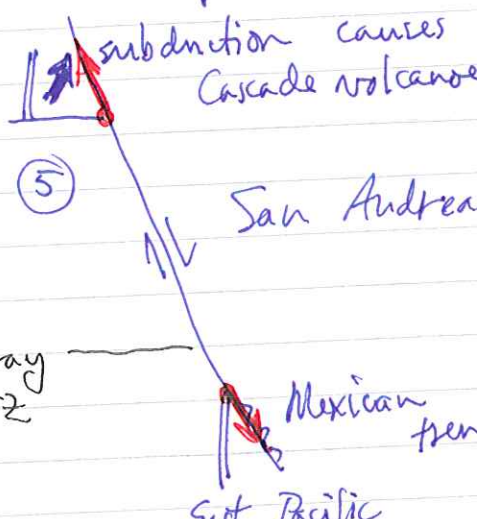

Evolution of the California Margin

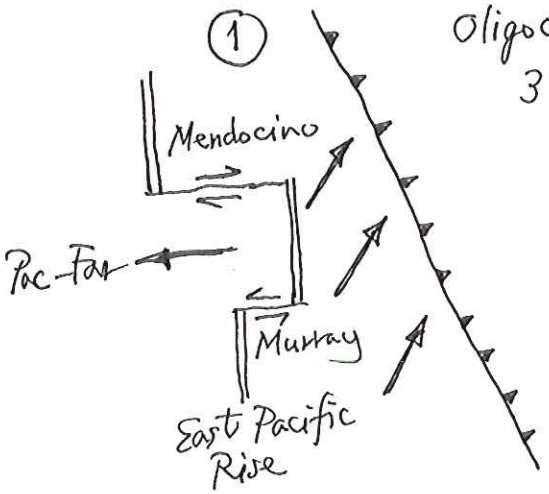

Velocity triangle

Pac: Pacific plate
Far: Farallon plate
Nam: North American plate

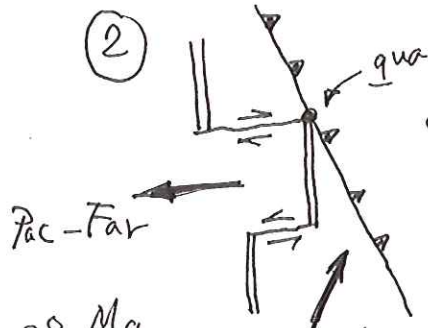

28 Ma
Farallon "splits" into Juan de Fuca (Gorda) and Cocos

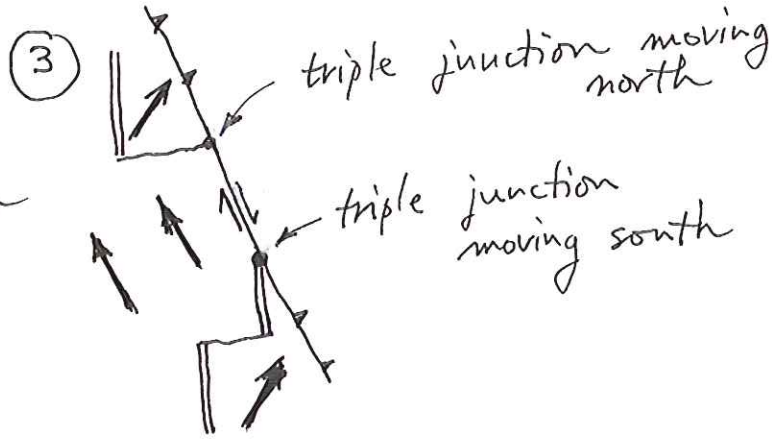

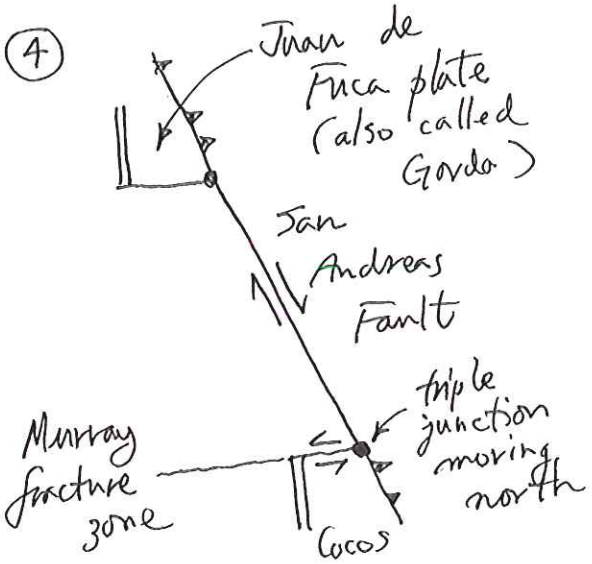

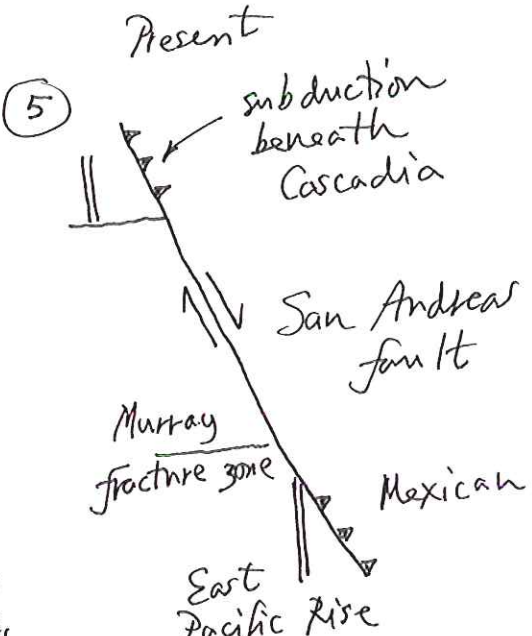

Relative motions and in particular rates of convergence along convergent boundaries can be inferred, e.g. northward motion of India (see "movie") is still continuing at 50 mm/yr.

Most of the Earth's volcanoes are situated in subduction zones

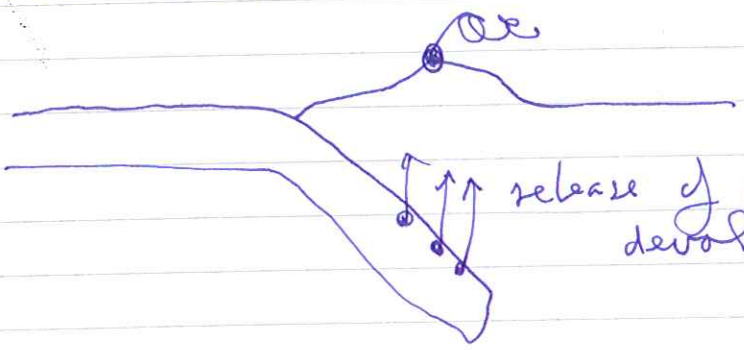

Causes volatile-rich (phreatic) eruptions

Example — Aleutian chain

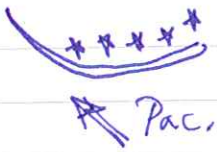

Example — Cascade chain — constrained to region where Juan de Fuca plate is subducting

Mt. Lassen in the south to Mt. Meager in the north

Strike-slip boundaries to the N & S of this

Plates are moving on the ⊕'s surface. Is it possible to determine their absolute motion relative to the deep mantle?

Answer: various aseismic ridges or linear chains of island appear to be tracks or scars left by quasi-stationary hot spots or upwelling plumes or diapirs in the mantle

Most prominent example is the Hawaii-Emperor chain in the Pacific

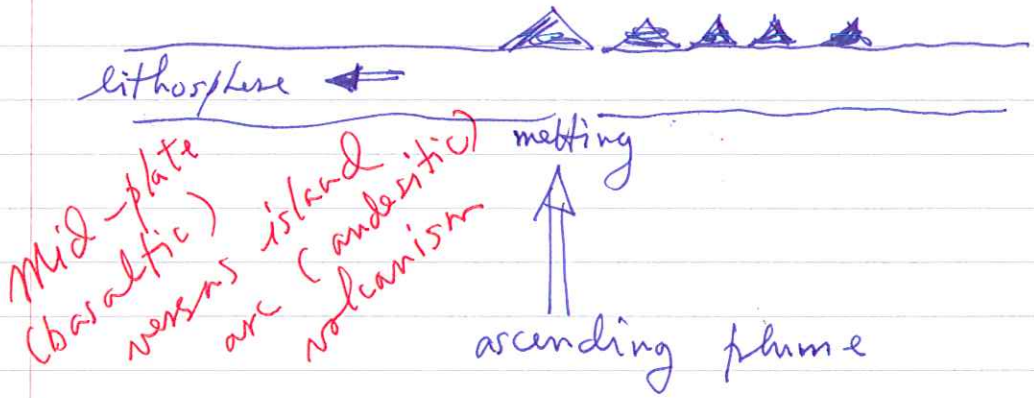

K-Ar dates up the chain show the expected age progression. There are dozens of such plumes or hot spots, e.g. Yellowstone. They appear to drift relative to one another considerably more slowly than plate motions.

Suffices to determine absolute direction and rate

Strong correlation between percent slab boundary and absolute velocity suggests strongly that the negative buoyancy of sinking slabs is the principal driving force of plate tectonics

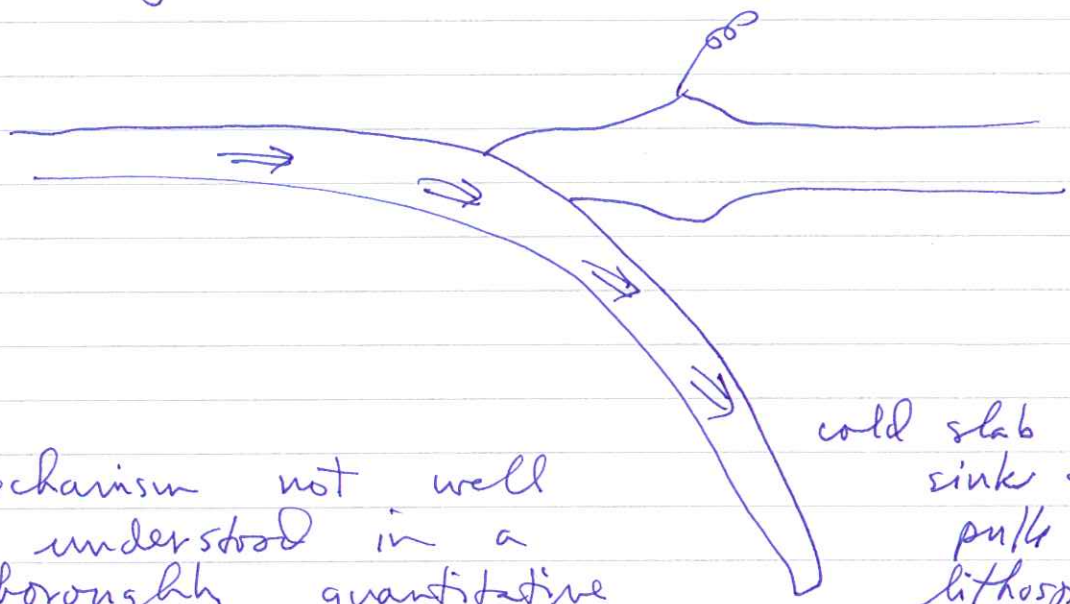

Mechanism not well understood in a thoroughly quantitative sense yet, however.

cold slab sinks & pulls the lithosphere with it

Note: excellent agreement with GPS in stable NAM plate. Residual ~ 1 mm/yr.

Note, however, that the Dixon et al. figure shows the residual w.r.t. the best-fitting rigid rotation to their data, not to NUVEL-1.

Looks, however, like it agrees well with NUVEL-1 no net rotation

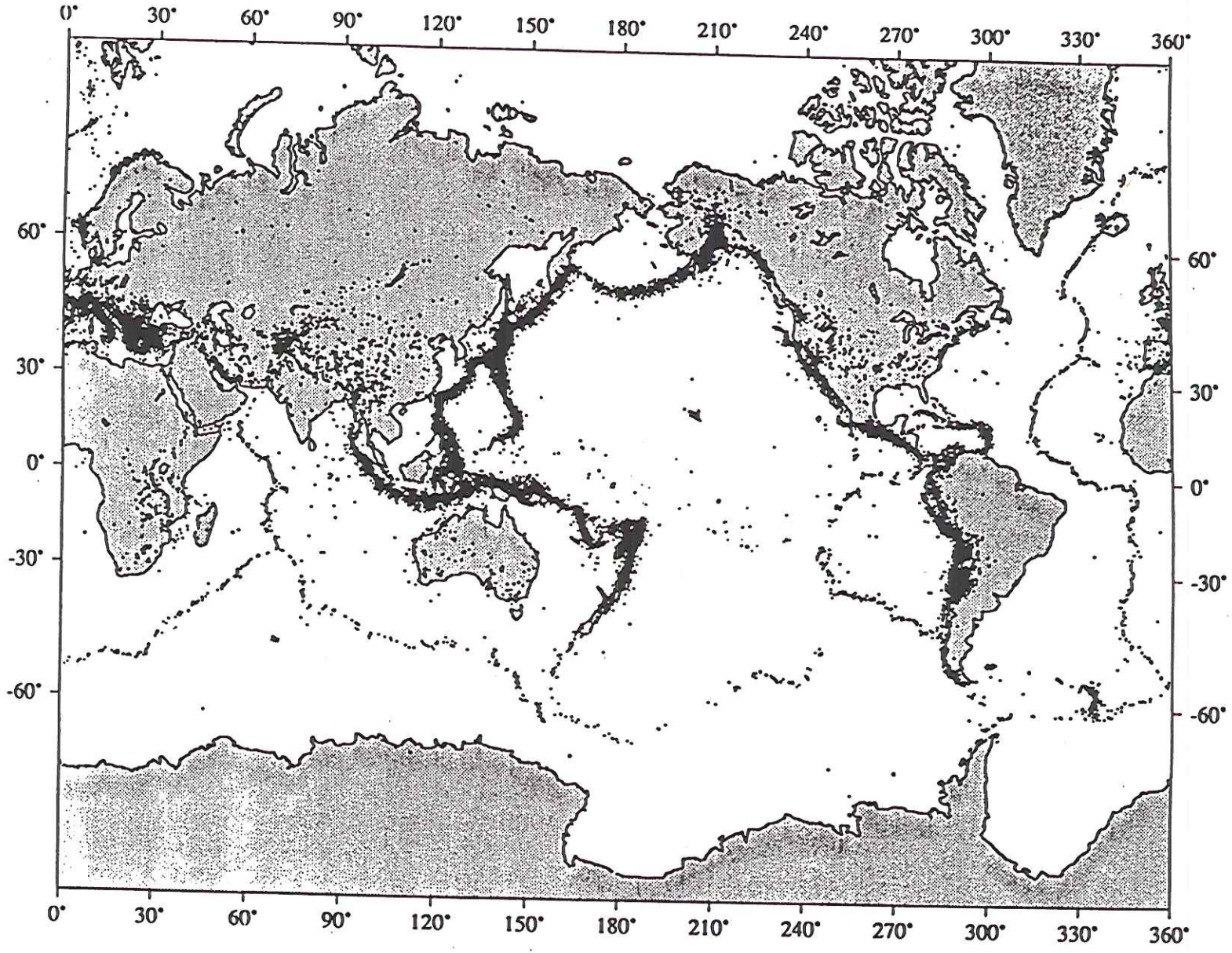
0°
30°
60°
90°
120°
150°
180°
210°
240°
270°
300°
330°
360°
60°
30°
0°
-30°
-60°

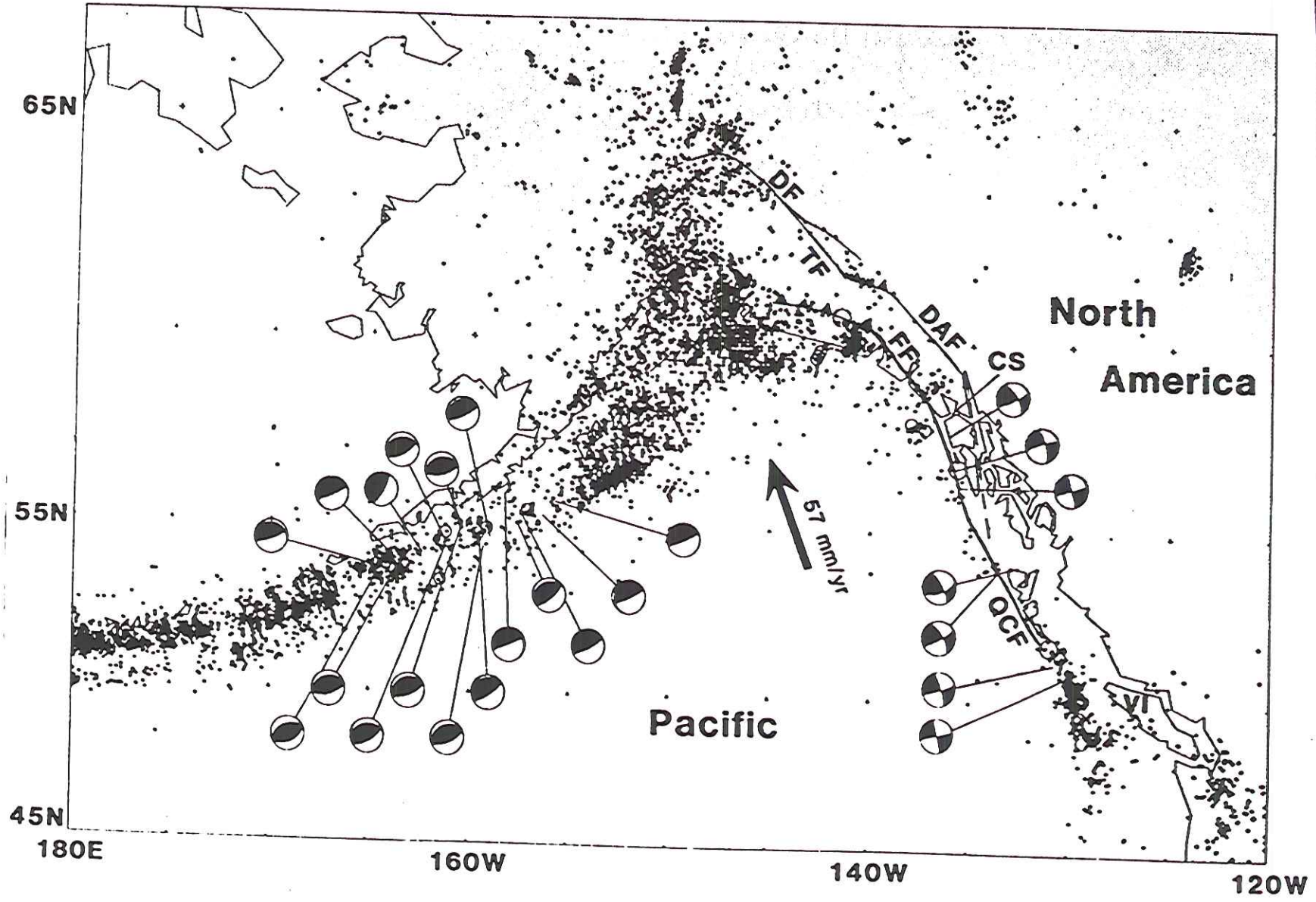
65N
55N
45N
180E
160W
140W
120W
DF
TF
DAF
FF
CS
QCF
VI
North
America
Pacific
57 mm/yr

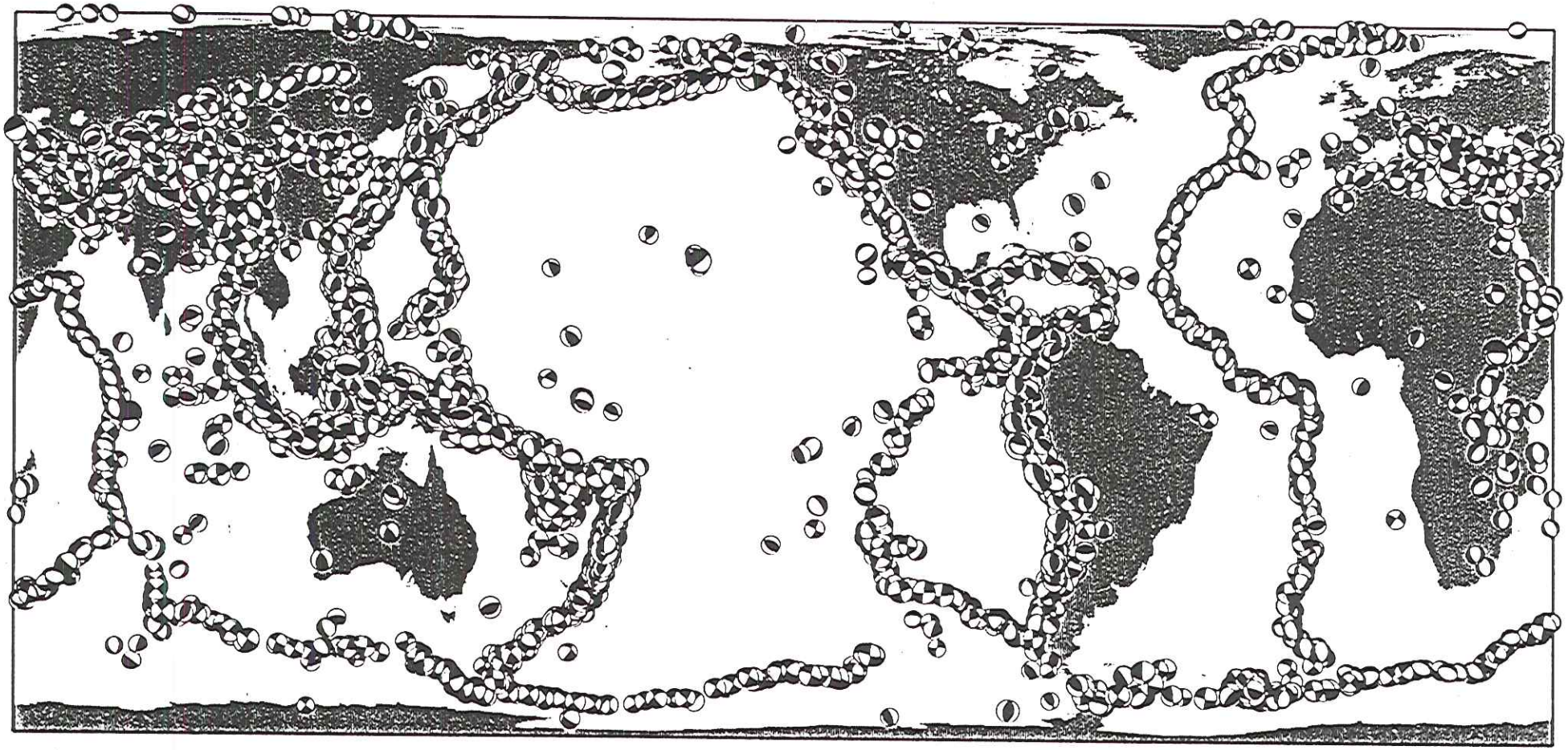

Figure 5.8. Epicentral locations and source mechanisms of 10,219 earthquakes in the Harvard CMT catalogue, with focal depths less than 50 km, during the period 1976–1997. The size of each beachball is proportional to the logarithm of the seismic moment M_0. The world map is a cylindrical equal-area projection, with landmasses shaded. (Courtesy of E. Larson.)

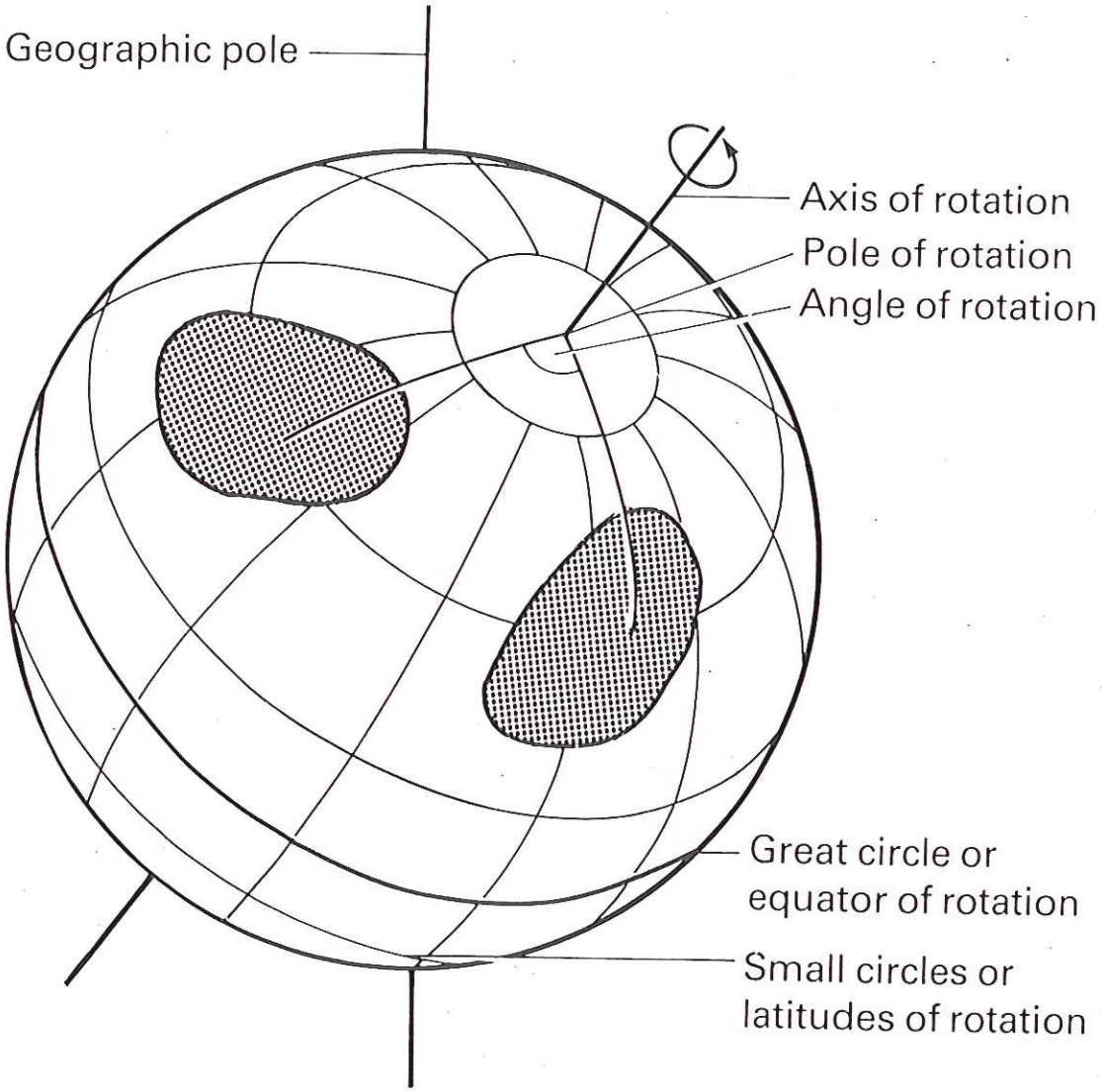

Fig. 3.1 Euler's theorem. Diagram illustrating how the motion of a continent on the Earth can be described by an angle of rotation about a pole of rotation.

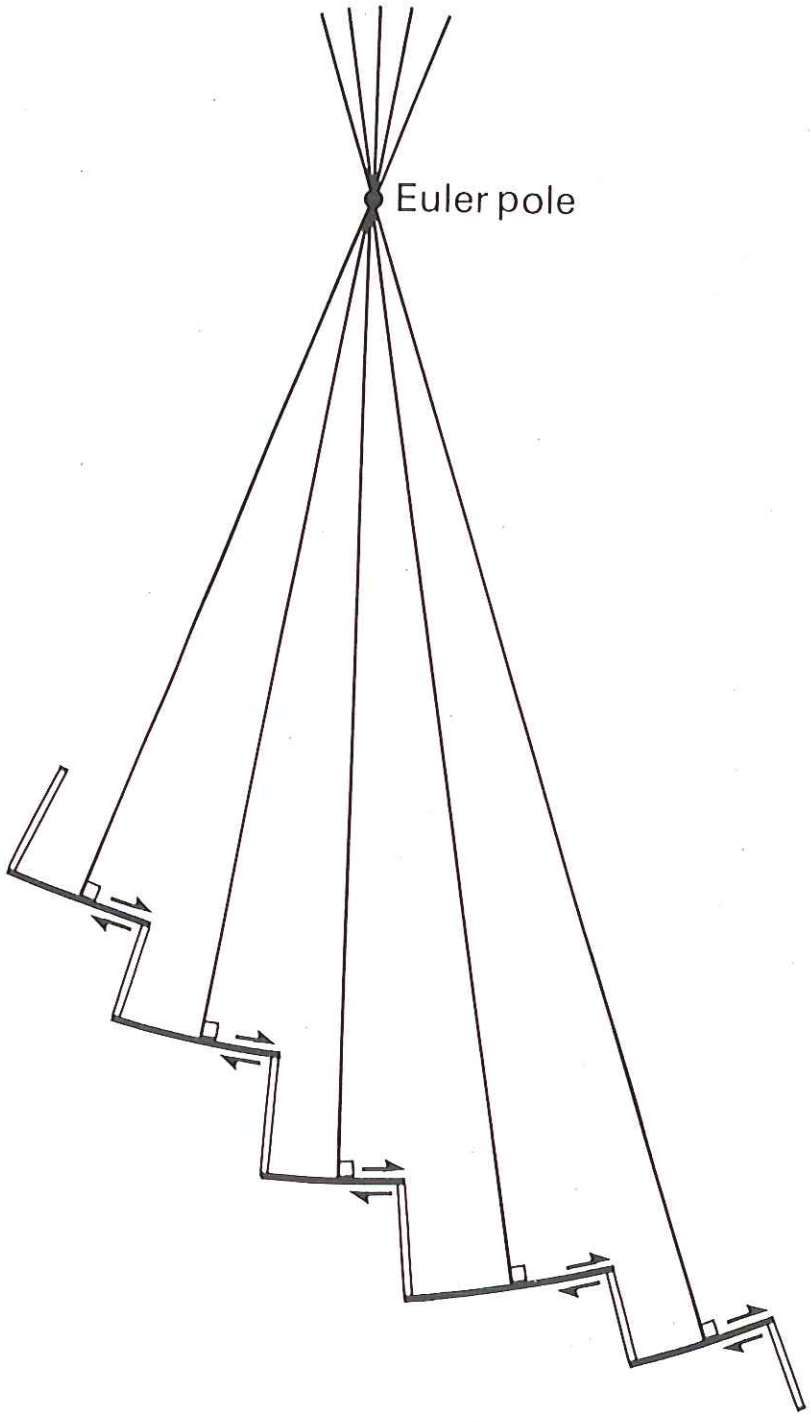

Fig. 5.3 Determination of the Euler pole for a spreading ridge from its offsetting transform faults which describe small circles with respect to the pole.

Table 1. NUVEL-1 Euler vectors (Pacific plate fixed).

Plate	Latitude °N	Longitude °E	ω (deg–m.y.$^{-1}$)	ω_x	ω_y (radians–m.y.$^{-1}$)	ω_z
Africa	59.160	–73.174	0.9695	0.002511	–0.008303	0.014529
Antarctica	64.315	–83.984	0.9093	0.000721	–0.006841	0.014302
Arabia	59.658	–33.193	1.1616	0.008570	–0.005607	0.017496
Australia	60.080	1.742	1.1236	0.009777	0.000297	0.016997
Caribbean	54.195	–80.802	0.8534	0.001393	–0.008602	0.012080
Cocos	36.823	–108.629	2.0890	–0.009323	–0.027657	0.021853
Eurasia	61.066	–85.819	0.8985	0.000553	–0.007567	0.013724
India	60.494	–30.403	1.1539	0.008555	–0.005020	0.017528
Nazca	55.578	–90.096	1.4222	–0.000023	–0.014032	0.020476
North America	48.709	–78.167	0.7829	0.001849	–0.008826	0.010267
South America	54.999	–85.752	0.6657	0.000494	–0.006646	0.009517
Additional Euler Vectors (Pacific Plate Fixed)						
Juan de Fuca	35.0	26.0	0.53	0.00681	0.00332	0.00531
Philippine	0.	–47.	1.0	0.0119	0.0128	0.000

Each named plate moves counterclockwise relative to the Pacific plate. The Juan de Fuca-Pacific 3.0 Ma Euler vector is taken from Wilson (1988) and the Philippine-Pacific Euler vector is taken from Seno *et al.* (1987).

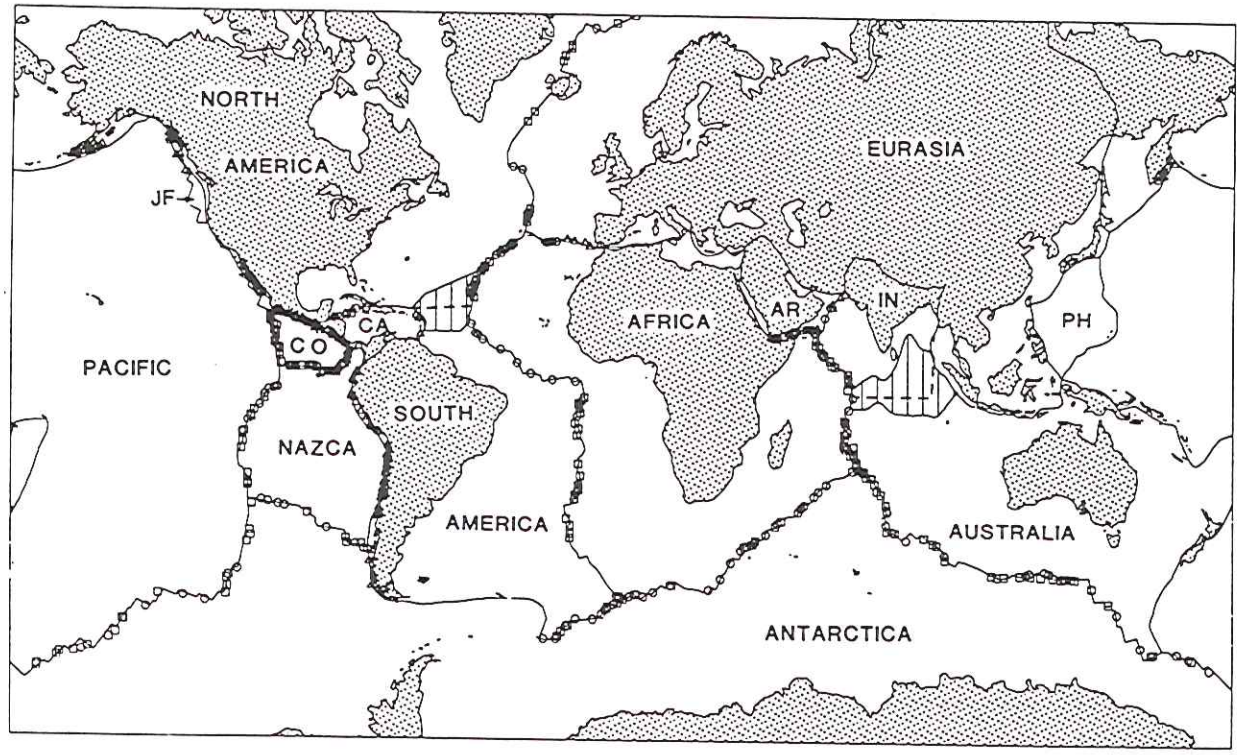

Figure 4. Data locations and plate geometry assumed for NUVEL-1. Regions with vertical lines mark diffuse plate boundaries between North and South America and between India and Australia. Within each of these diffuse boundaries a dashed line shows the discrete boundary assumed in NUVEL-1. Squares show locations of spreading rates, circles show locations of transform azimuths, and triangles show earthquake locations for slip vectors (except those along transform faults offsetting mid-ocean ridges, which are omitted for clarity). Also shown are two plates (Philippine and Juan de Fuca) omitted from NUVEL-1, but included in Table 1 for completeness. Plate name abbreviations: Cocos (CO), Caribbean (CA), Indian (IN), Arabian (AR), Philippine (PH), and Juan de Fuca (JF). Mercator projection.

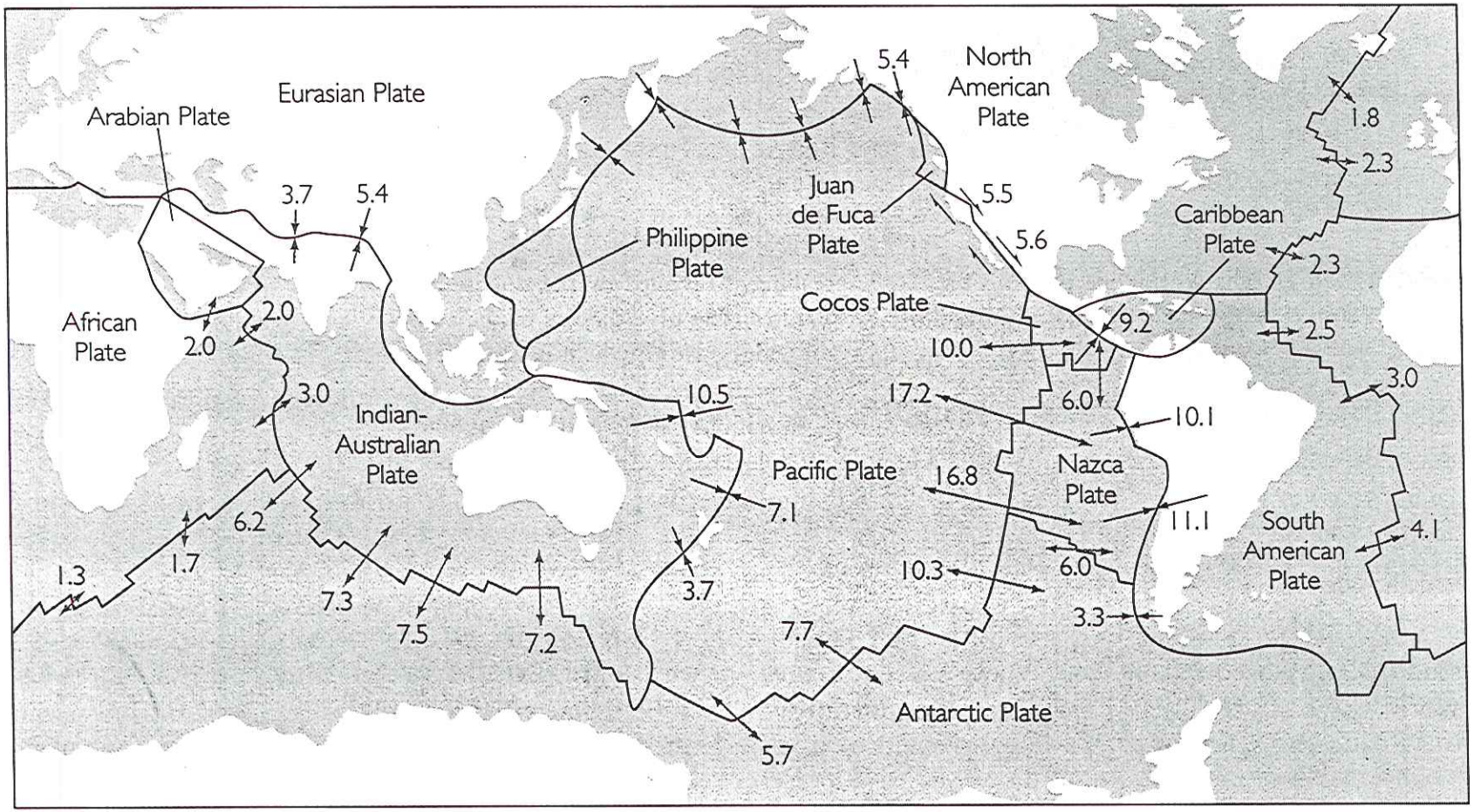

FIGURE 20.12 Relative velocities (in centimeters per year) and directions of plate separation and convergence. Opposed arrowheads indicate convergence. Diverging arrowheads indicate plate separation at ocean ridges. Parallel arrowheads, as along the San Andreas fault in California, indicate transform faults, where plates slide past each other. Spreading is fastest between the Pacific and Nazca plates and slowest between the North American and Eurasian plates. (Data from C. Demets, R. G. Gordon, D. F. Argus, and S. Stein, Model Nuvel-1, 1990.)

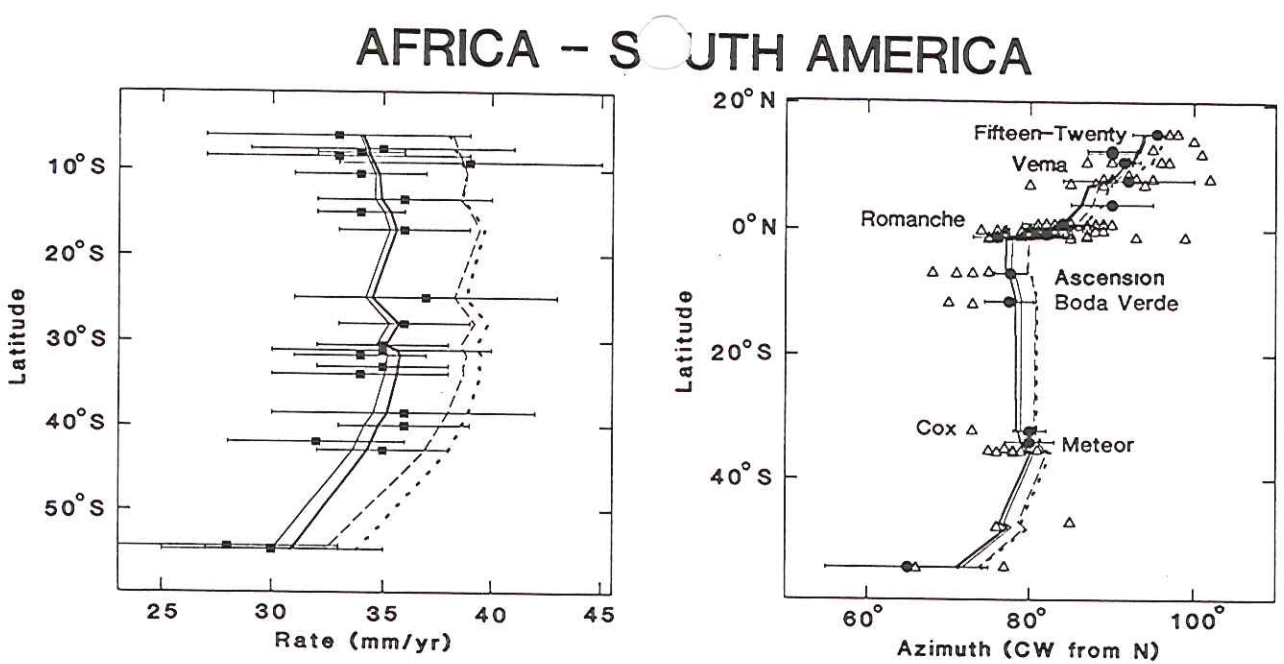

Figure 13. Spreading rates (squares), transform fault azimuths (circles), and slip vector azimuths (triangles) observed along the southern Mid-Atlantic Ridge are compared with directions and rates from the NUVEL-1 (bold solid), best-fitting (thin solid), RM2 (long dashed), and P071 (short dashed) Africa–South America Euler vectors. Horizontal error bars show assigned 1-σ errors.

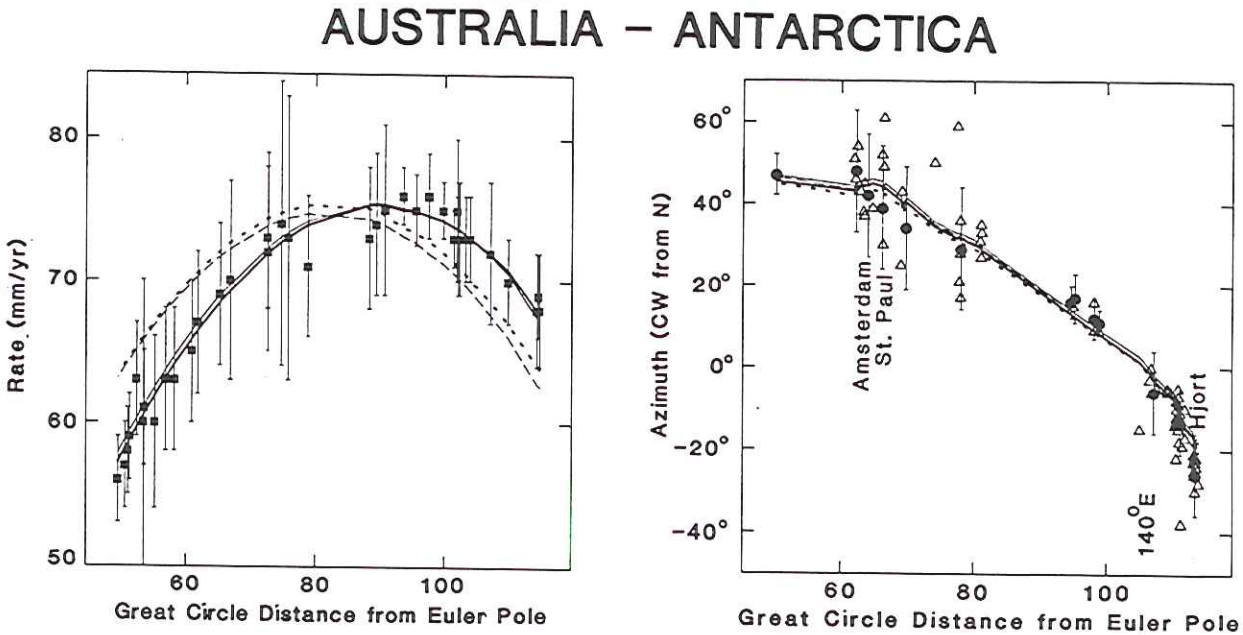

Figure 15. Spreading rates (squares), transform fault azimuths (circles), and slip vector azimuths (triangles) observed along the Southeast Indian Ridge are compared with directions and rates from the NUVEL-1 (bold solid) and best-fitting (thin solid) Australia–Antarctica Euler vectors, and the RM2 (long dashed) and P071 (short dashed) India–Antarctica Euler vectors. The horizontal axis shows the angular distance from the best-fitting Euler vector (Table 4). Vertical error bars show assigned 1-σ errors.

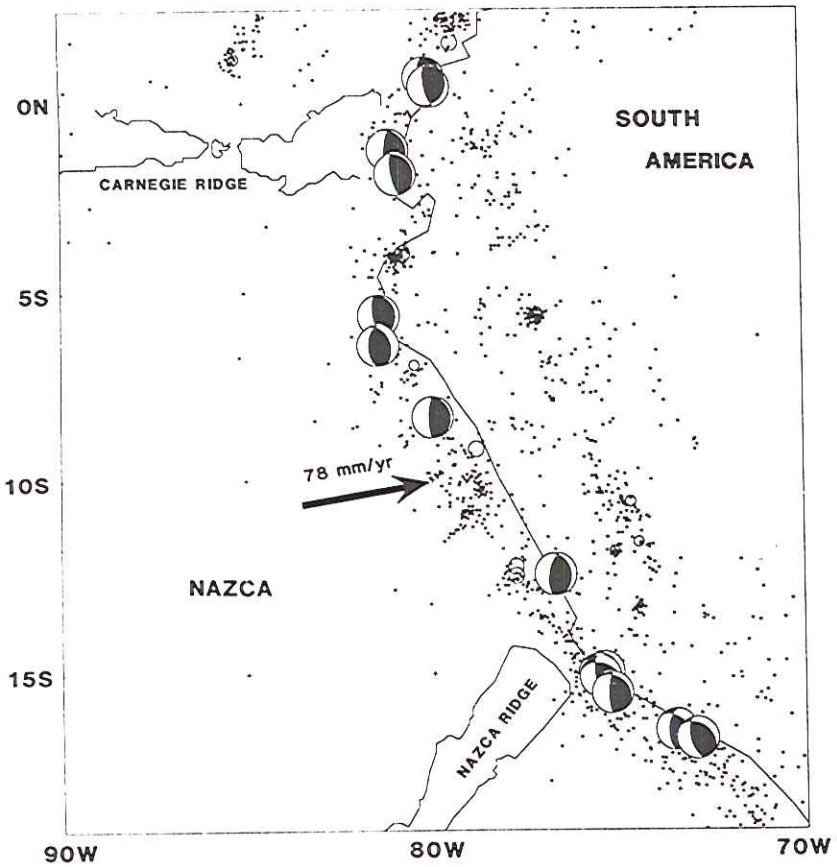

Figure 34. Harvard centroid-moment tensor focal mechanisms along the Ecuador and Peru–Chile trenches from 2.5 °N to 19 °S. Black dots show epicentres of earthquakes from 1963 to 1985 with depths shallower than 60 km. South of 15 °S, the strikes of the fault planes are counter-clockwise of those farther north, mirroring the counter-clockwise change in the strike of the trench. However, the auxiliary planes of the earthquakes south of 15 °S strike N–S giving E–W slip vectors similar to those from the equator to 15 °S and from 20 °S to 45 °S.

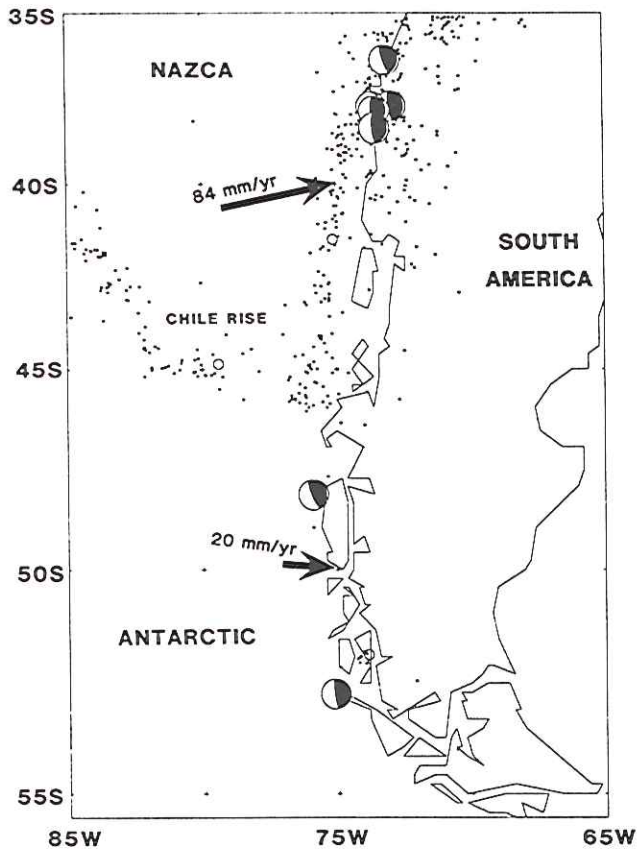

Figure 36. Harvard centroid-moment tensor focal mechanisms along the Peru–Chile trench from 35 °S to 56 °S. Black dots show epicentres of earthquakes from 1963 to 1985 with depths shallower than 60 km.

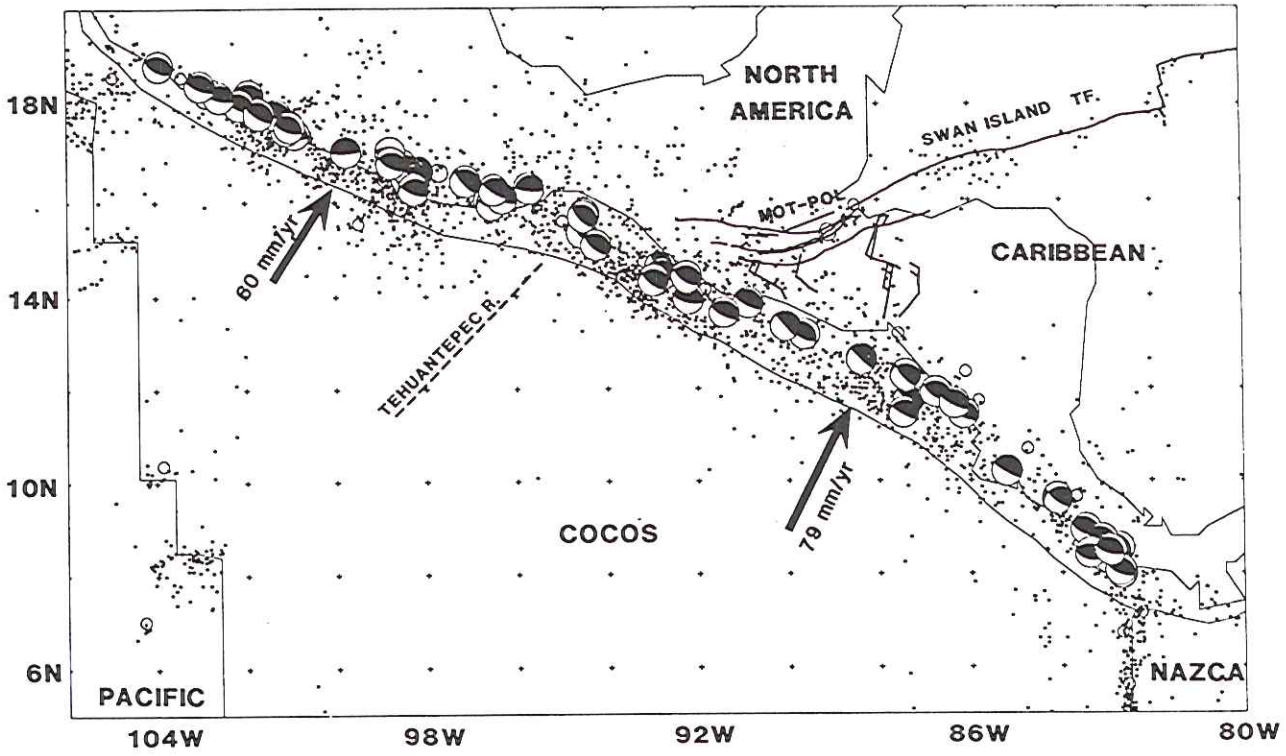

Figure 32. Focal mechanisms along the Middle America trench from the Harvard centroid-moment tensor solutions. The focal mechanisms give even slip vector coverage along the trench. Open circles and black dots show epicentres of earthquakes from 1963 to 1985 with depths shallower than 60 km. The black dots mark events with magnitudes less than 5.5, the small open circles mark events with magnitudes between 5.5 and 7.0, and the larger open circles mark events with magnitudes greater than 7.0. 'MOT-POL' labels the Motagua–Polochic fault system.

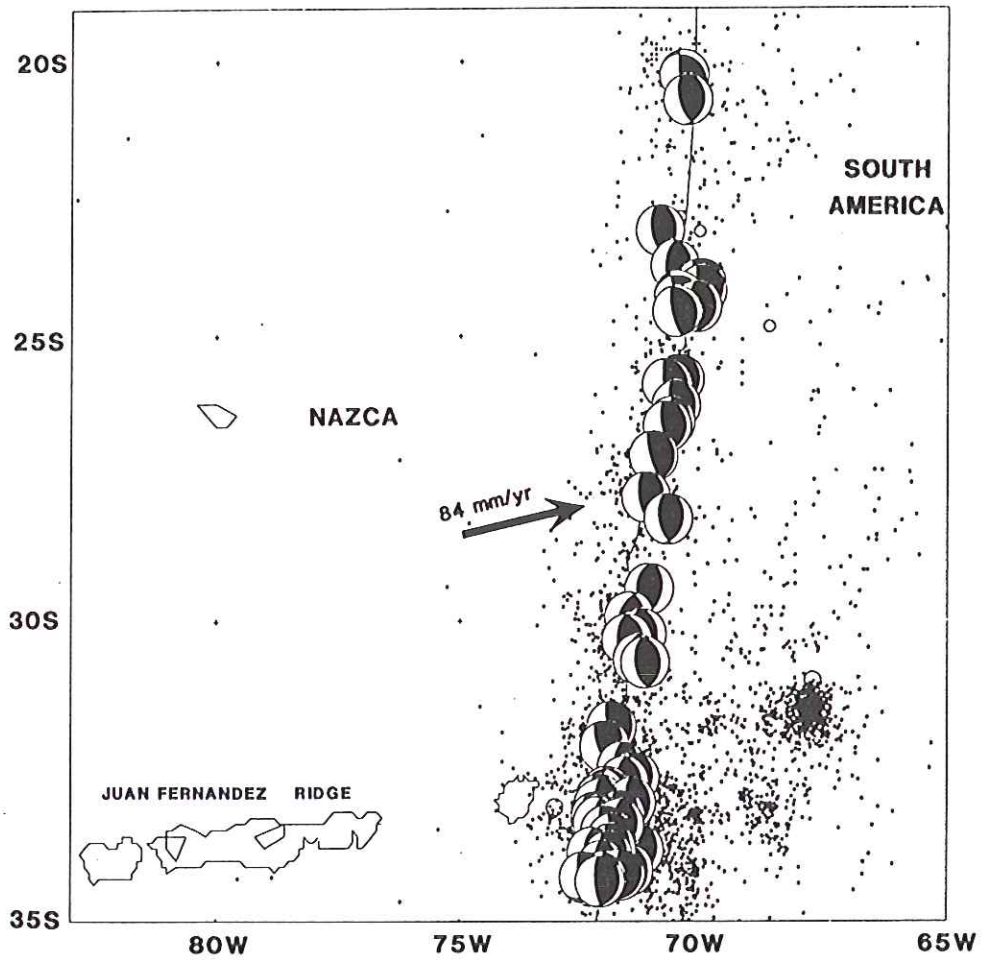

Figure 35. Harvard centroid-moment tensor focal mechanisms along the Peru–Chile trench from 19° to 35 °S. Black dots show epicentres of earthquakes from 1963 to 1985 with depths shallower than 60 km.

This is how we know that there was a spreading ridge offshore of Calif.

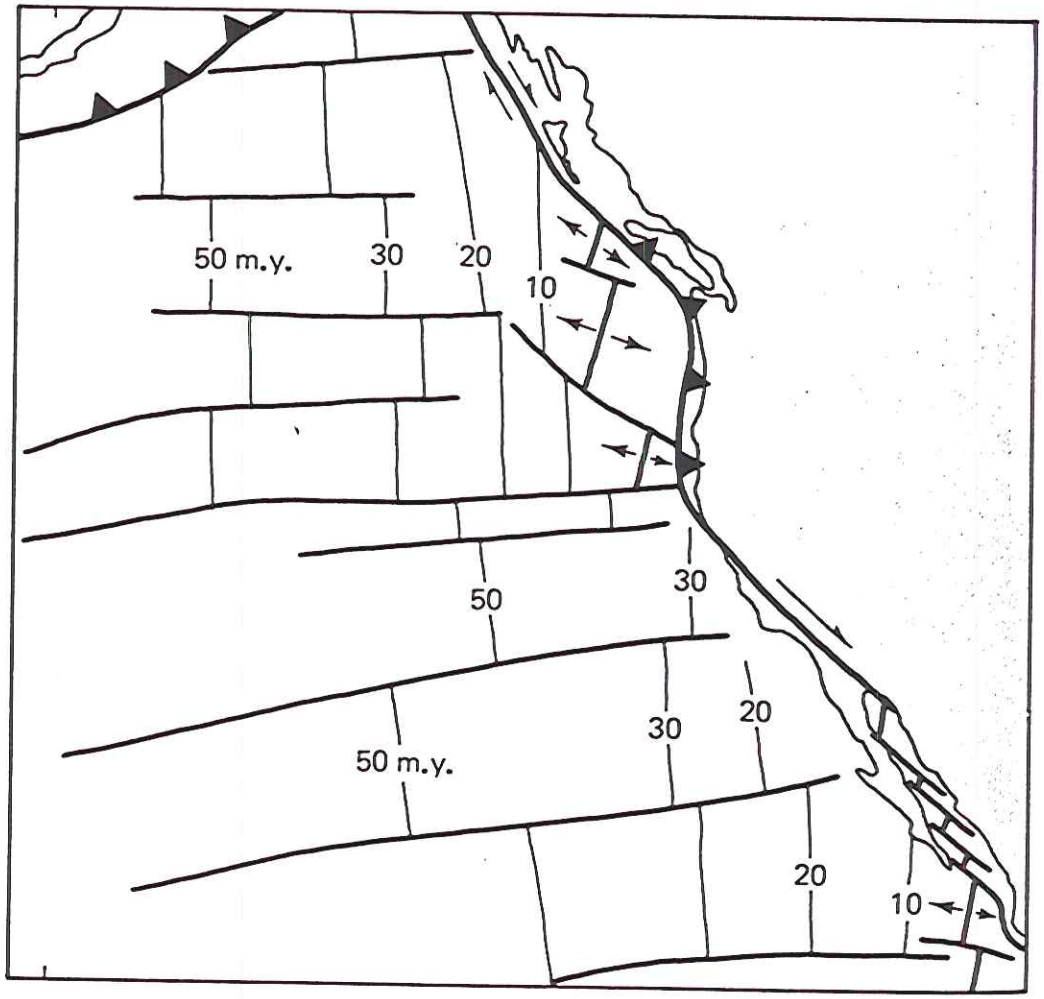

RE 13–35 Map of magnetic anom-
offshore of western North America.
that the anomalies generally be-
older toward the west, implying a
amount of subduction along the
eran margin of North America.
ified after Atwater, 1970.)

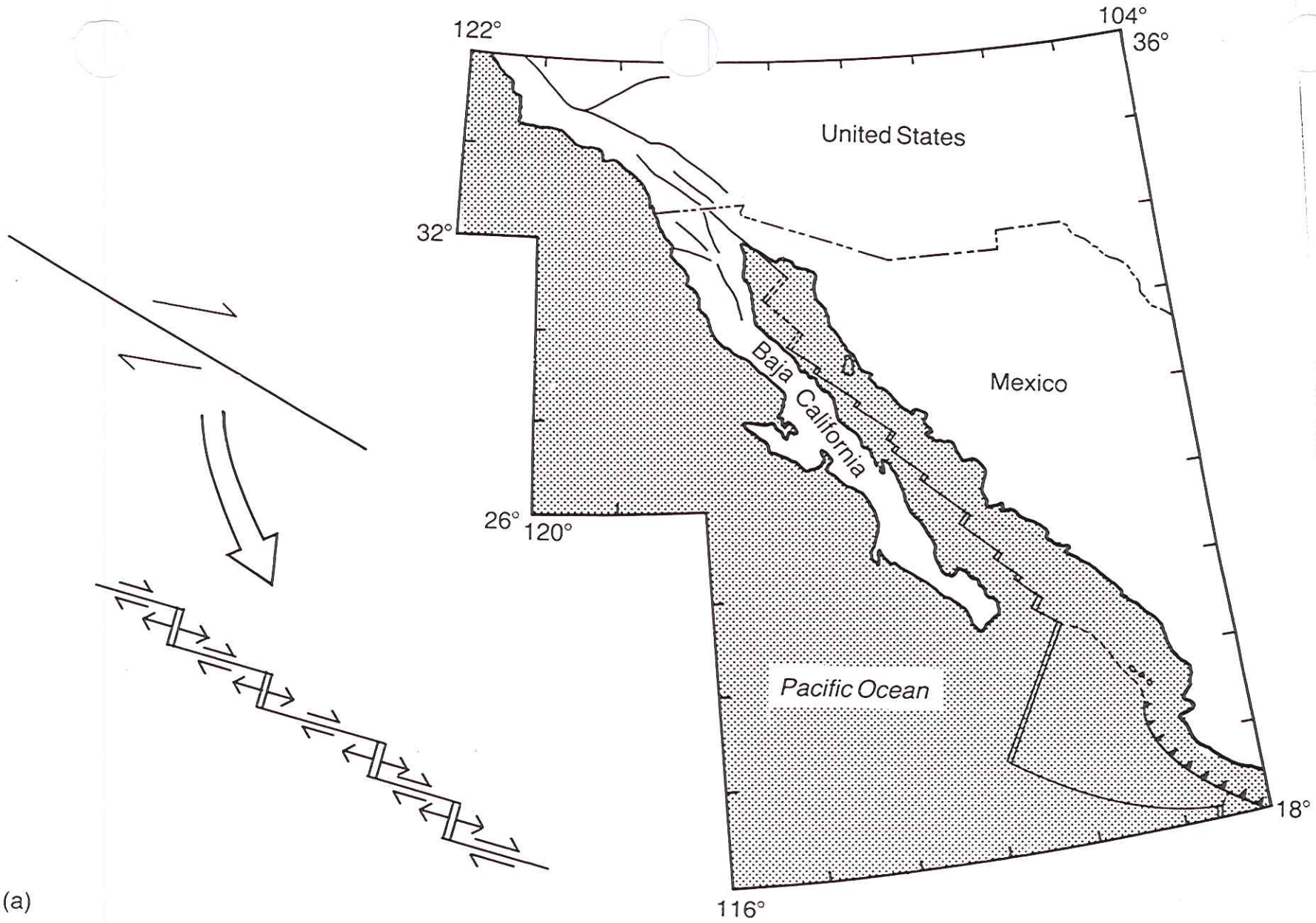

Fig. 7.7 (a) Development of a leaky transform fault because of a change in the pole of rotation. (b) Leaky transform fault in the Gulf of California.

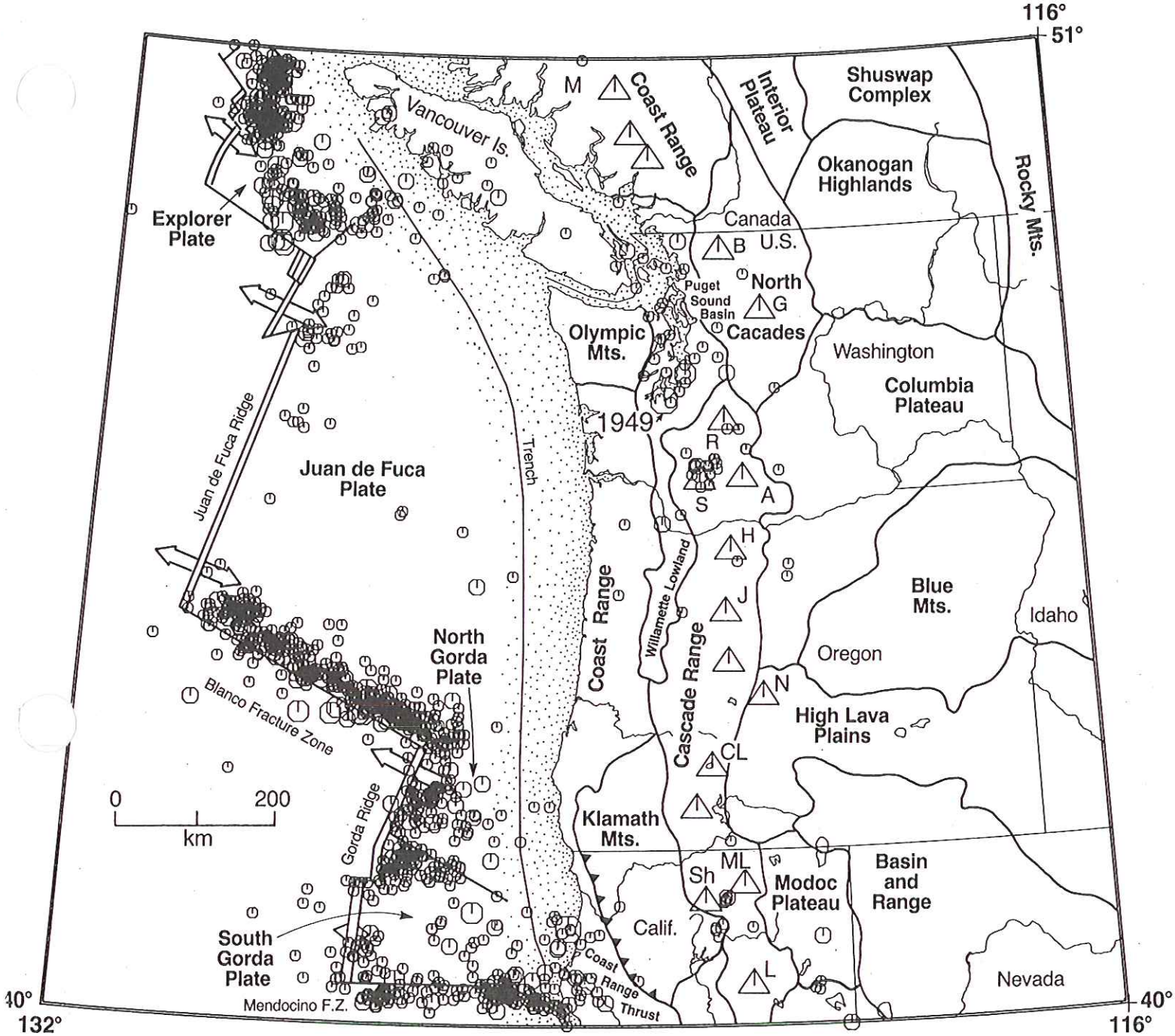

Figure 11–32. Plate boundaries, physiographic provinces, and seismicity for northwestern United States and adjacent parts of Canada. Octagons show earthquakes of $M > 4$ from National Oceanic and Atmospheric Administration catalog through 1985; largest earthquakes noted by year of occurrence. Open triangles show Quaternary volcanoes. From Shedlock and Weaver (1991).

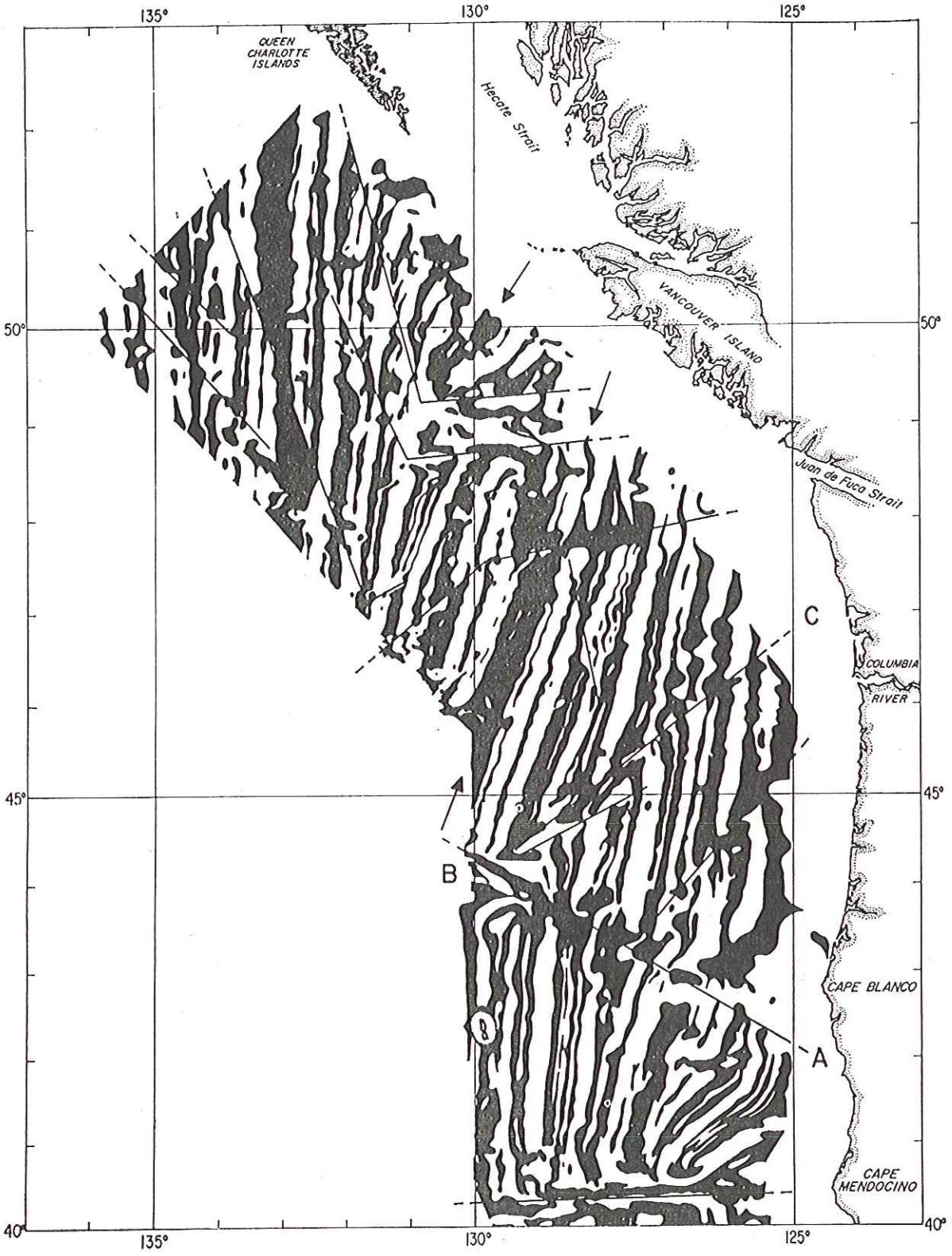

Fig. 13. Superposed on Raff and Mason's summary diagram of the magnetic anomalies in the Juan de Fuca region are arrows that indicate the axes of the three short ridge lengths in the area and straight lines that indicate faults offsetting the anomaly pattern [*Vine*, 1966].

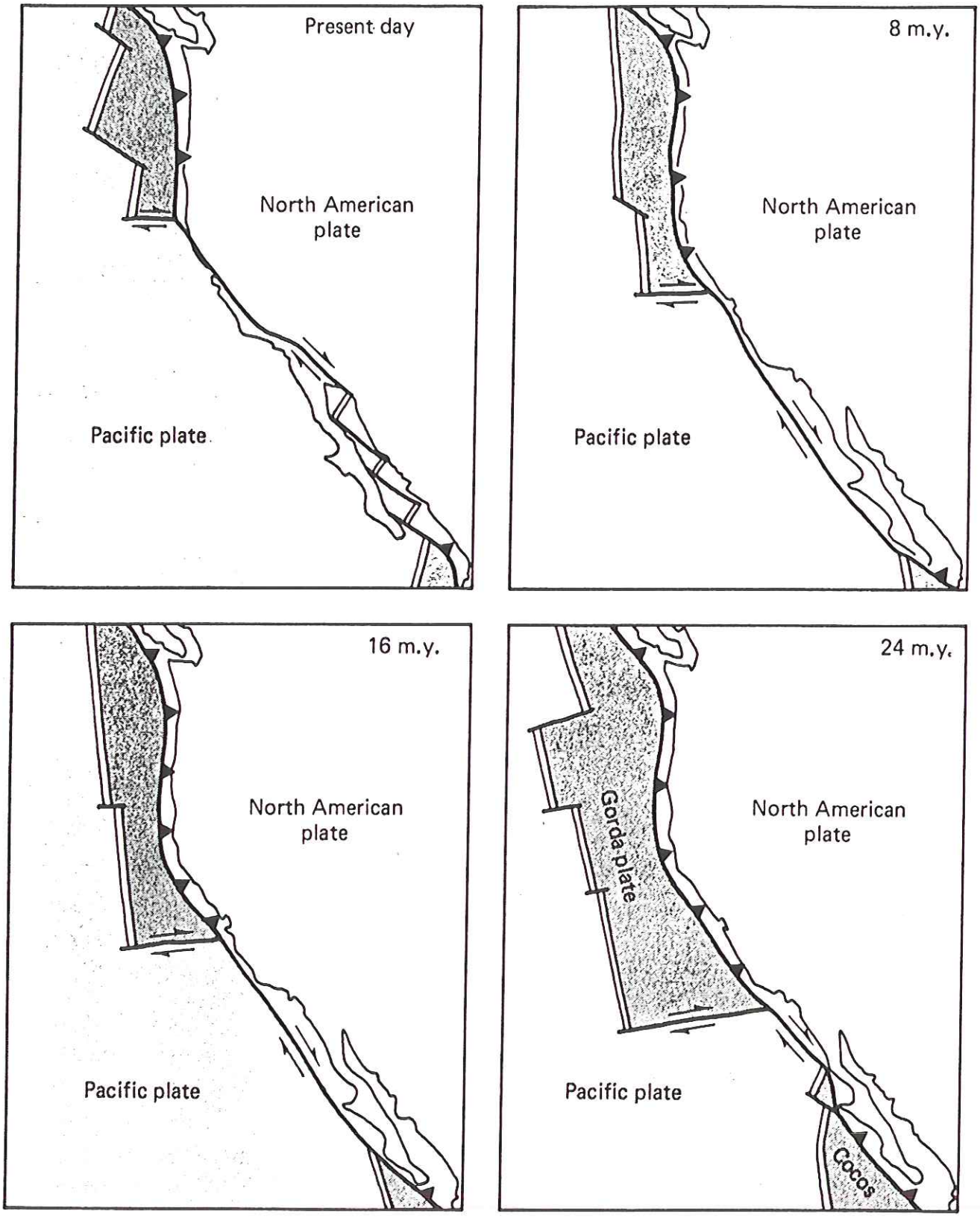
Present day
North American plate
Pacific plate
8 m.y.
North American plate
Pacific plate
16 m.y.
North American plate
Pacific plate
24 m.y.
Gorda plate
North American plate
Pacific plate
Cocos

400 km depth

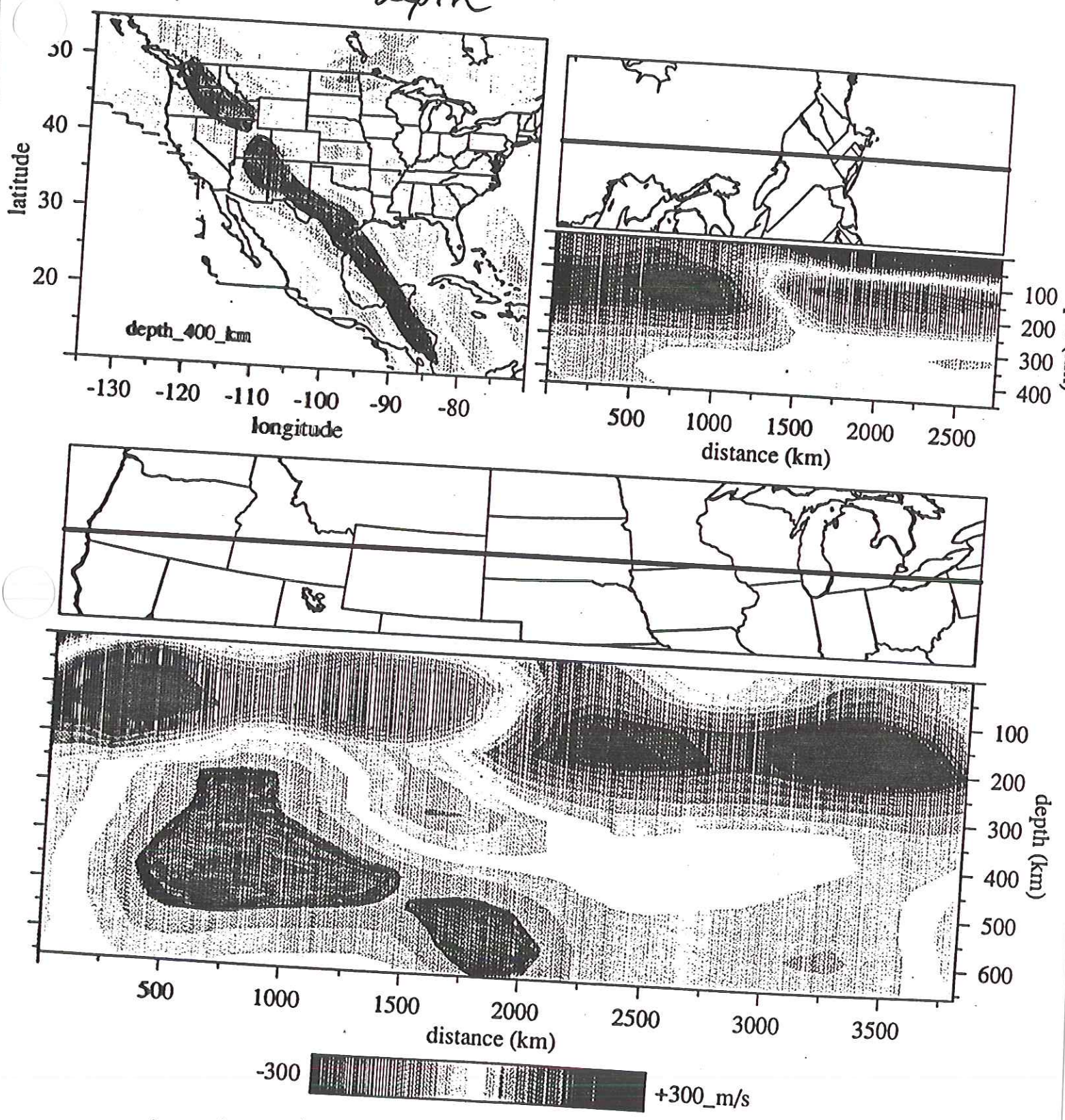

Seismic tomographic image of subducted Farallon plate — Suzan van der Lees

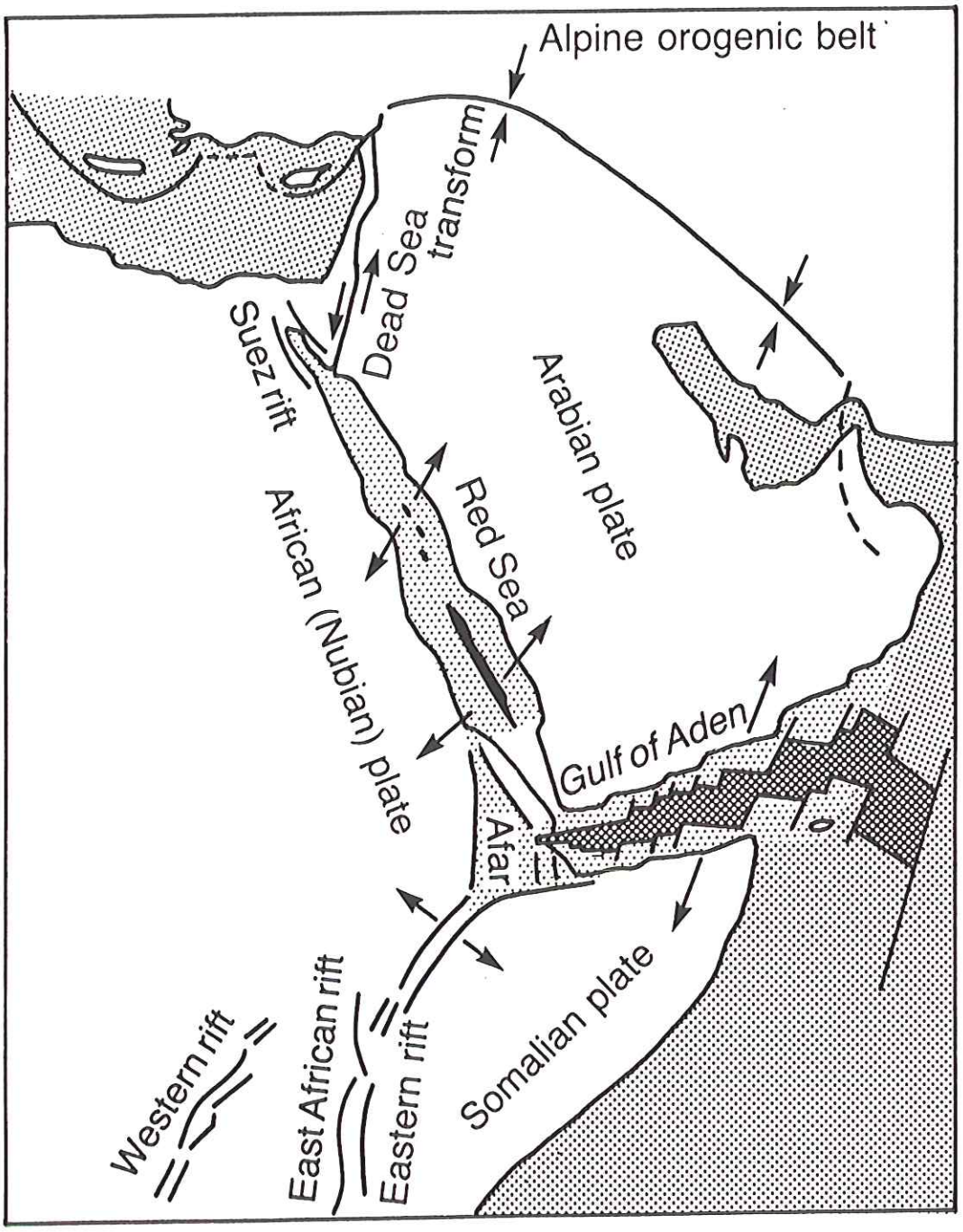

Fig. 11.4 Simplified plate tectonic framework of the Red Sea–Gulf of Aden area. Dark areas, oceanic crust; light stippled areas, transitional crust consisting of stretched, thinned continental crust invaded by basaltic dykes (redrawn from Bonatti, 1987, with permission from *Nature*, **330**, 692. Copyright © 1987 Macmillan Magazines Ltd).

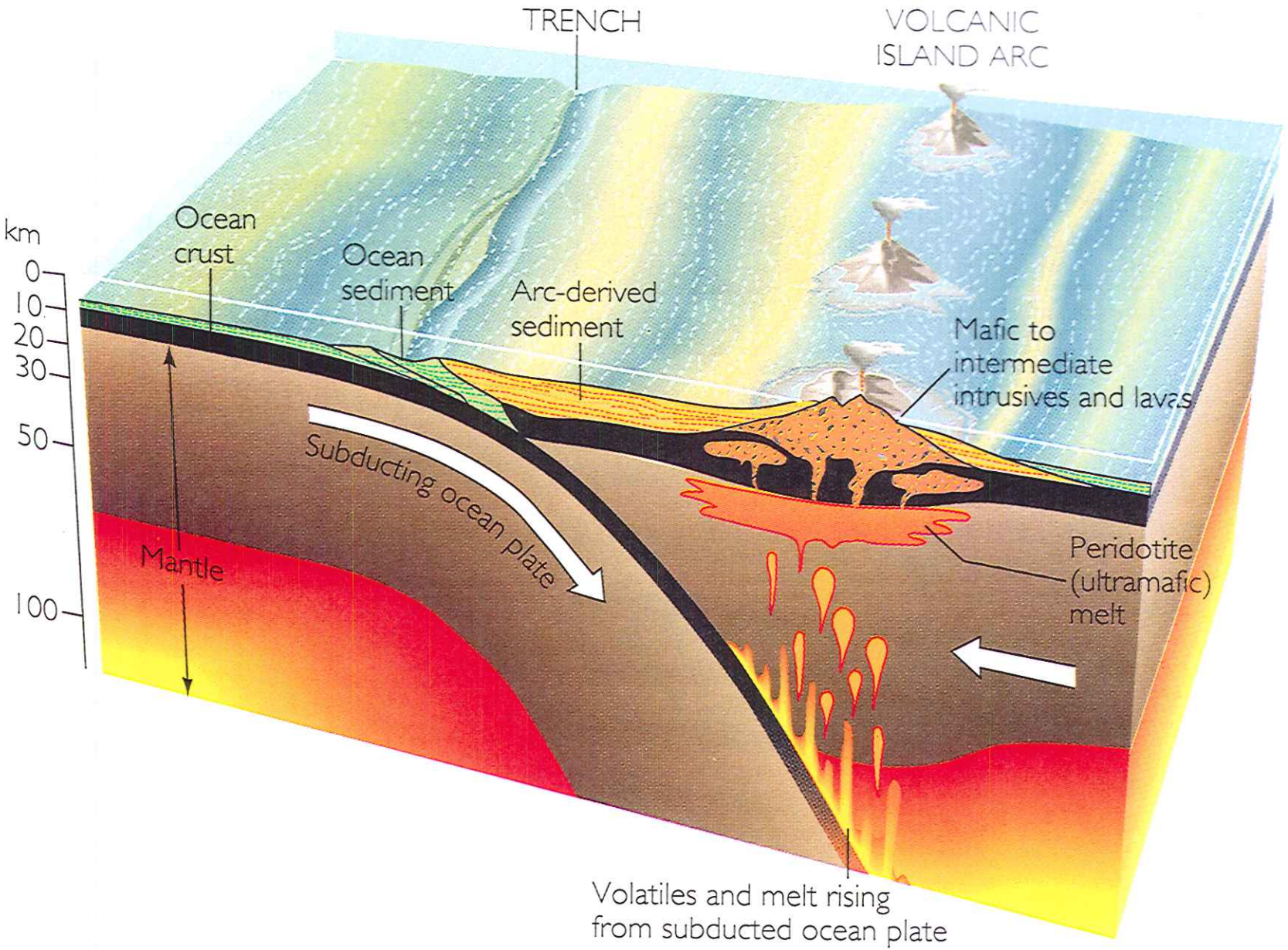
TRENCH
VOLCANIC ISLAND ARC
km
0
10
20
30
50
100
Ocean crust
Ocean sediment
Arc-derived sediment
Mafic to intermediate intrusives and lavas
Subducting ocean plate
Mantle
Peridotite (ultramafic) melt
Volatiles and melt rising from subducted ocean plate

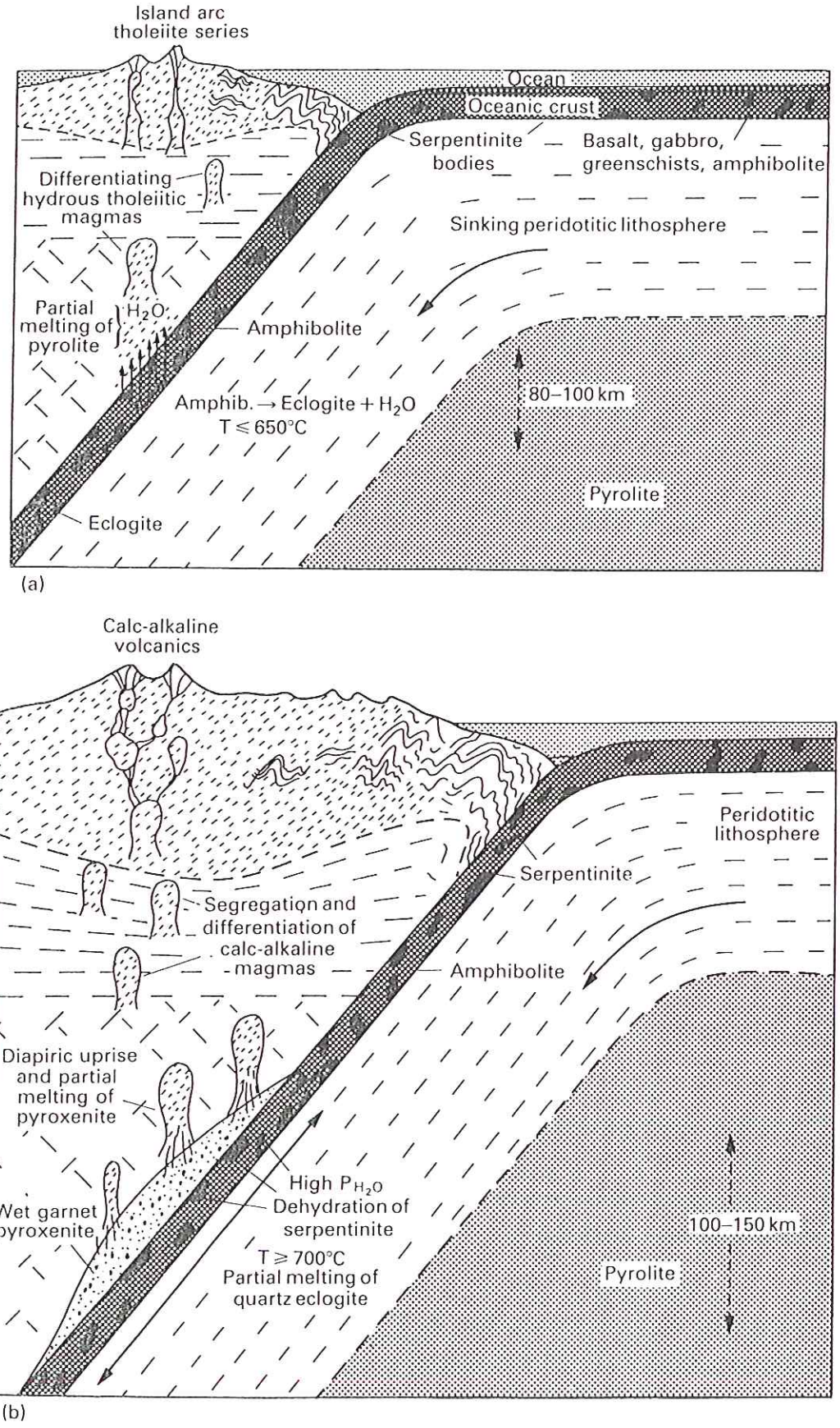

Fig. 8.32 (a) Early phase of development of an island arc. (b) Later phase of island arc development (redrawn from Ringwood, 1974, in *Journal of the Geological Society of London*, 1974, with permission from the Geological Society).

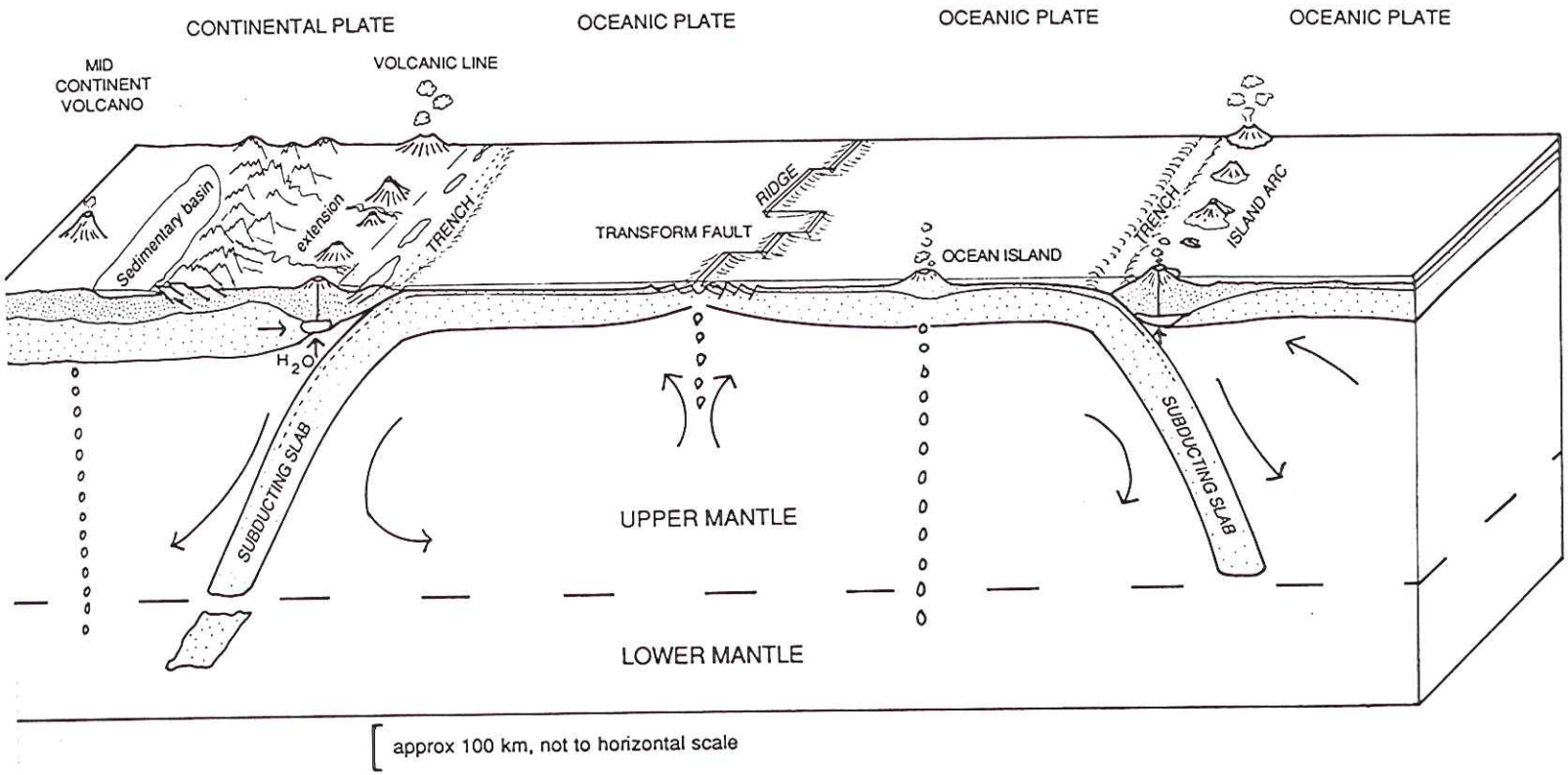

Figure 7.21. Schematic illustrating the formation of new oceanic lithosphere along the midocean ridges and its eventual subduction back into the mantle. Lithosphere is stippled. Crust is indicated by dense stipple. Oceanic island basalts may be derived from the lower mantle.

arc volcanism caused by fluxing of volatiles from slab

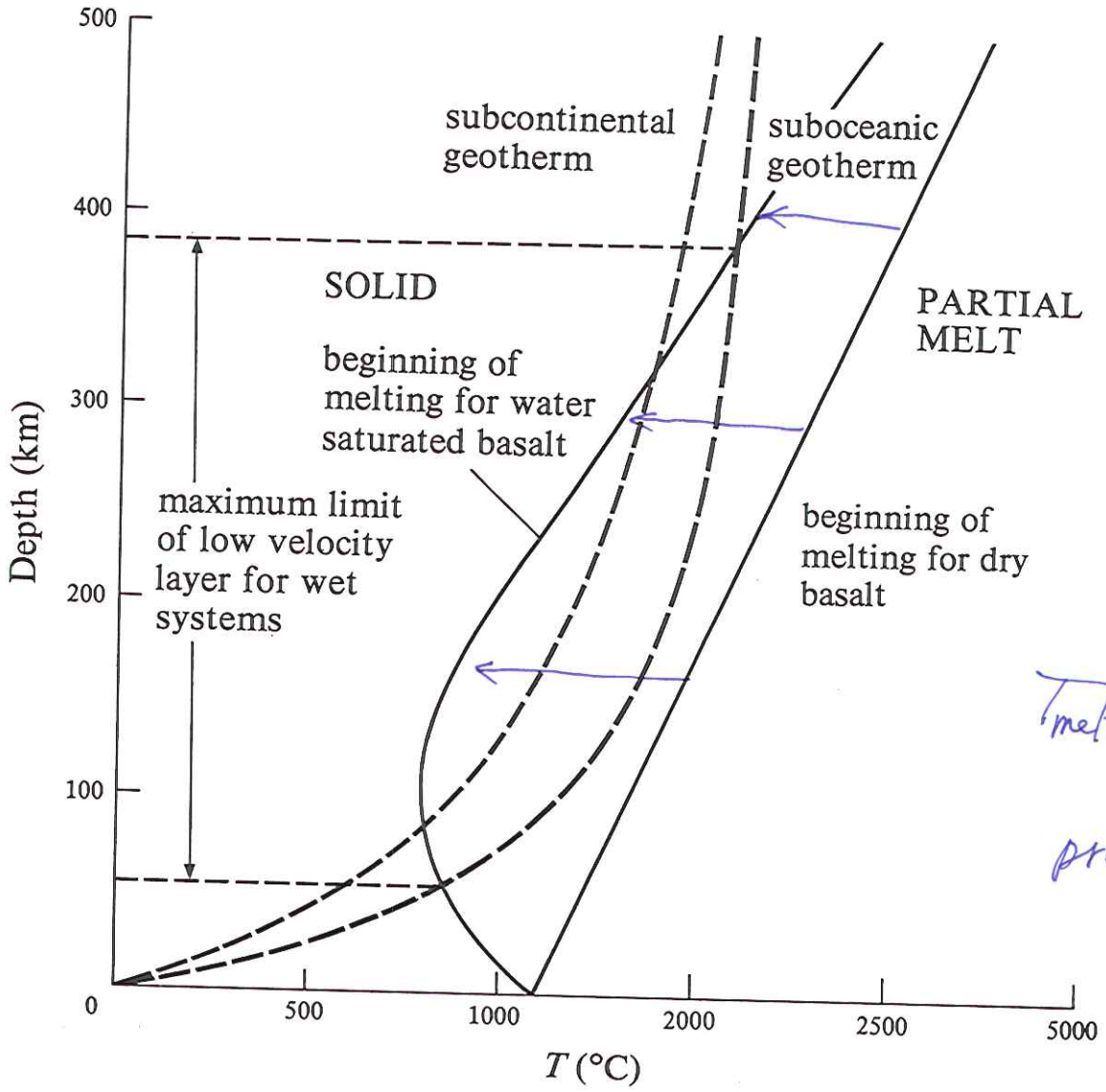

Tmelting lowered by presence of fluids

Figure 7.3 Upper mantle geothermal gradients (dashed, from Fig. 7.2) and their relationship to wet and dry melting curves for peridotite (solid) to give basalt partial melt. If excess water were present, the low-velocity layer would reach its maximum theoretical limits between the horizontal dashed lines.

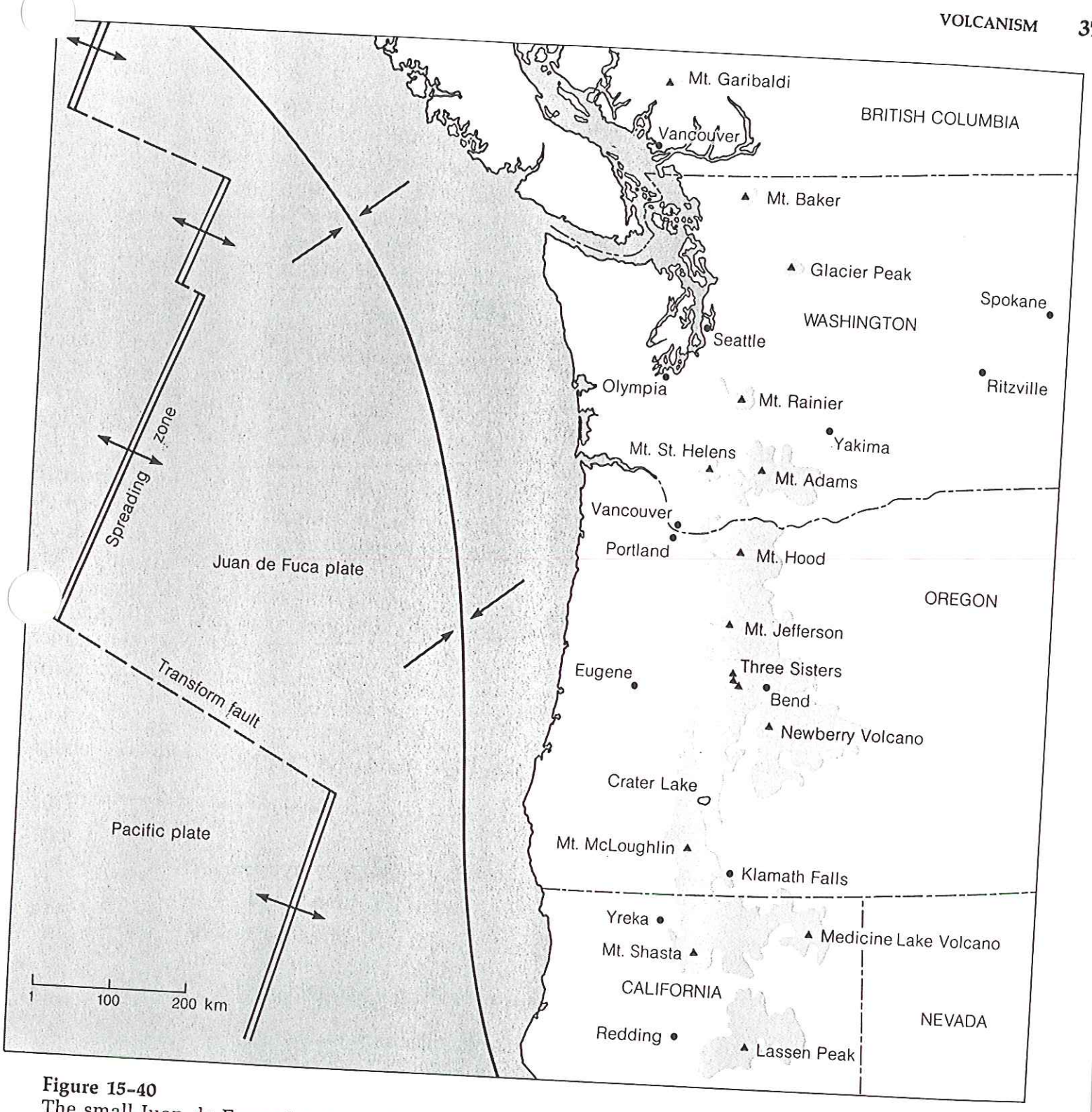

Figure 15-40
The small Juan de Fuca plate is sandwiched between the Pacific and the North American plates. Subduction of the Juan de Fuca plate under North America gives rise to the volcanoes (small triangles) of the Cascade Range, including Mt. St. Helens. [After "The Eruptions of Mt. St. Helens" by R. Decker and B. Decker. Copyright © 1981 by Scientific American, Inc. All rights reserved. Data from U.S. Geological Survey.]

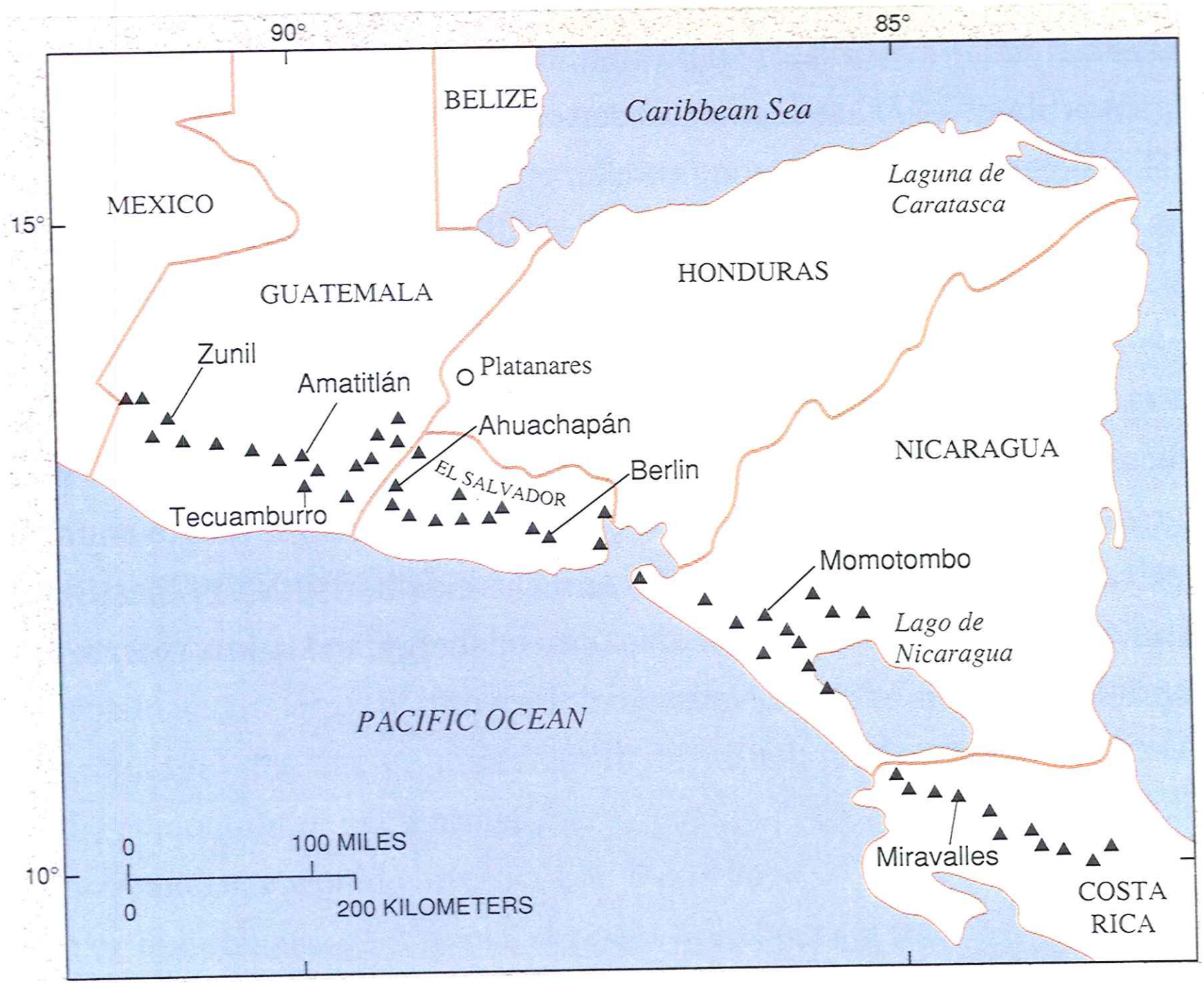
90°
85°
15°
10°
BELIZE
Caribbean Sea
MEXICO
Laguna de
Caratasca
GUATEMALA
HONDURAS
Zunil
Amatitlán
Platanares
Ahuachapán
EL SALVADOR
Berlin
NICARAGUA
Tecuamburro
Momotombo
Lago de
Nicaragua
PACIFIC OCEAN
Miravalles
COSTA
RICA
0
100 MILES
0
200 KILOMETERS

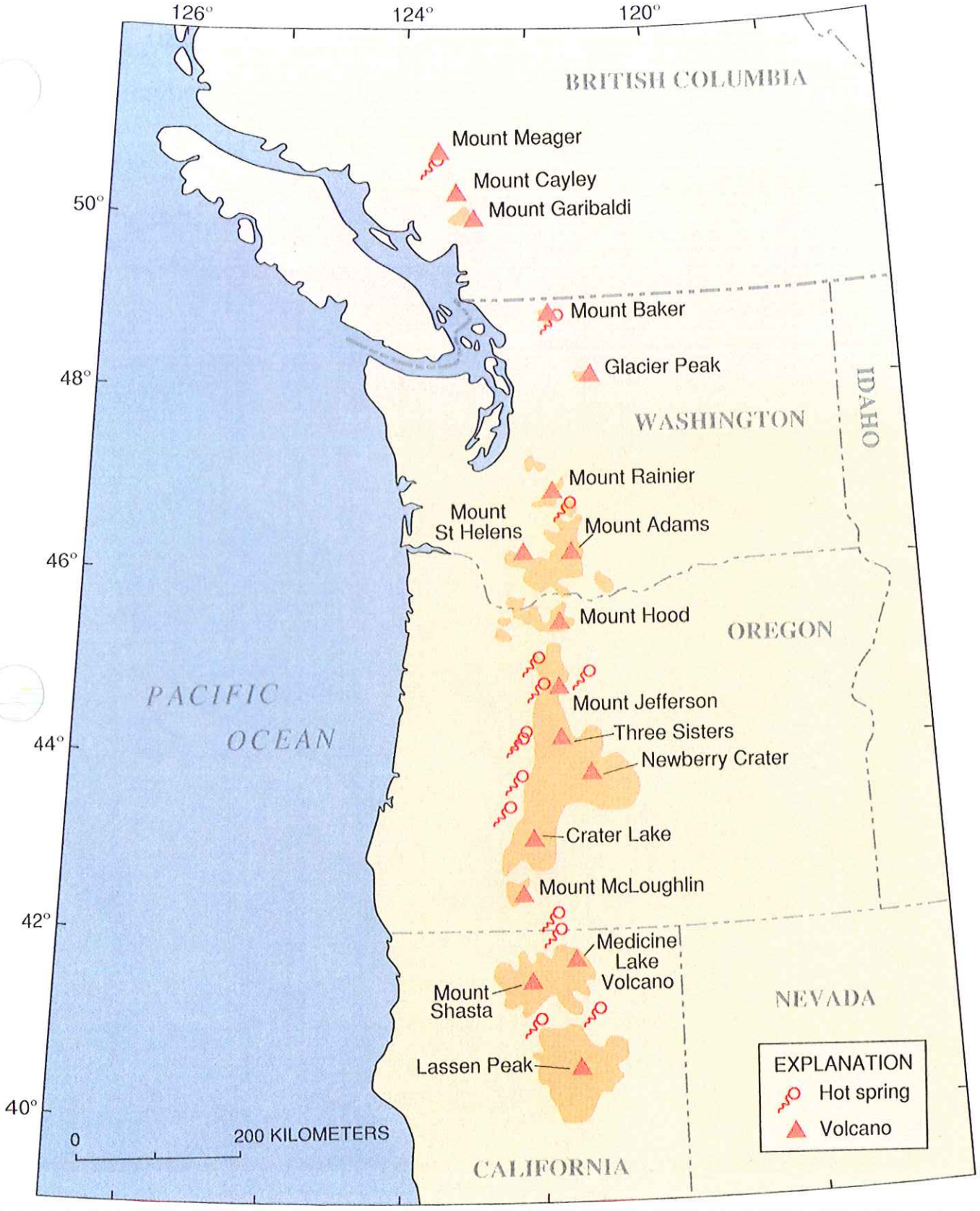

ook Toward the Future

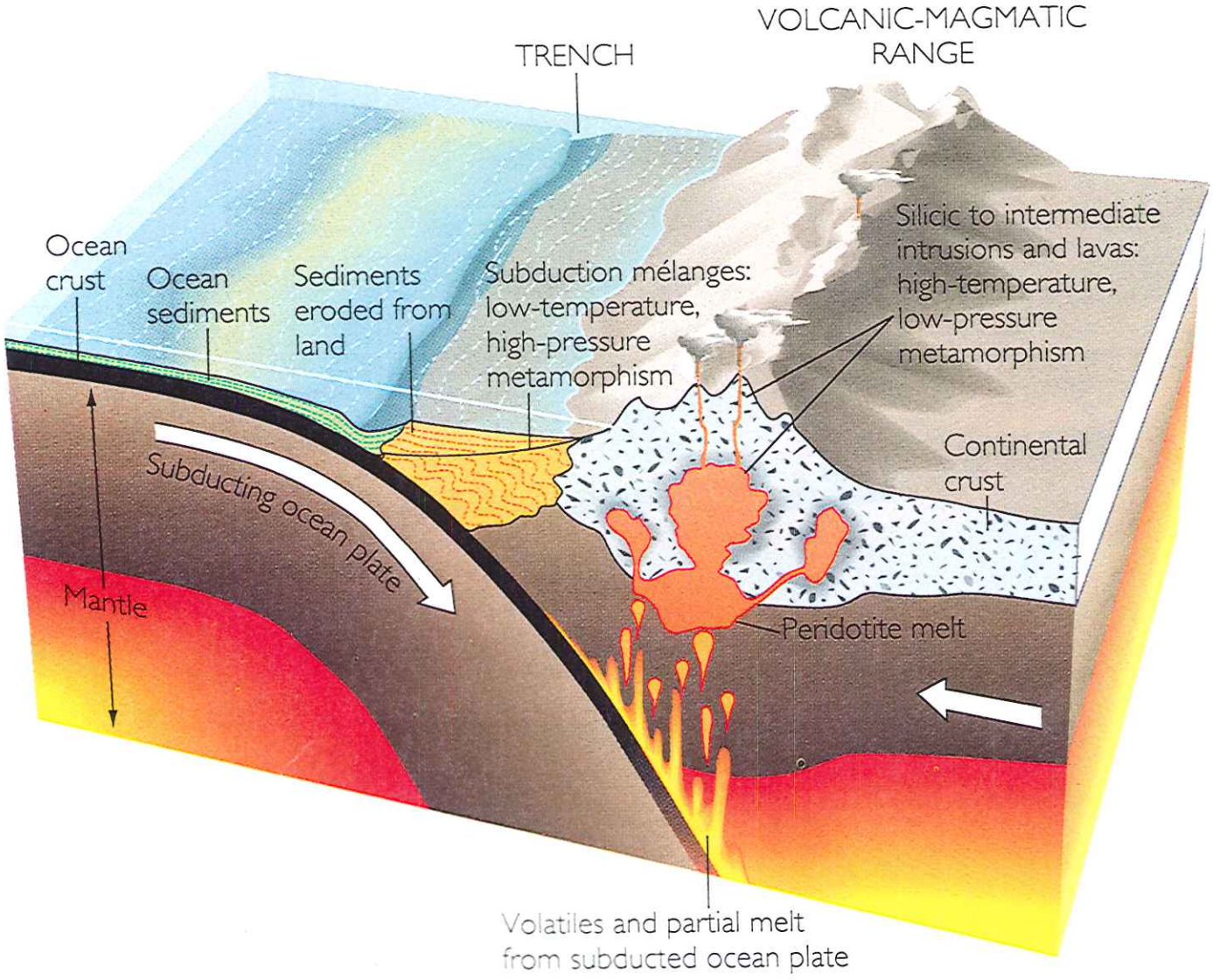

FIGURE 20.19 Rock assemblages associated with ocean-continent plate collisions and subduction: ocean trenches, mélange deposits, magmatic belts, metamorphism, and volcanism. The drawing is not to scale; the thickness of the lithosphere is about 70 km, the depth of the ocean trench is about 10 km, and the distance from trench to magmatic belt is 300 to 400 km.

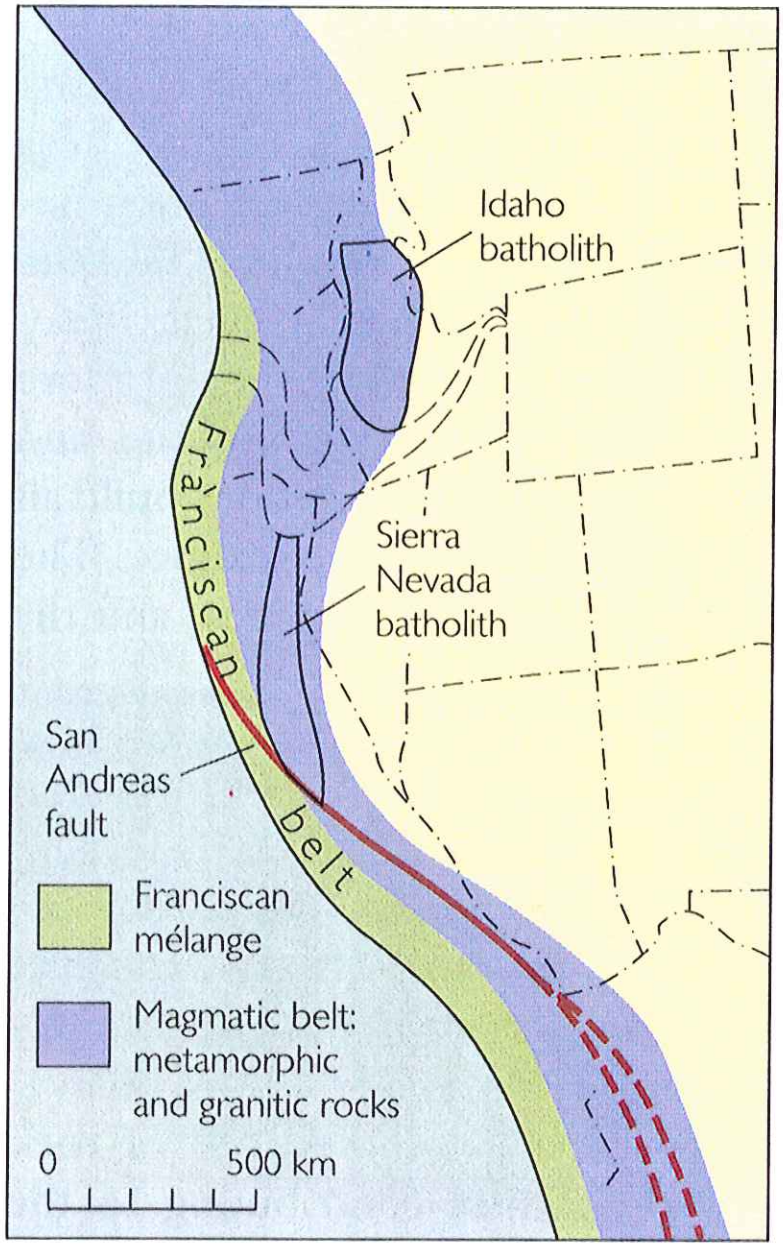

FIGURE 20.20 The geology of the western United States at the beginning of Tertiary time, some 60 million years ago. The paired mélange and magmatic belts indicate a collision of the North American Plate to the east and the Farallon Plate to the west; the Farallon Plate was subducted. The Franciscan mélange formation and the batholiths of the Sierra Nevada to the east as they exist today are indicated. (After W. Hamilton and W. B. Myers, "Cenozoic Tectonics," *Reviews of Geophysics,* vol. 4, 1966, p. 541.)

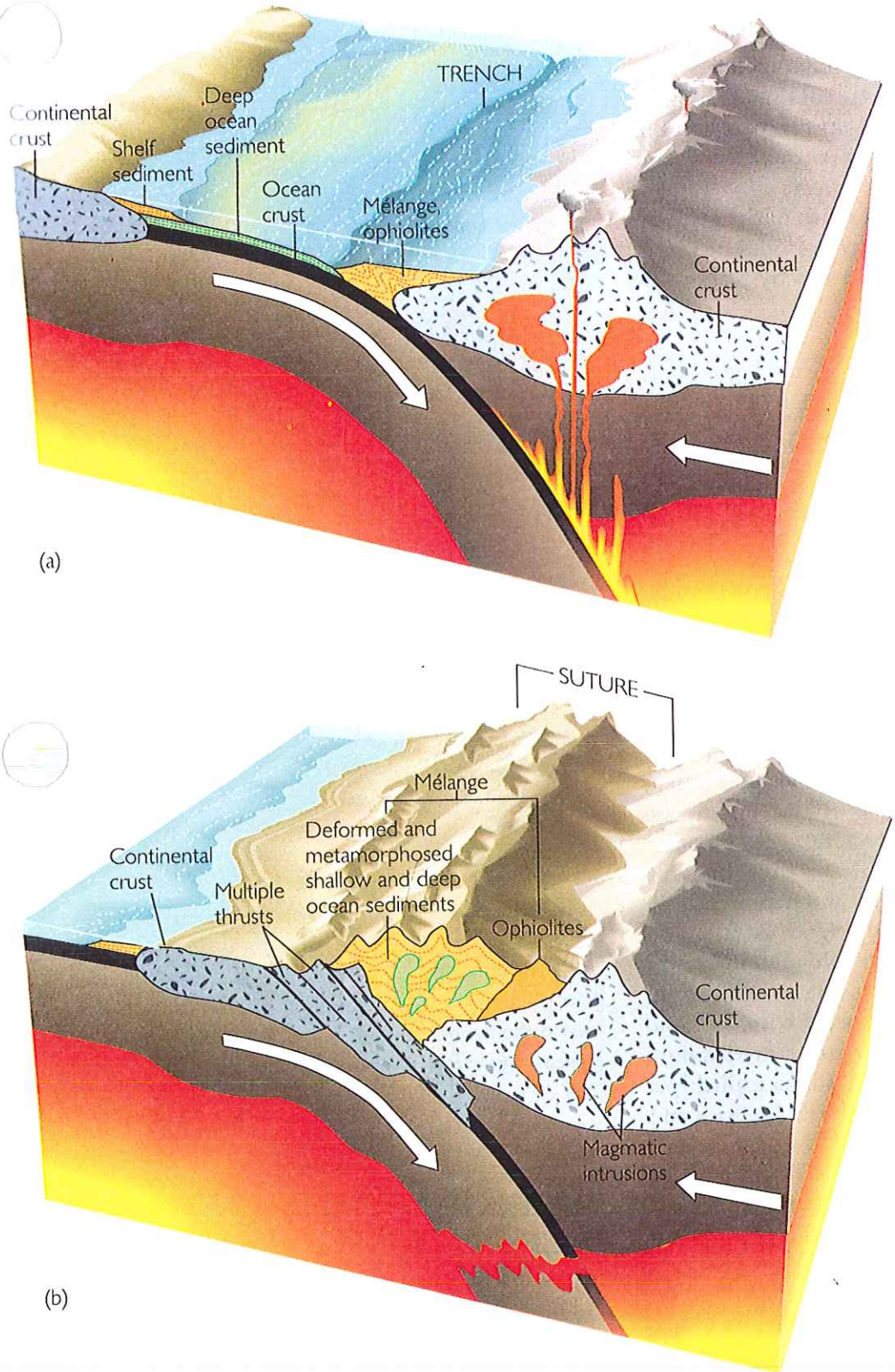

FIGURE 20.21 (a) A plate carrying a continent is subducted under a plate with a continent at its leading edge. (b) The two continents collide. The continent at left breaks into several thrust sheets, thickening the continental crust and raising a high mountain range. Other rocks associated with plate convergence are caught up in the collision zone: magmatic intrusions, deformed and metamorphosed shelf and deep-water sediments, and ophiolite fragments.

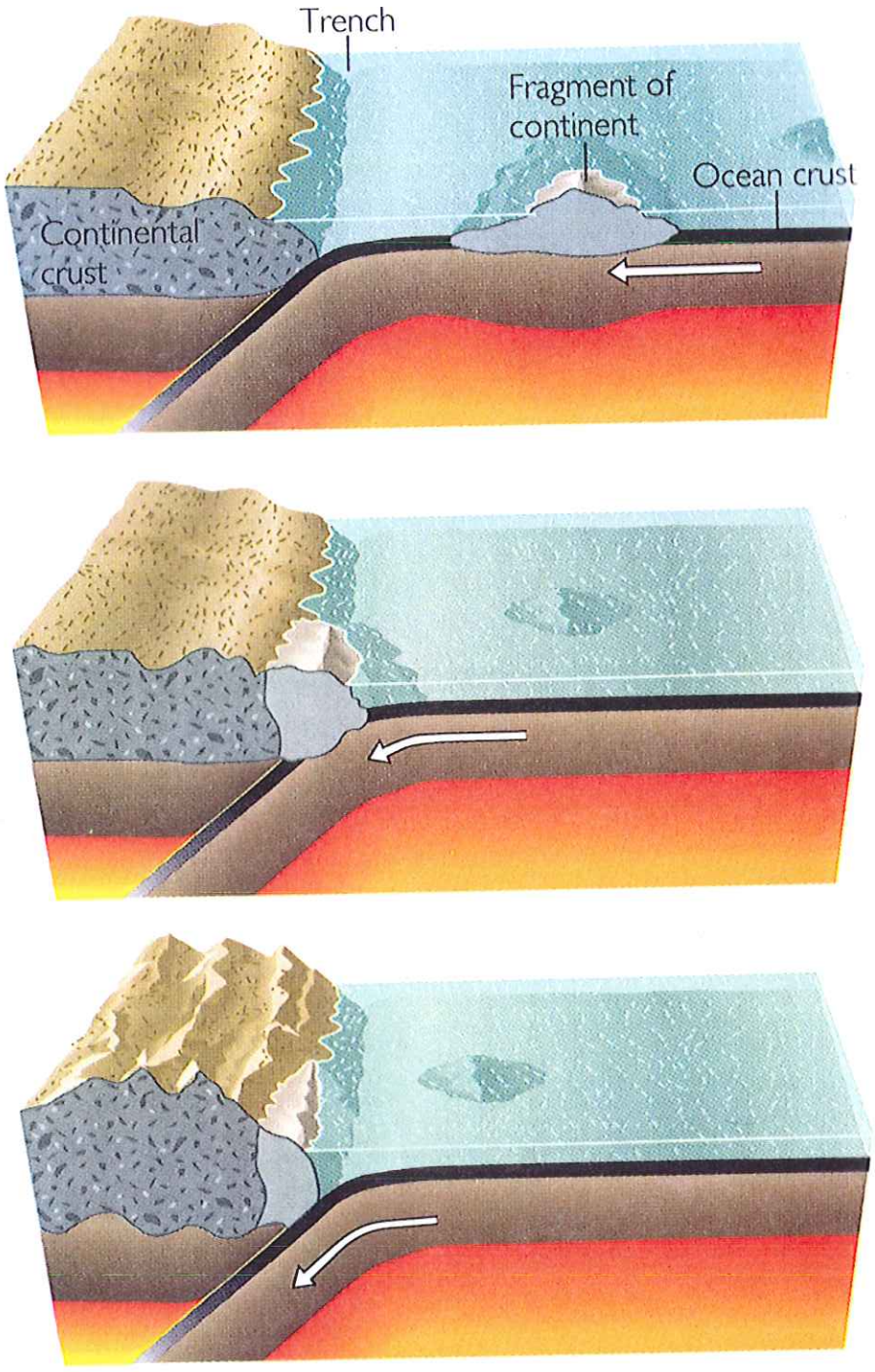

FIGURE 20.22 Origin of a microplate terrane. An oceanic island arc or a fragment of continent is carried into a plate collision zone. Instead of being subducted, it is welded onto the overriding plate. Because the fragment may have originated thousands of kilometers away, it differs in its rock assemblages from the surrounding geological terrain.

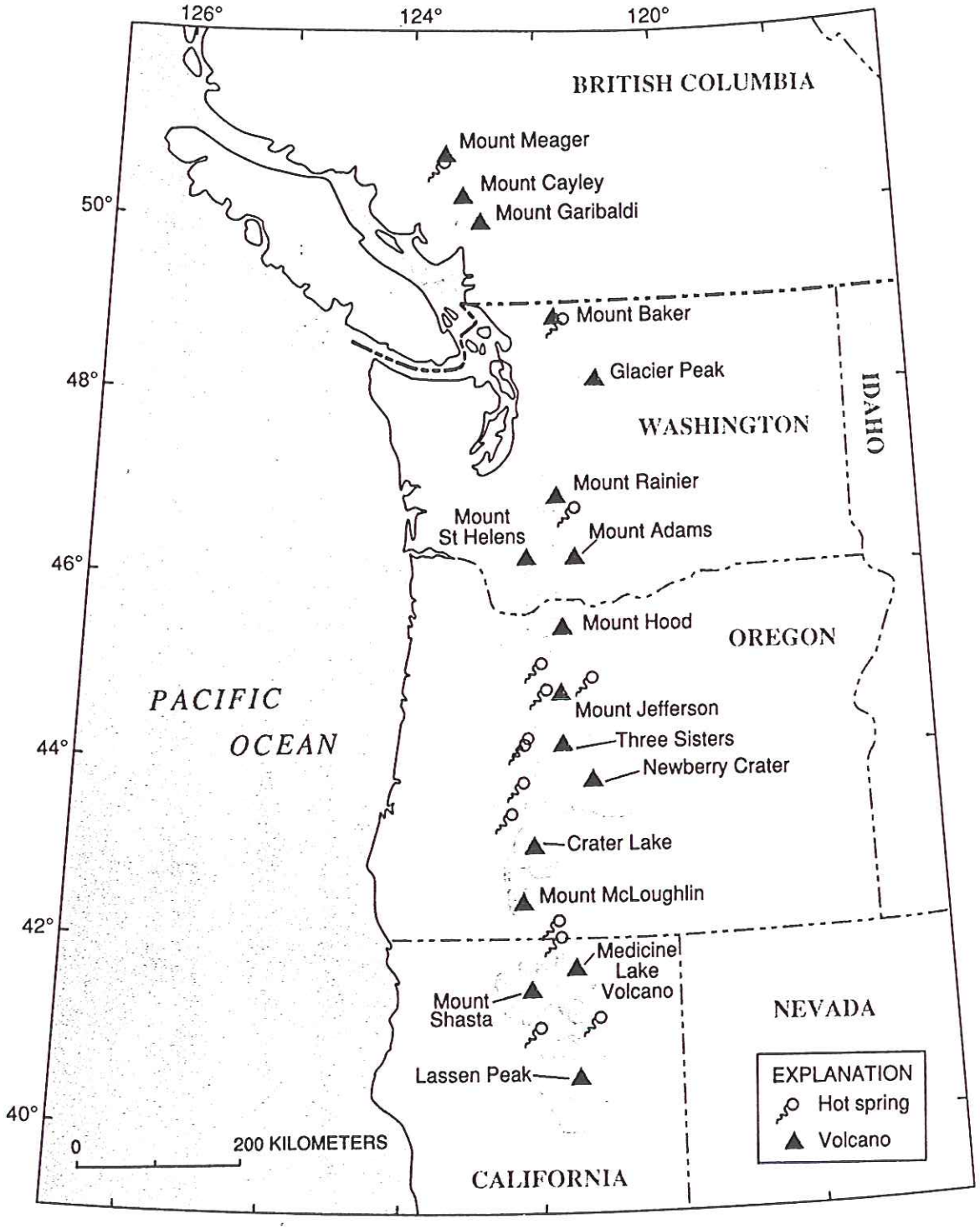
126°
124°
120°
BRITISH COLUMBIA
Mount Meager
Mount Cayley
Mount Garibaldi
50°
Mount Baker
Glacier Peak
48°
WASHINGTON
IDAHO
Mount Rainier
Mount St Helens
Mount Adams
46°
Mount Hood
OREGON
PACIFIC OCEAN
Mount Jefferson
44°
Three Sisters
Newberry Crater
Crater Lake
Mount McLoughlin
42°
Medicine Lake Volcano
Mount Shasta
NEVADA
Lassen Peak
40°
EXPLANATION
Hot spring
Volcano
0
200 KILOMETERS
CALIFORNIA

FIGURE 12.28 Quaternary volcanoes in Japan are concentrated in two belts, one associated with the active Northeast Japan Arc and the other with subduction along the Ryukyu Arc, which extends southwestward toward Taiwan. There are no active volcanoes in southern Honshu or Shikoku. *(A map derived from Figure 15.2 in A. Miyashiro,* Metamorphism and Metamorphic Belts, *p. 351, George Allen and Unwin © 1973 by Routledge, Chapman & Hall, Inc.)*

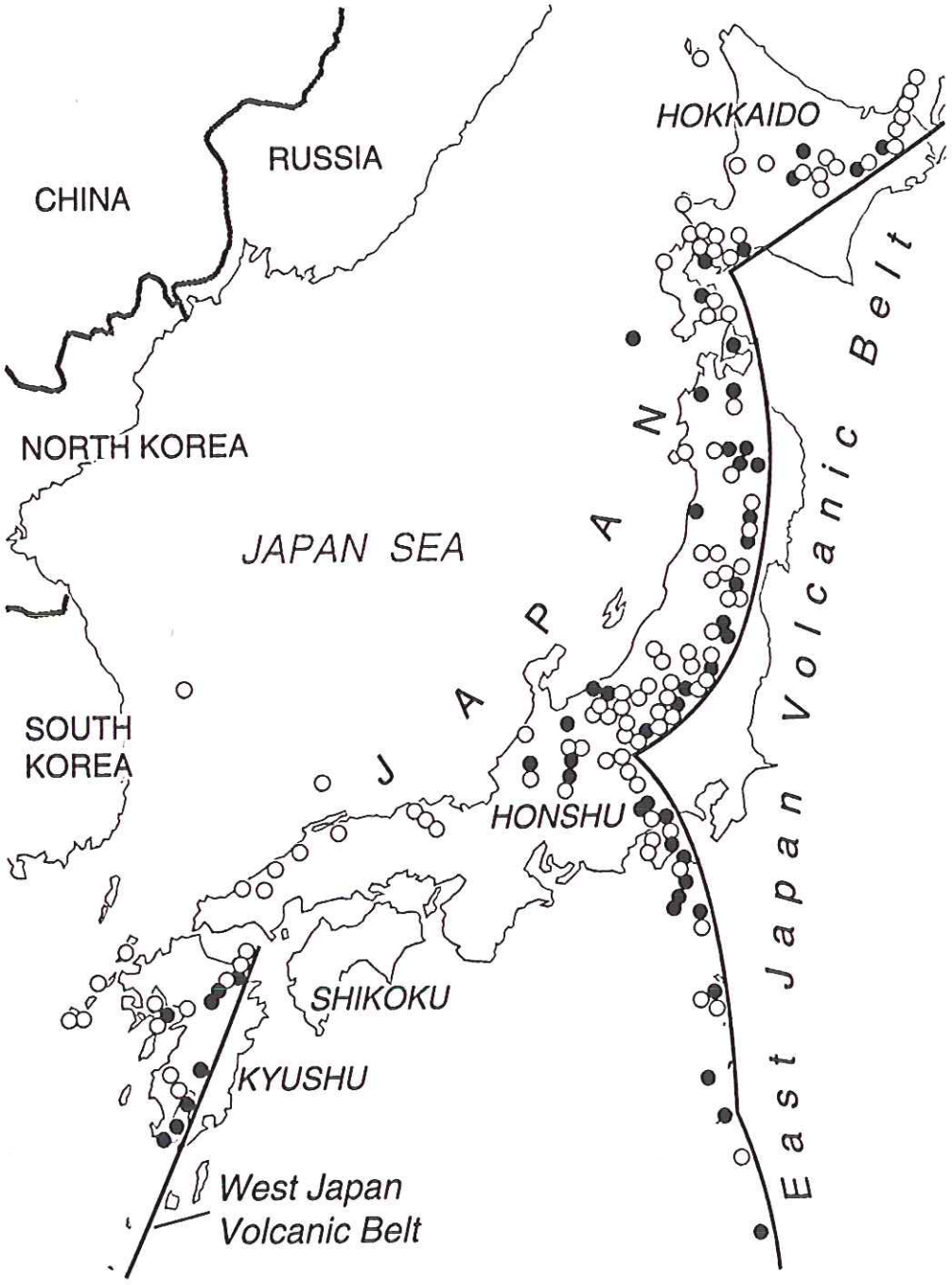

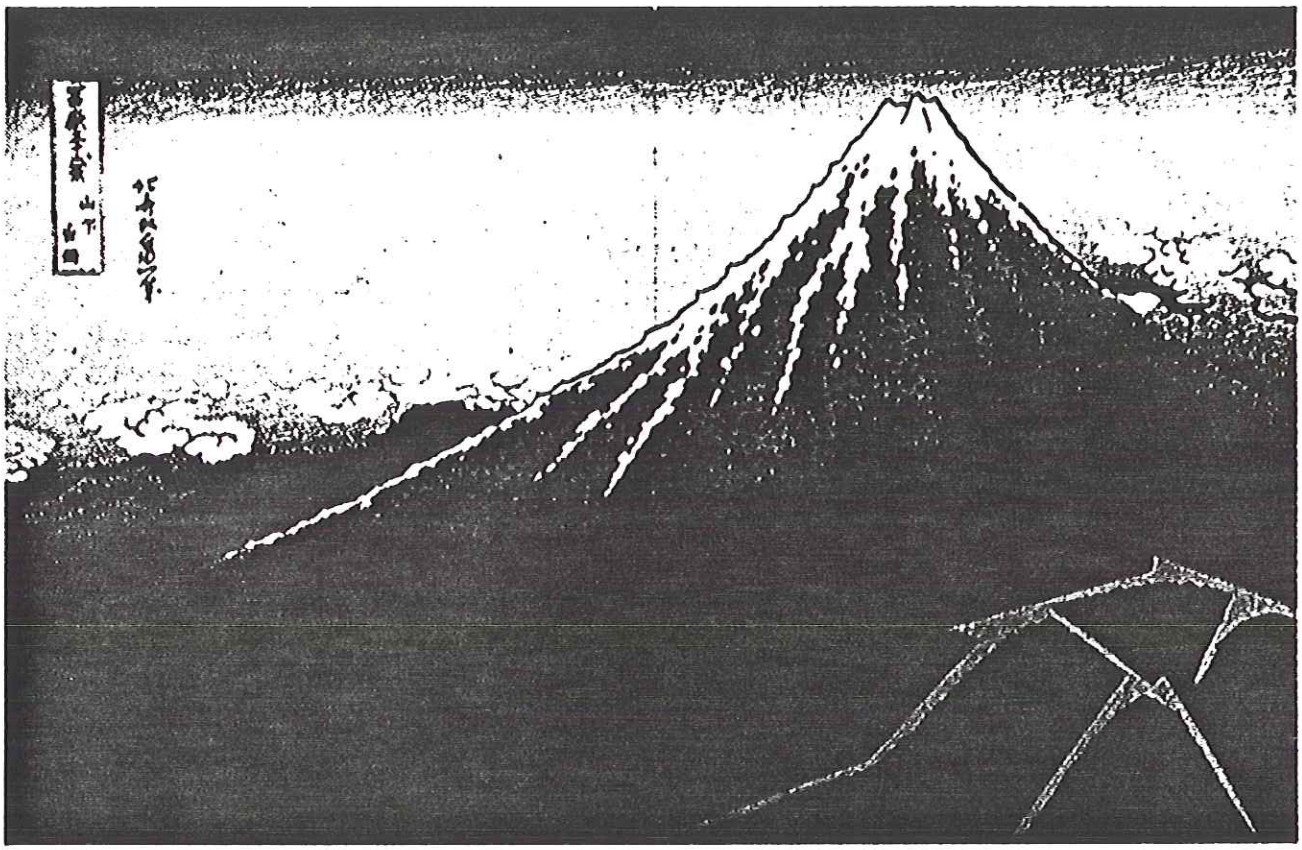

FIGURE 12.29 Mount Fuji, the Japanese volcano that is most familiar to Westerners, has a picturesque shape that has made it a favorite subject for artists. Mount Fuji is 3,776 m tall and has a circumference of 30 km at its base. This woodblock print by Hokusai (1760–1849) is one of a well-known series of 36 views. *(Giraudon, Art Resource)*

classic andesitic volcano high viscosity magma

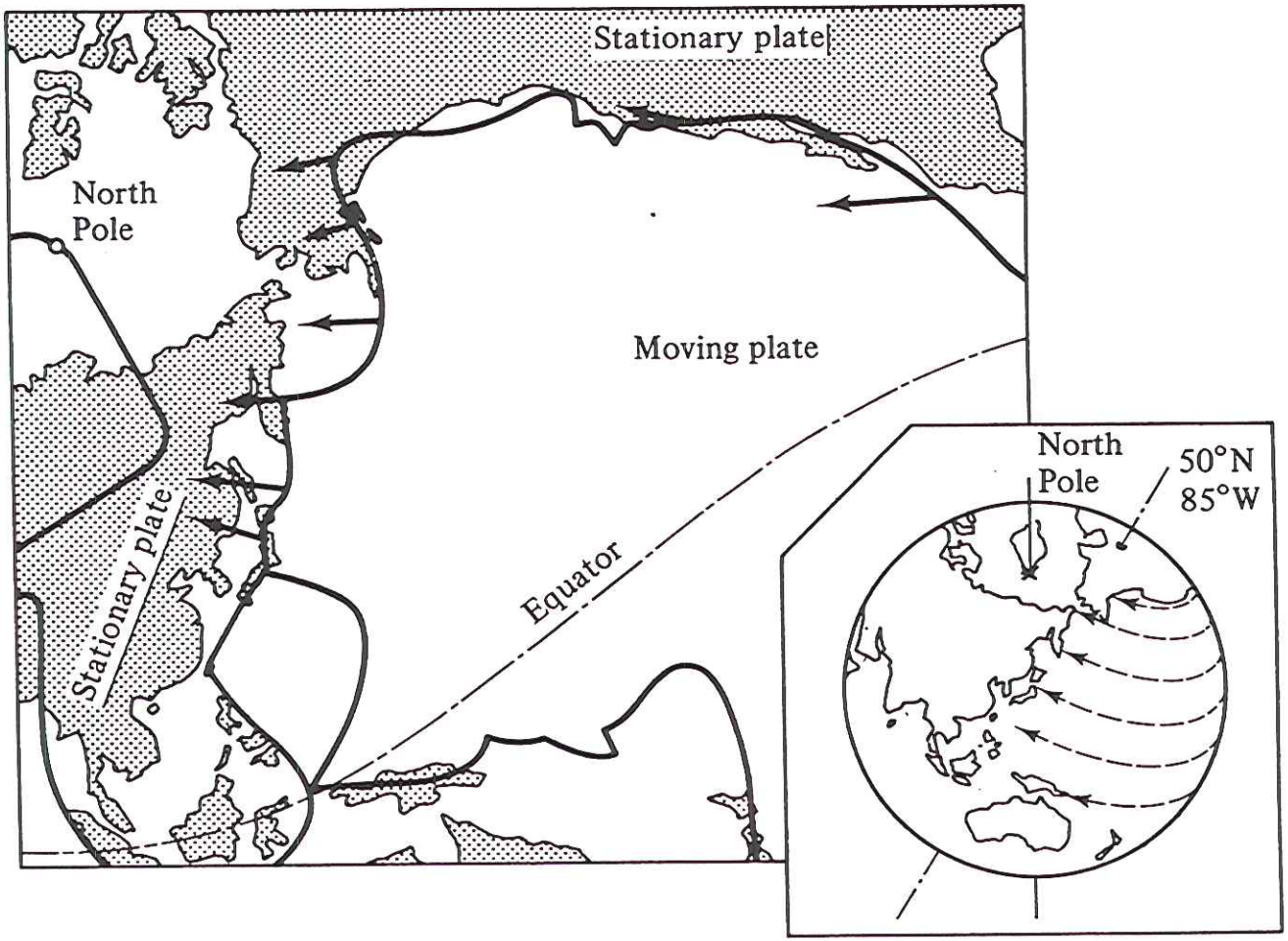

Fig. 7.5. A Mercator projection of the Pacific with a pole at 50°N 85°W. The arrows show the direction of motion of the Pacific plate relative to that containing North America and Kamchatka. If both plates are rigid all slip vectors must be parallel with each other and with the upper and lower boundaries of the figure. Possible boundaries of other plates are sketched. (After McKenzie & Parker, 1967.)

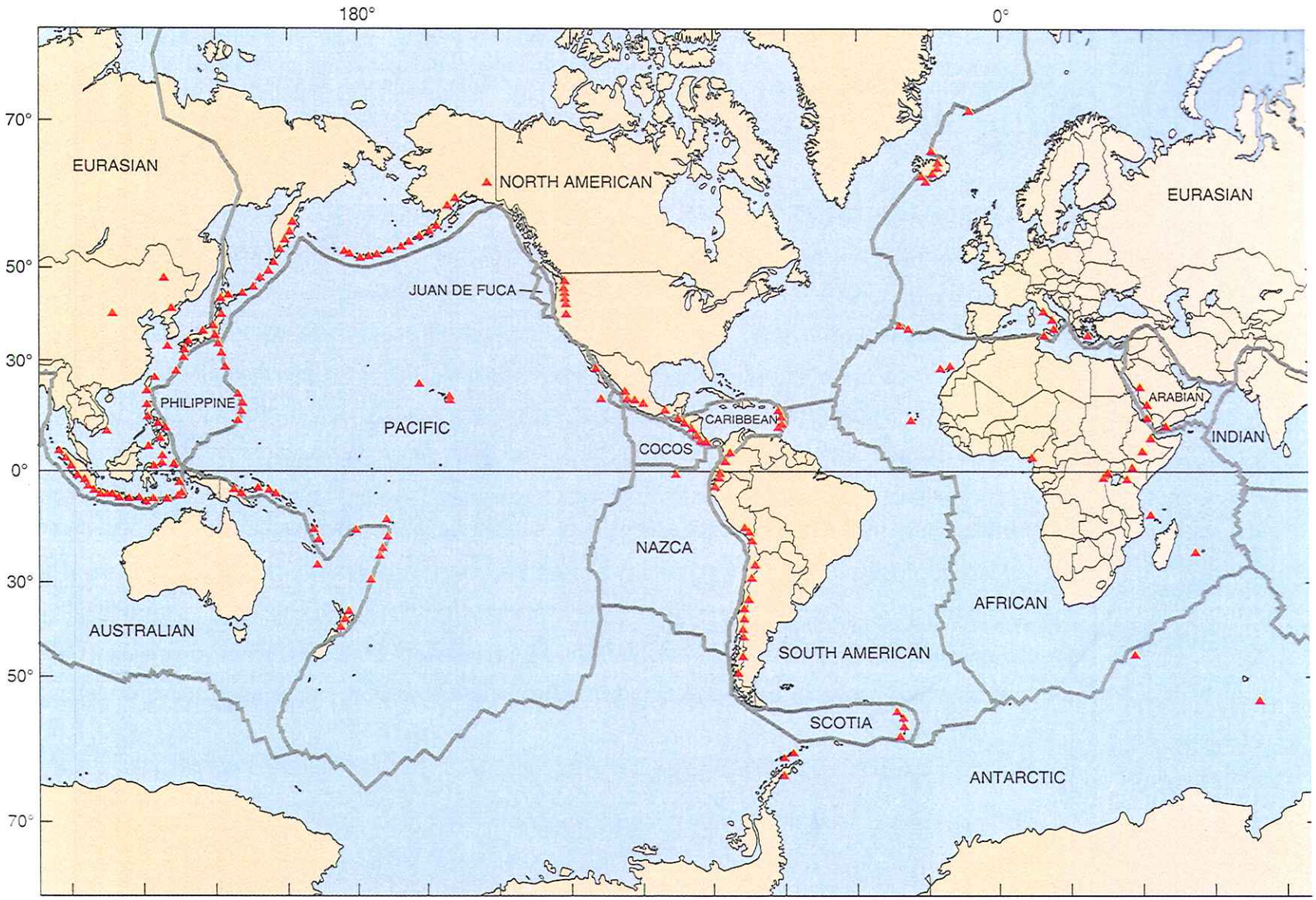

no volcanoes on end of Aleutians
also point out hotspot volcanoes: Hawaii & Iceland

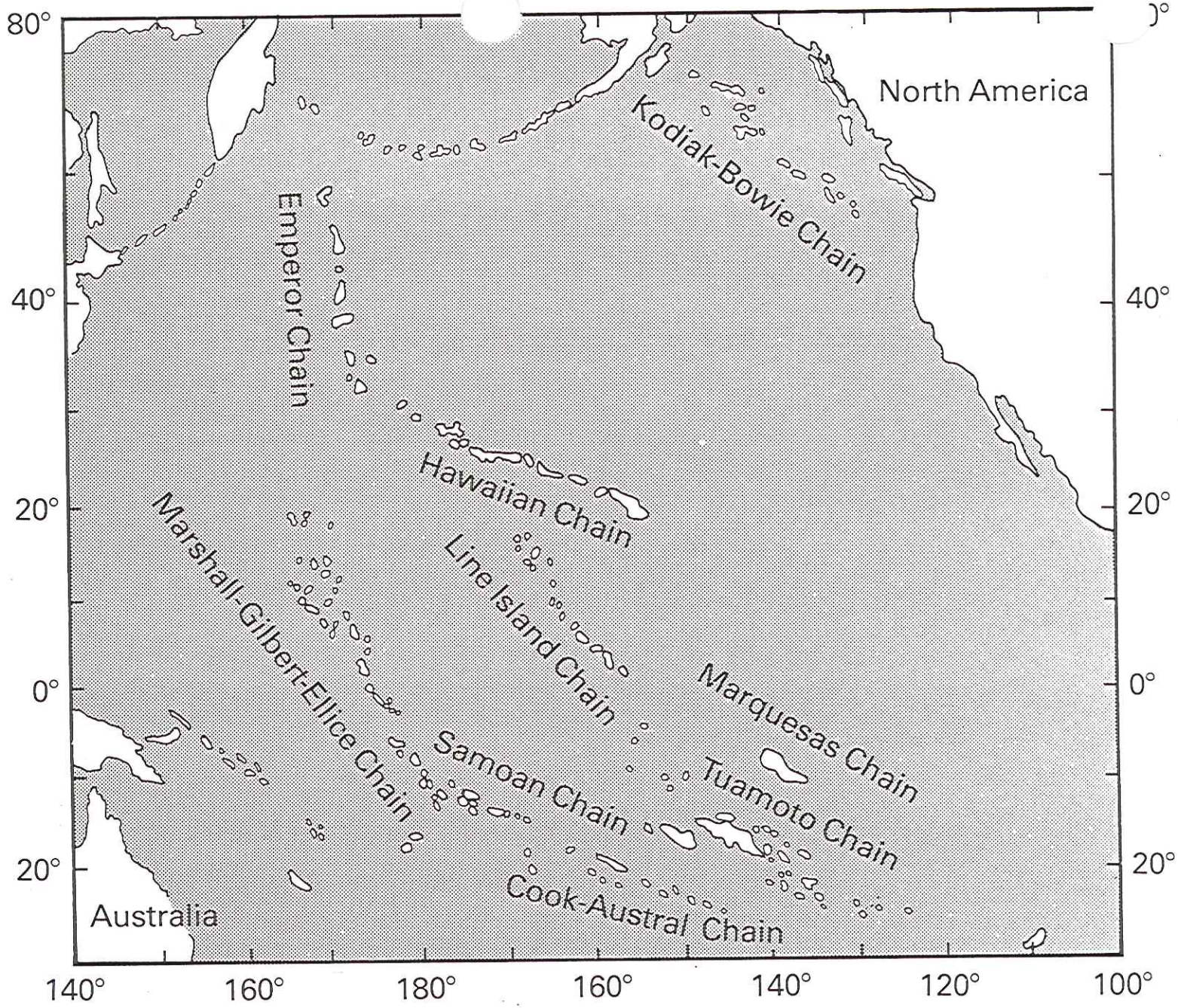

Fig. 5.6 Linear island chains in the Pacific Ocean on a Mercator projection. The chains young to the east.

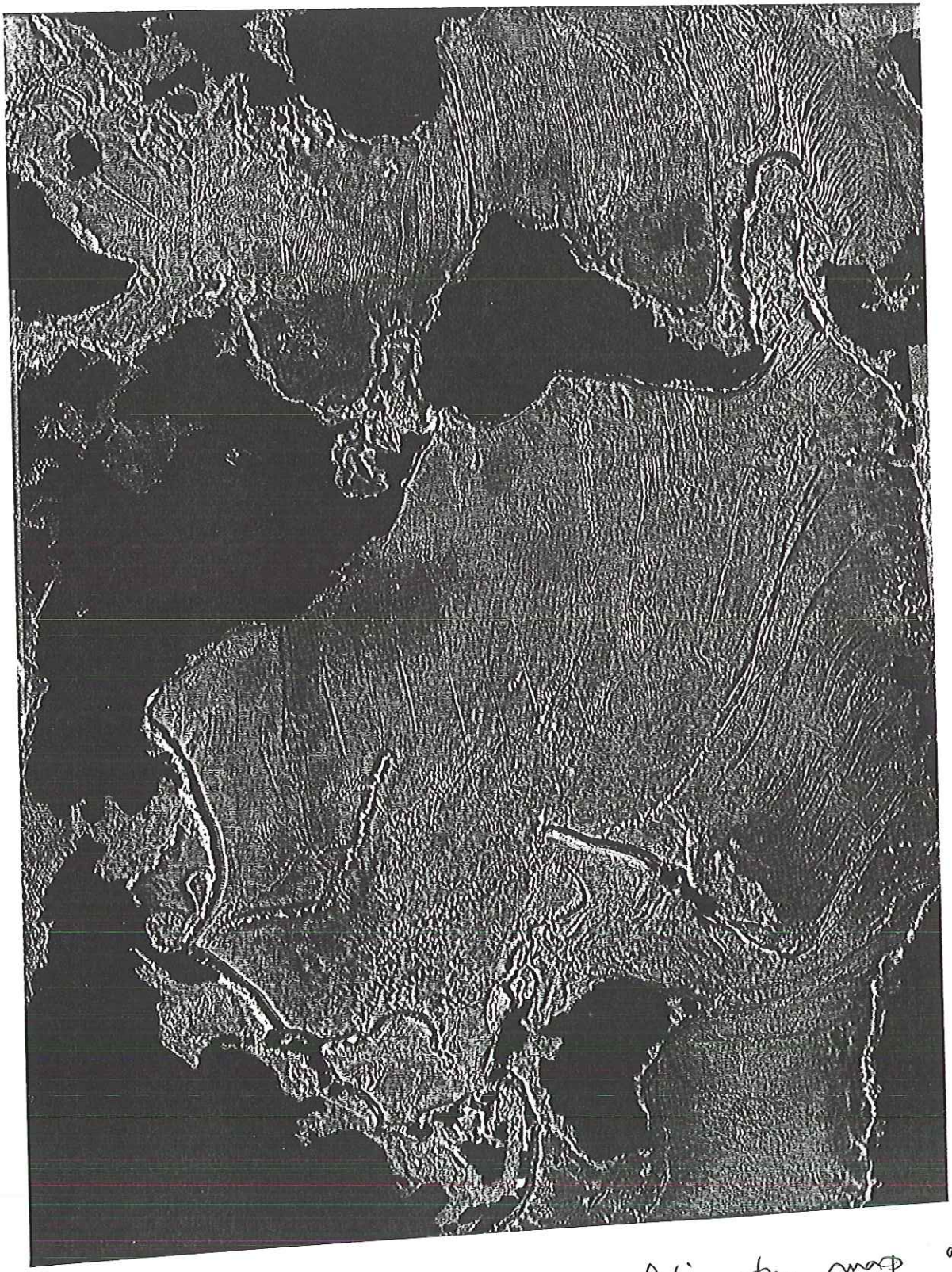

radar altimetry map of sea surface

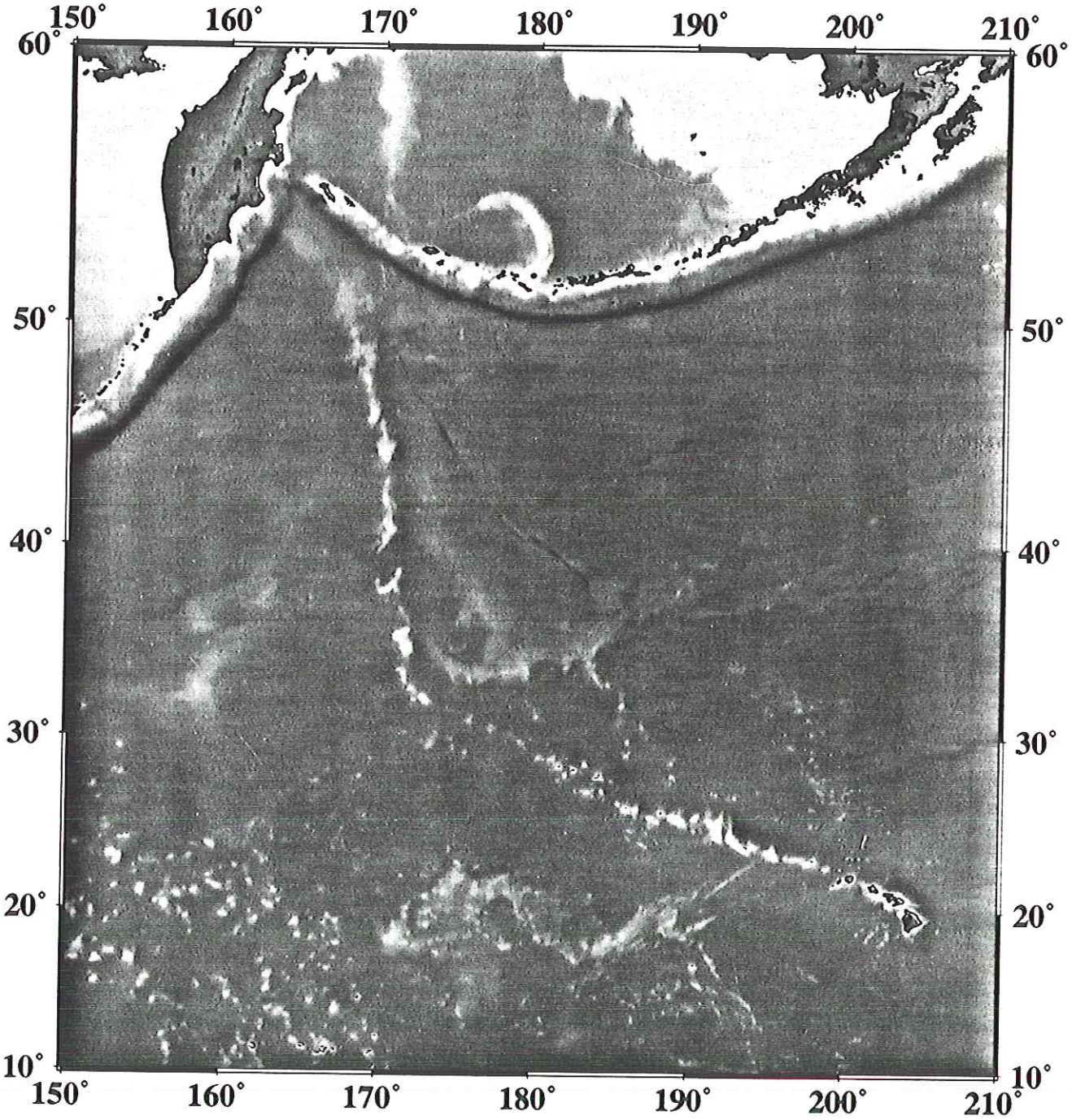
150°
160°
170°
180°
190°
200°
210°
60°
50°
40°
30°
20°
10°

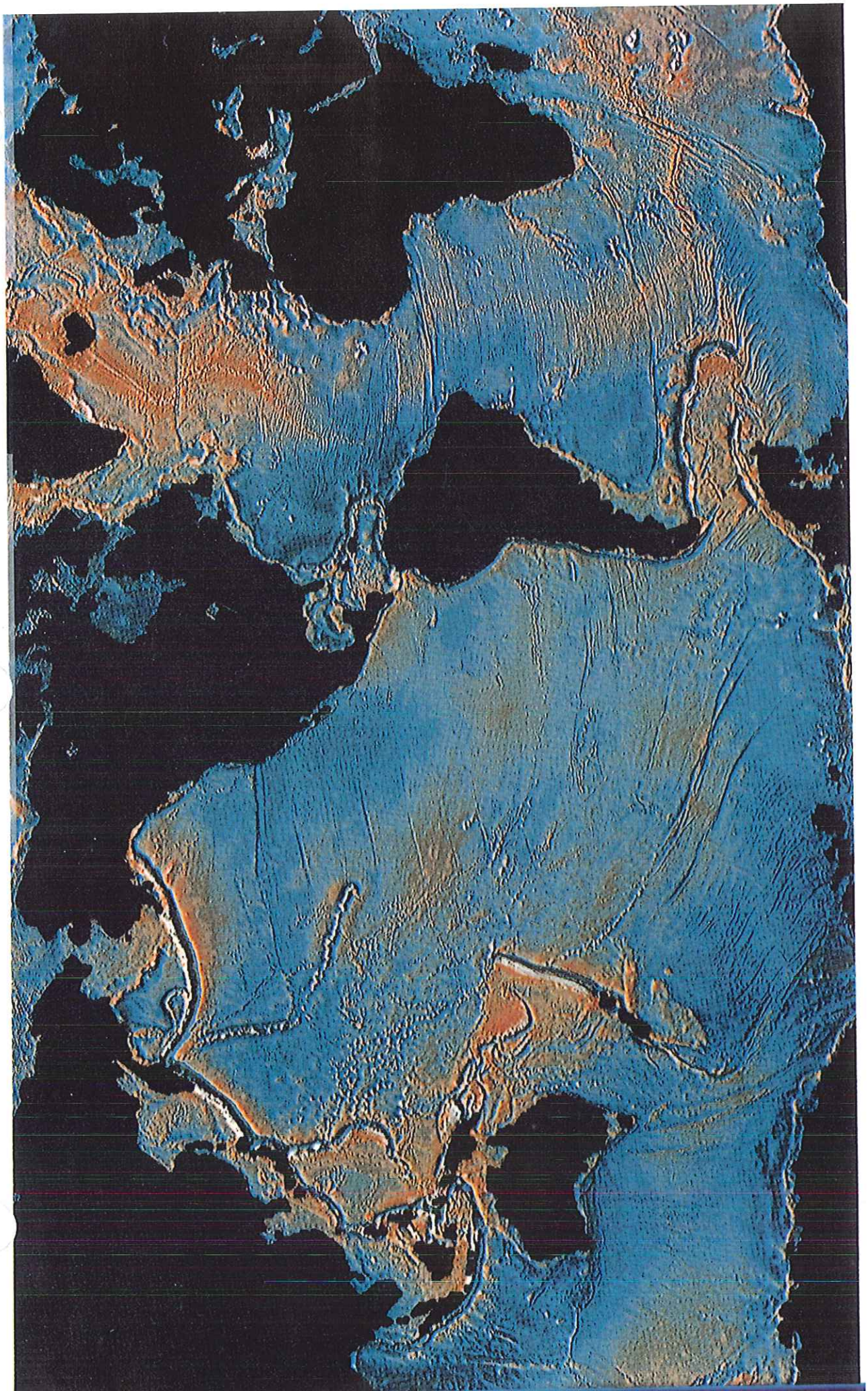

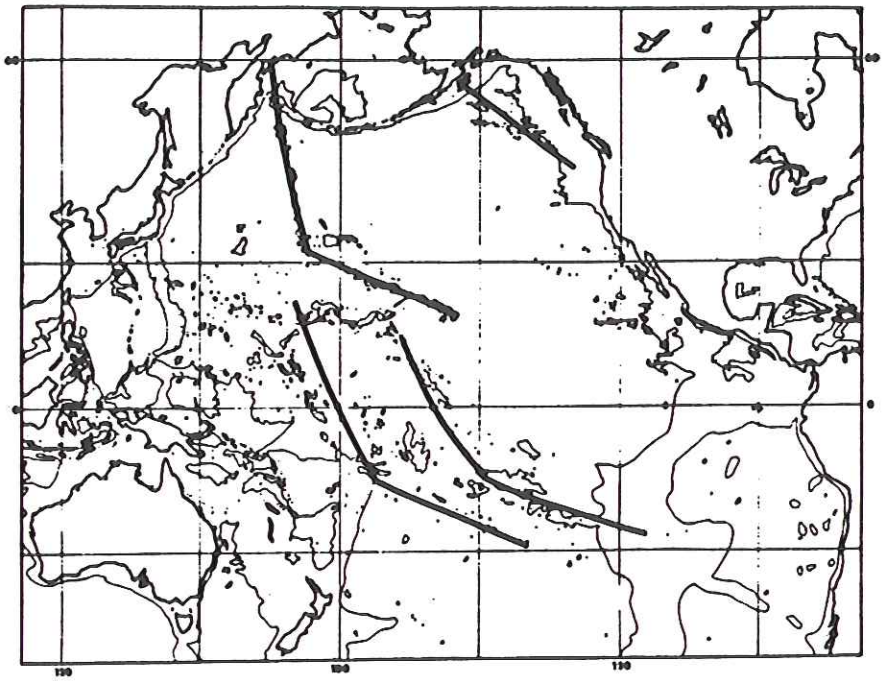

Figure 3. Hot spot trajectories constructed by rotating the Pacific plate 34 degrees about a pole at 67° N., 73° W., and then 45 degrees about a pole at 23° N., 110° W.

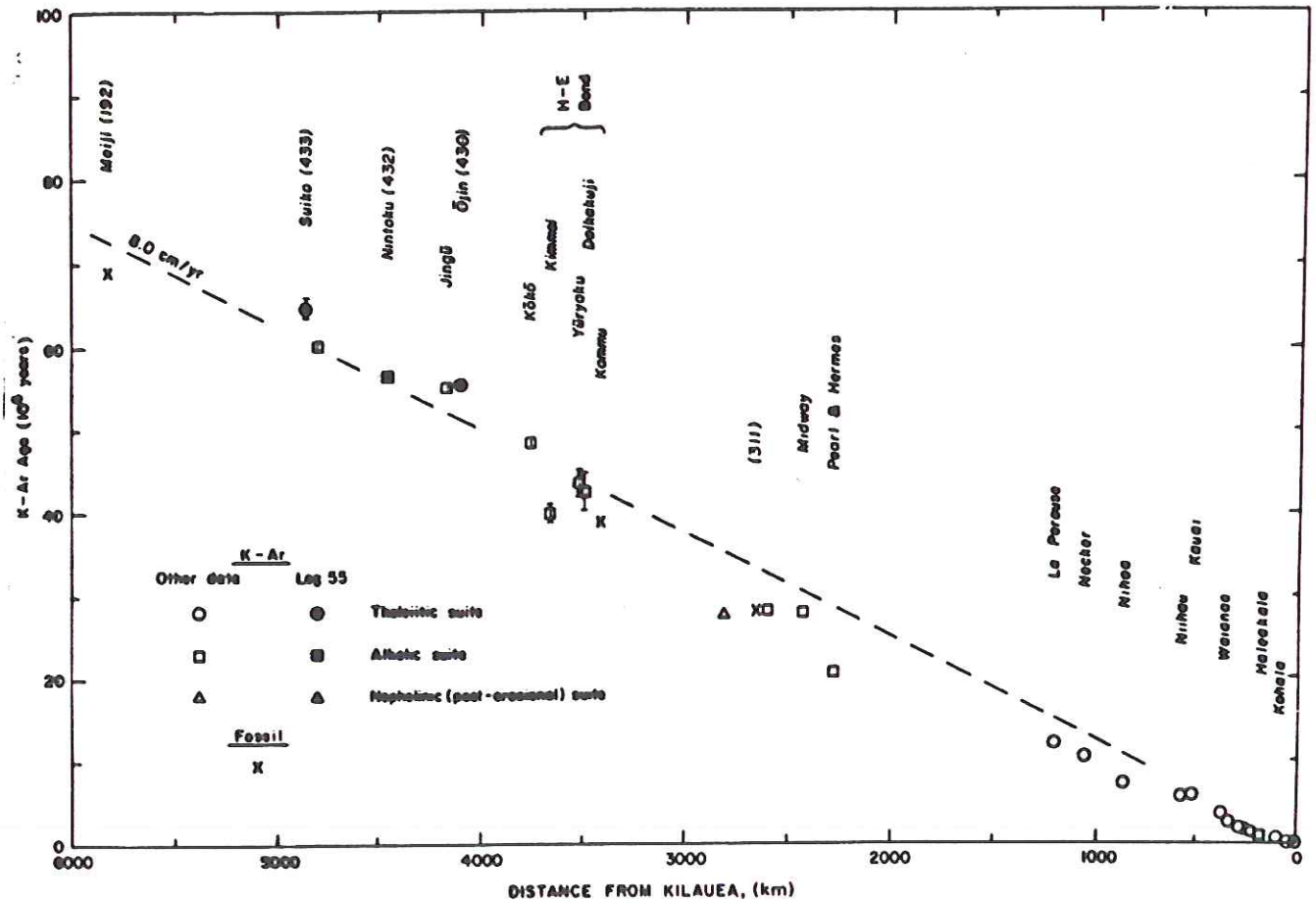

Figure 7. *Age of volcanoes in the Hawaiian-Emperor chain as a function of distance from Kilauea Volcano. Errors shown are standard deviations, and are less than symbol size where omitted. K-Ar data from Table 6. Fossil minimum ages are shown only where radiometric data are unavailable (see text). DSDP sites in parentheses.*

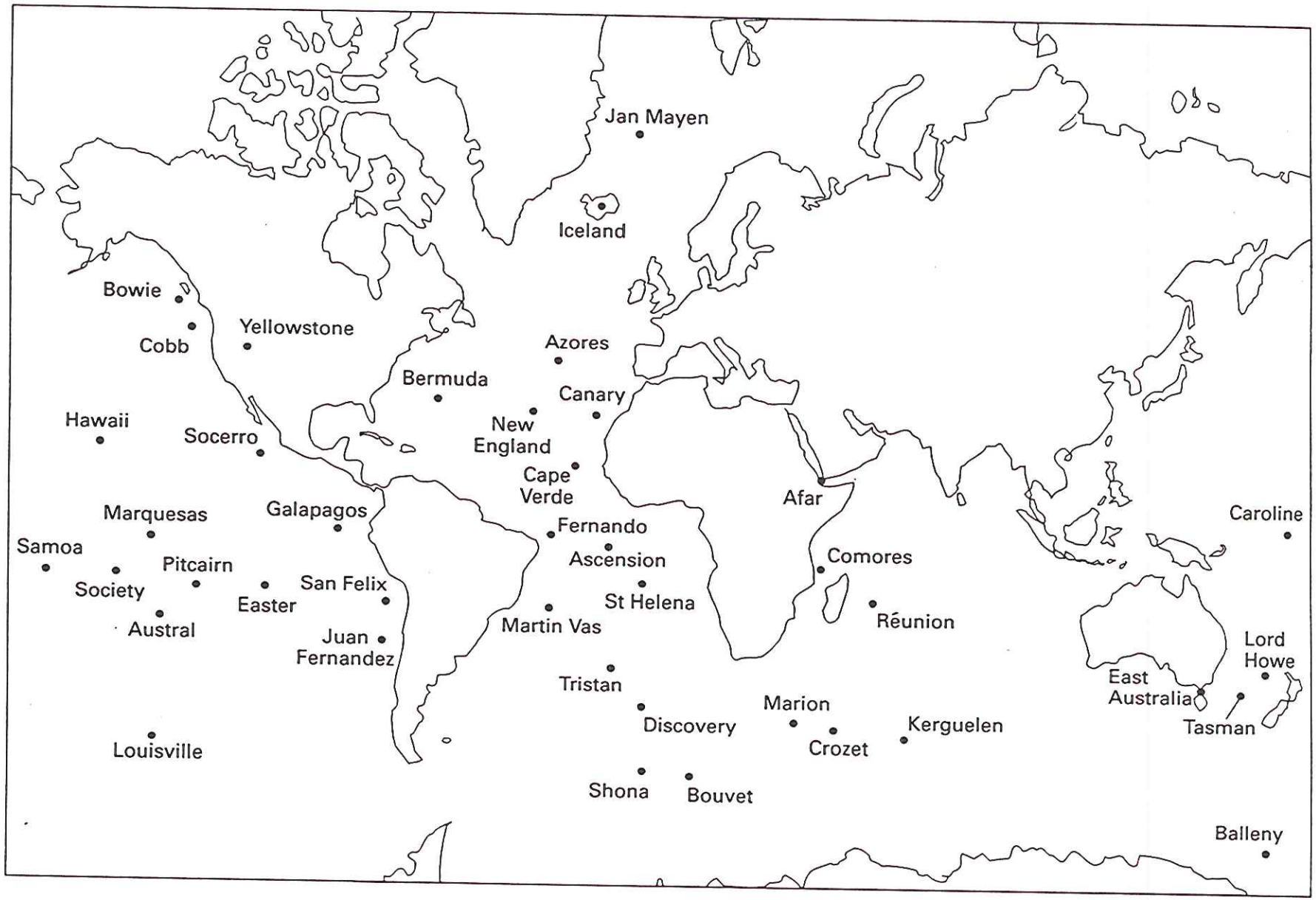

Fig. 5.7 World-wide distribution of hotspots (after Duncan & Richards, 1991).

note the "wheeling" motion of NAM plate

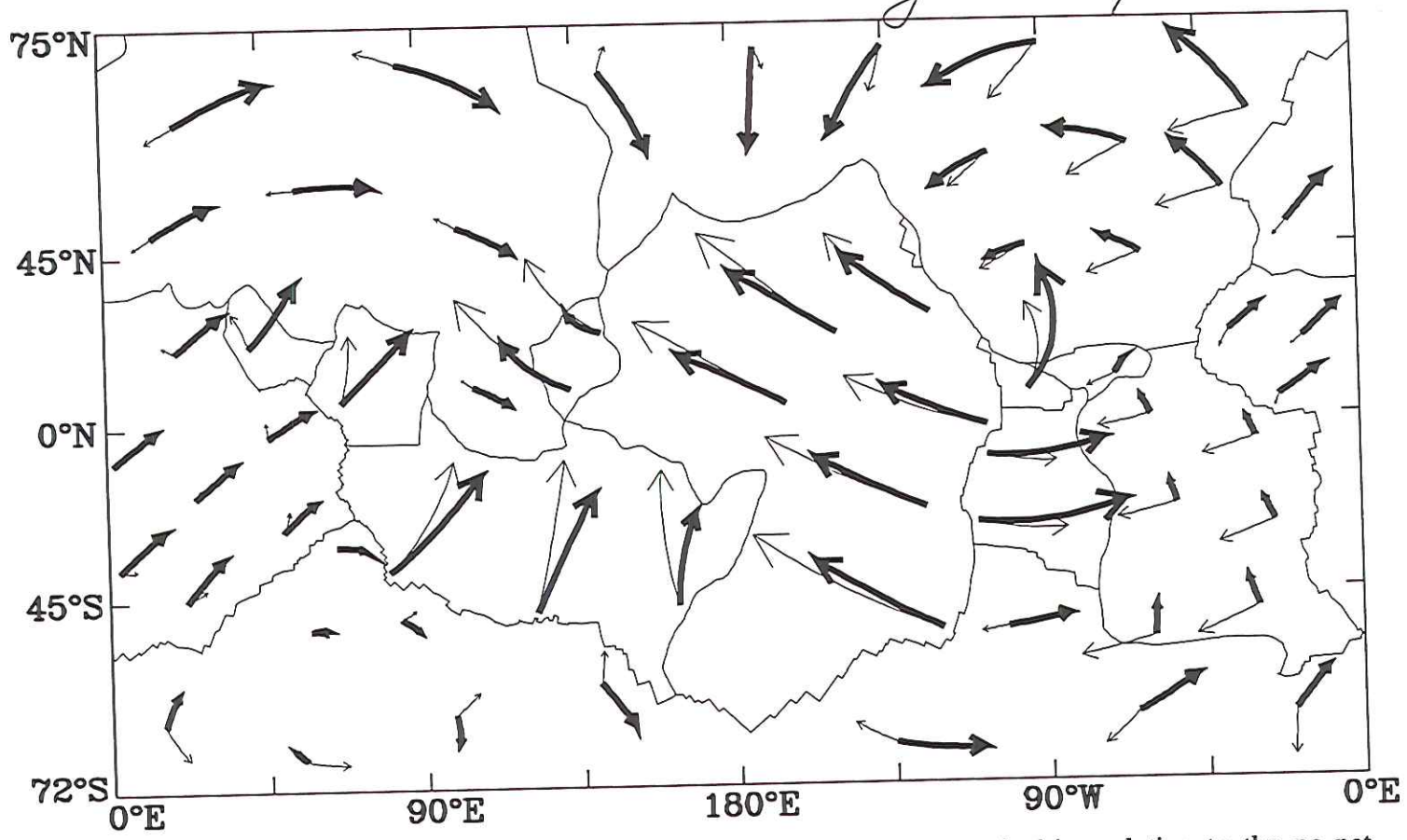

Fig. 2. Plate boundaries assumed to determine NNR-NUVEL1, plate velocities relative to the no-net-rotation reference frame in NNR-NUVEL1 (thick arrows) [4], and plate velocities relative to the hotspots in HS2-NUVEL1 (thin arrows) [39]. Arrows show the trajectory of the lithosphere if the current angular velocities remained unchanged over 50 Myr The map uses Mercator's projection, which distorts lengths of arrows so that the speed of plates near the geographic poles appears too fast. Several simplifications have been made relative to the plate geometries shown in Figure 1, including the following. All plate boundaries are assumed to be narrow. Nubia and Somalia were treated as a single African plate. The Rivera plate has been incorporated into the Cocos plate. The Scotia Sea plate has been incorporated into the Antarctic plate. Southeast Asia has been incorporated into the Eurasian plate. The Caroline plate has been incorporated into the Pacific plate. From Argus and Gordon [4].

GRL 23, 3635–38 (1996)

Eight permanent GPS sites Two years of data 1994–95 Residual ~ 1 mm/yr (constraint on non-rigidity of NAM plate)

Note: we are comparing 2 yrs with 5–10 Myr!

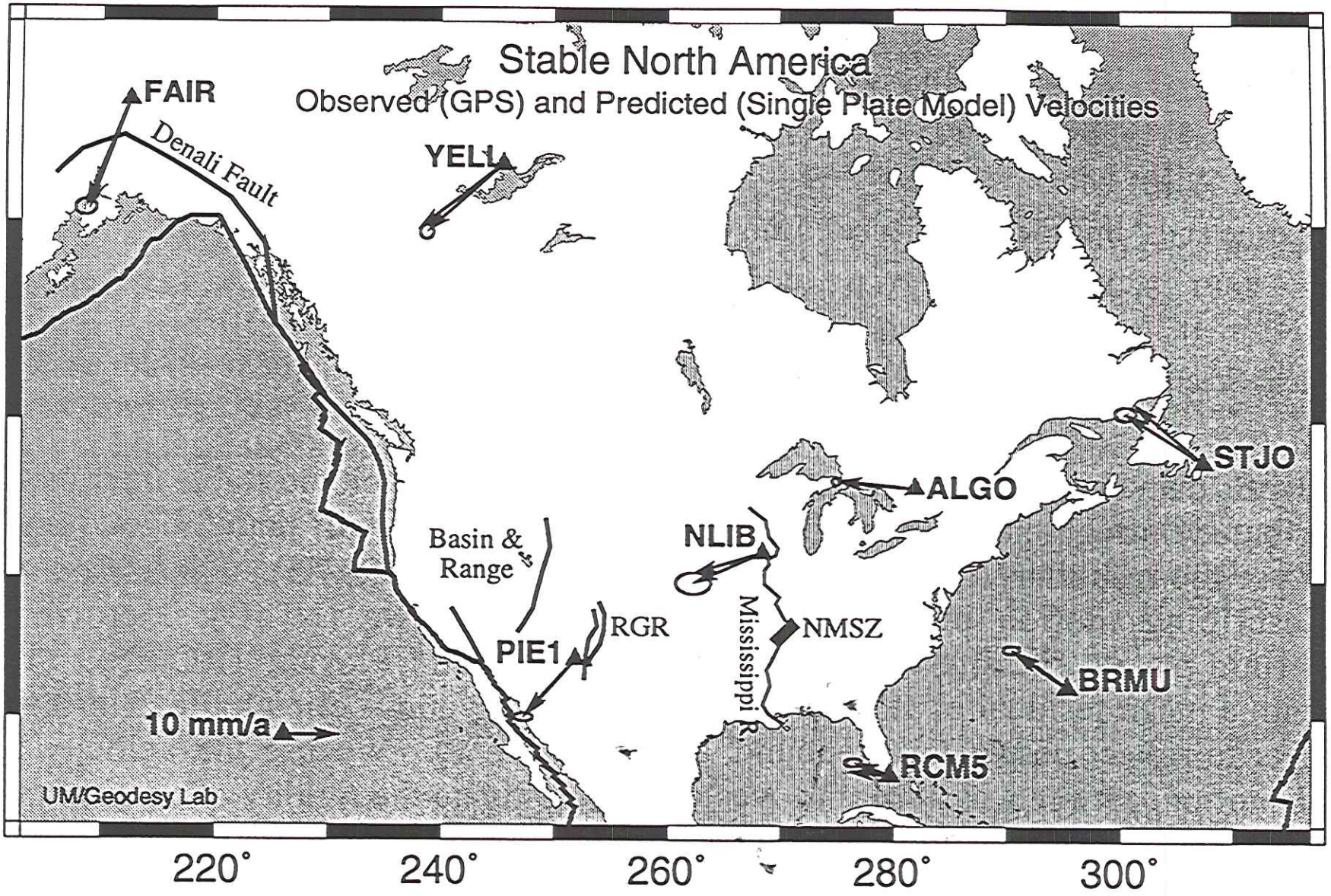

Figure 1. Stations used in this study, their GPS-derived velocities and 95% confidence ellipses, and t velocities predicted by the single rigid plate model in Table 1 (arrows with no ellipse). Major tect features cussed in text are also shown. RGR is F Grande Rift; NMSZ in New Madrid S nic Zone.

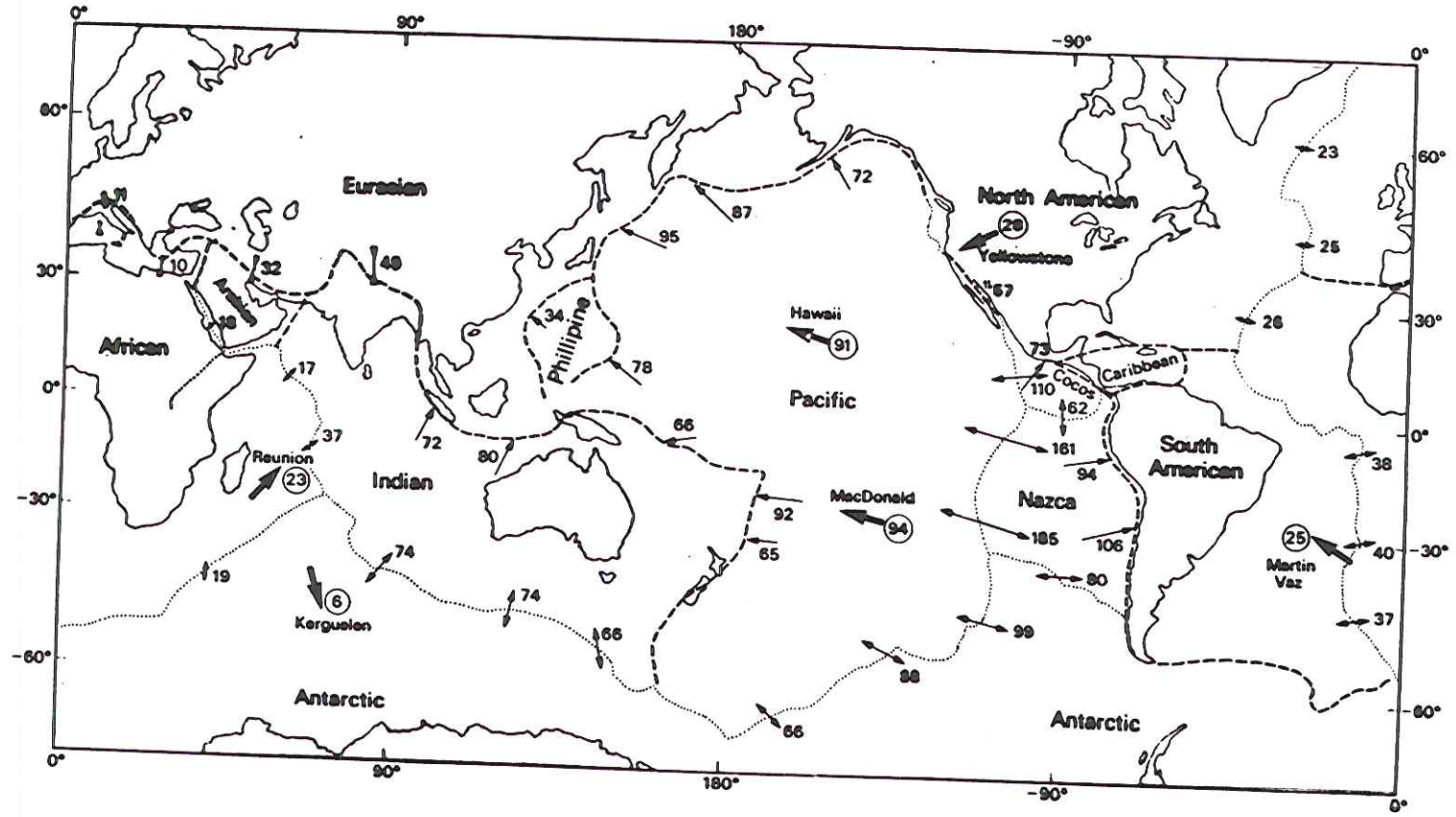

Fig. 3.30 The main plates forming the Earth's surface, showing divergent plate boundaries as a dotted line and convergent and transform fault boundaries as a dashed line. The directions and rates (in mm y^{-1}) of the relative motion, as computed by CHASE (1978), are shown at selected points on the plate boundaries. The computed relative motions of the plates at six selected hot spots relative to the mean hotspot reference frame are also shown (in mm y^{-1}).

Plate motions relative to mean hotspot reference frame.

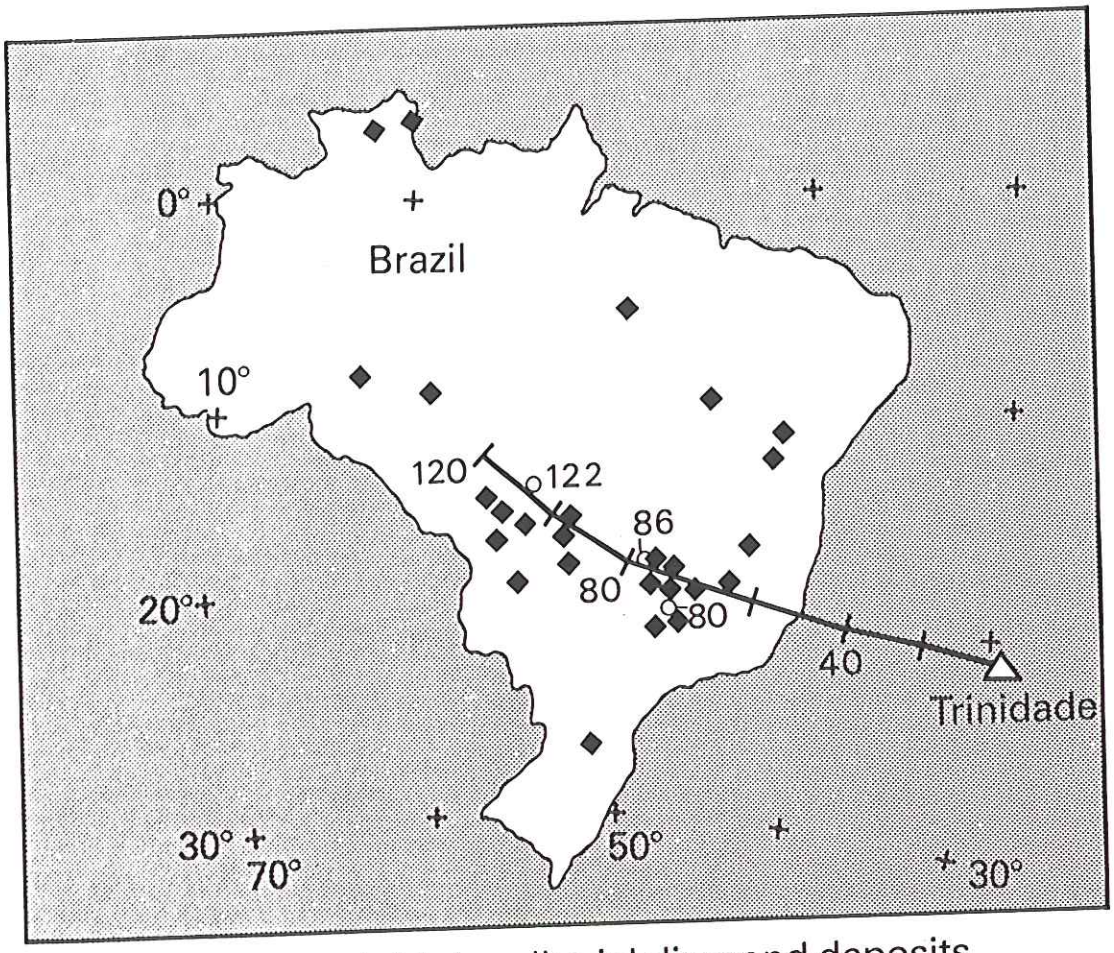

Fig. 5.9 Locations of kimberlites and major alluvial diamond deposits in Brazil compared to the predicted track of the Trinidade hotspot (ages in Ma) (redrawn from Crough *et al.*, 1980).

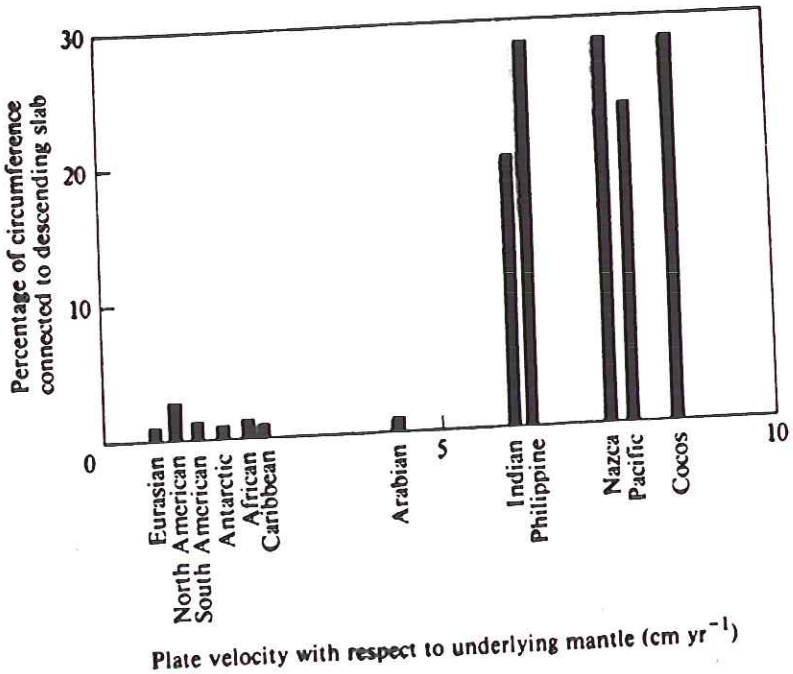

Figure 8.17 Plate velocities versus percentage of subducting edge. The strong correlation suggests subducting edges drive the plates. (From Forsyth & Uyeda 1975, by permission of the Royal Astronomical Society.)

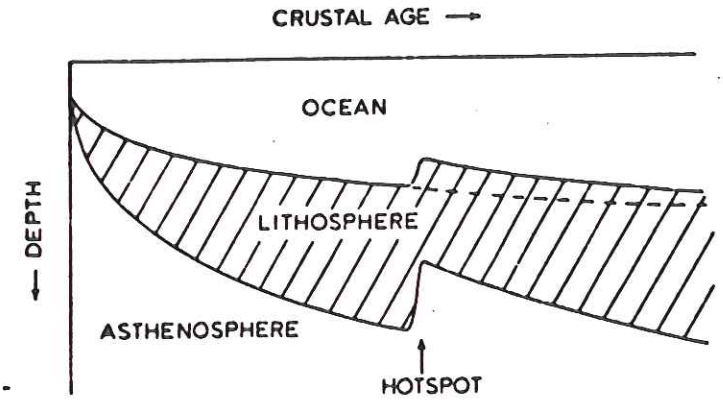

Figure 1. Inferred interaction of the lithosphere with a mid-plate hot-spot. From the ridge to the hot-spot the lithosphere thickens and subsides by cooling. At the hot-spot, extra heat drives the isotherms upwards, thins the lithosphere and causes uplift. Beyond the hot-spot, the lithosphere cools rapidly because it is thin and thus subsides as younger lithosphere at the same depth, rather than as normal lithosphere of the same age (dashed line).

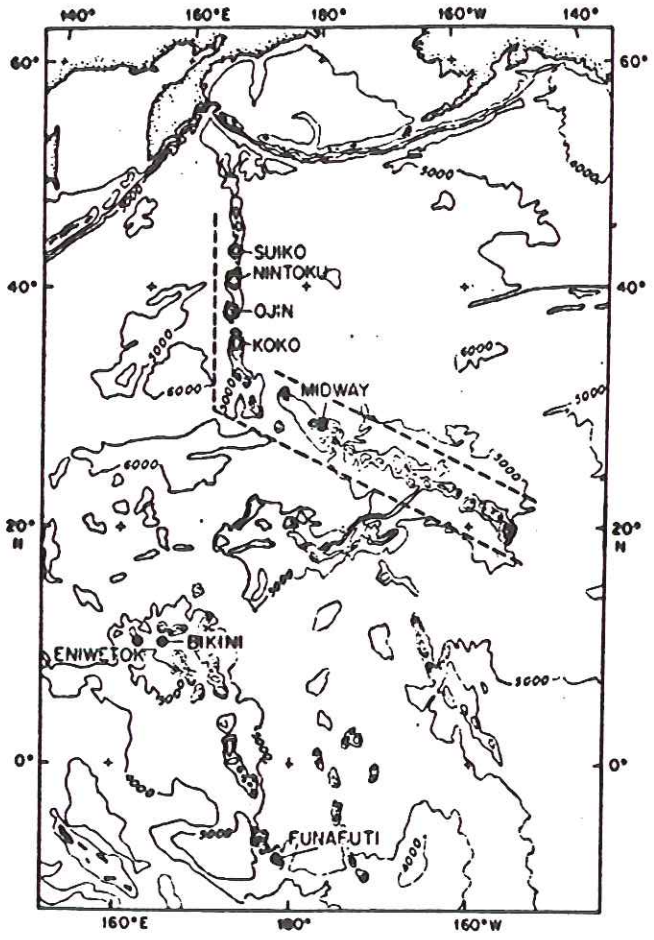

Fig. 1. Bathymetric map of the western Pacific. Solid circles indicate the locations of drilled western Pacific atolls, and open circles the locations of the guyots listed in Table 1. Average depths along dashed lines are plotted in Figure 6.

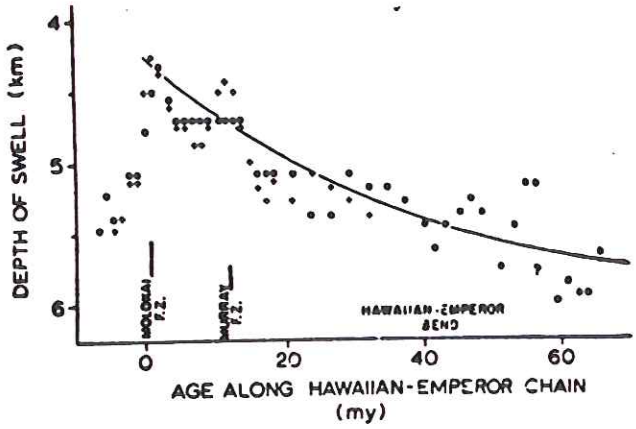

Fig. 6. Depth of the crest of the Hawaiian swell plotted against age along the Hawaiian-Emperor chain (location approximately indicated by dashed lines in Figure 1). Hawaii is assumed to be 0 m.y. old. Age along the chain is taken from Clague and Jarrard [1973], negative ages corresponding to points southeast of Hawaii along the trend of the Hawaiian ridge. Shaded band indicates expected depth if normal age/depth relationship existed in this area. Solid line is empirical age-depth curve for normal oceanic crust between 30 and 100 m.y. old [Parsons and Sclater, 1977].

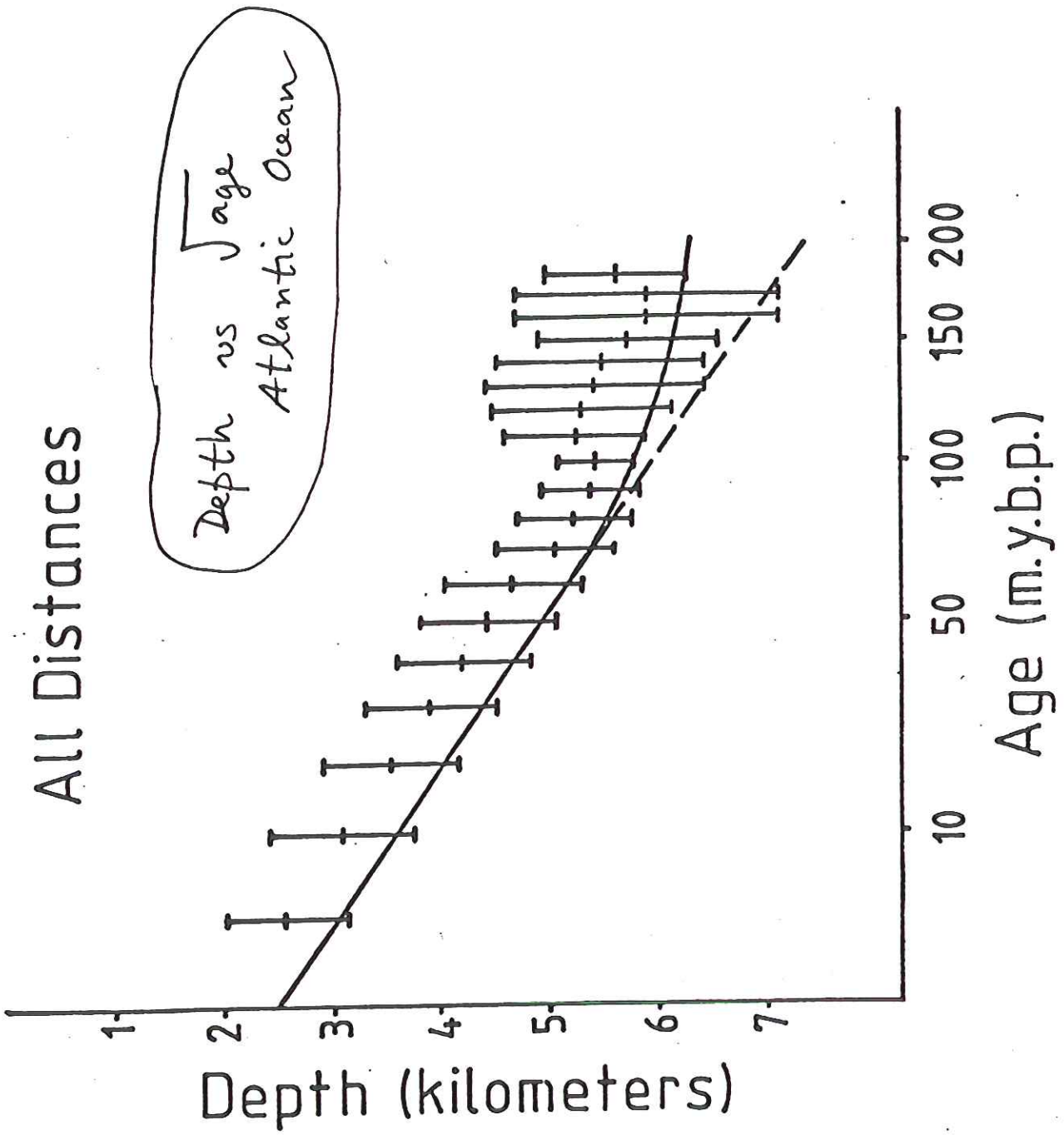

Fig. 7. Seafloor depth versus distance, unsorted by distance from a hotspot track.

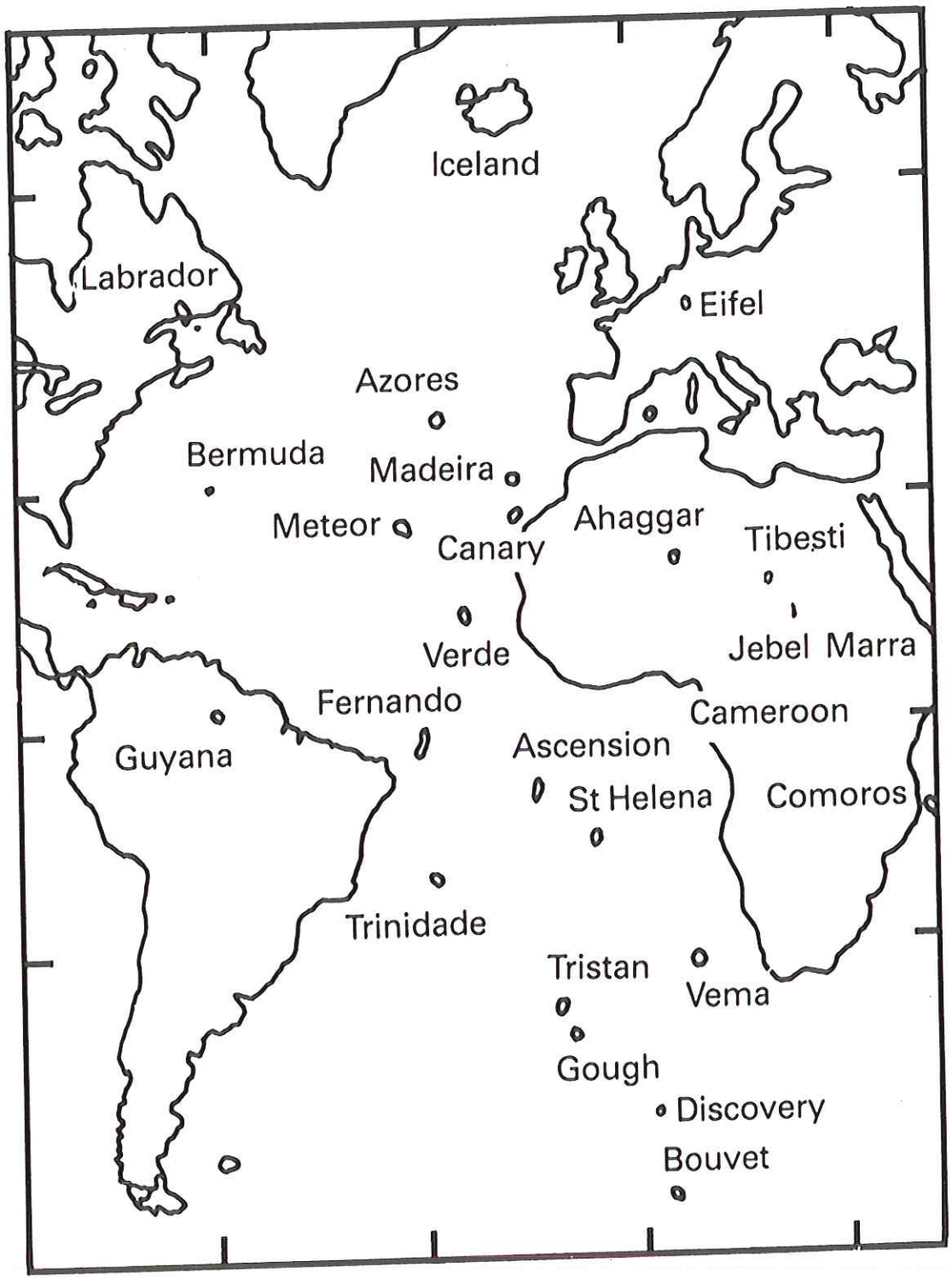
Iceland
Labrador
Eifel
Azores
Bermuda
Madeira
Meteor
Canary
Ahaggar
Tibesti
Verde
Jebel Marra
Fernando
Cameroon
Guyana
Ascension
St Helena
Comoros
Trinidade
Tristan
Vema
Gough
Discovery
Bouvet

Atlantic Ocean : depth vs. $\sqrt{\text{age}}$ for regions that have <u>not</u> passed over a hotspot (within 400 – 600 km)

Linear out to 180 m.y.b.p.

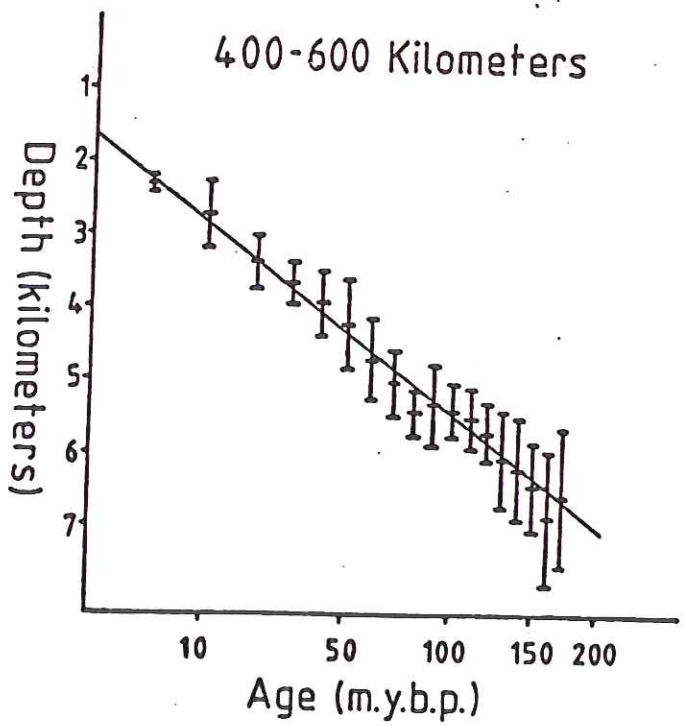

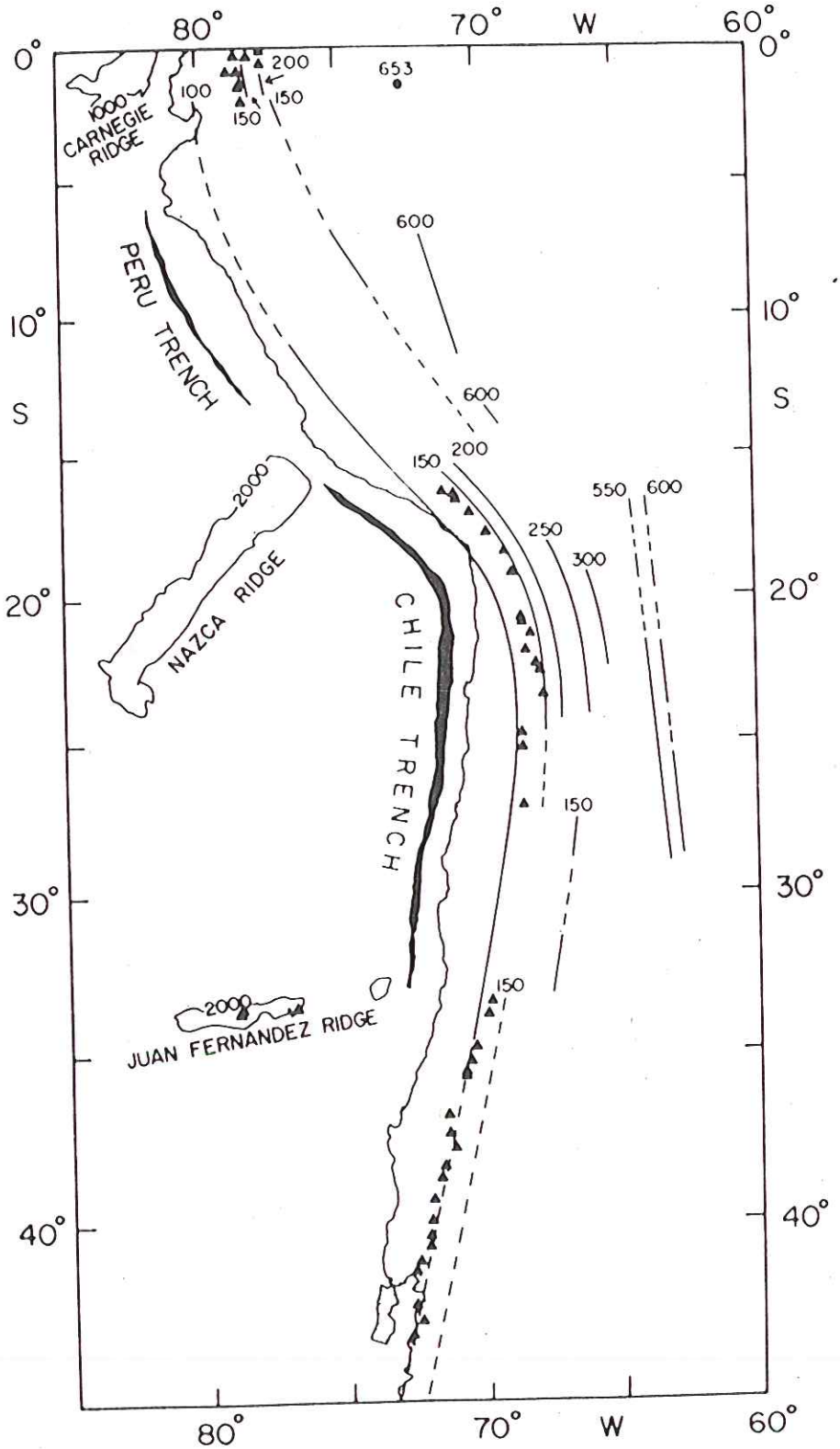
80°
70°
W
60°
0°
10°
S
20°
30°
40°
653
200
150
100
150
CARNEGIE RIDGE
600
600
PERU TRENCH
150
200
550
600
250
300
2000
NAZCA RIDGE
CHILE TRENCH
150
150
2000
JUAN FERNANDEZ RIDGE

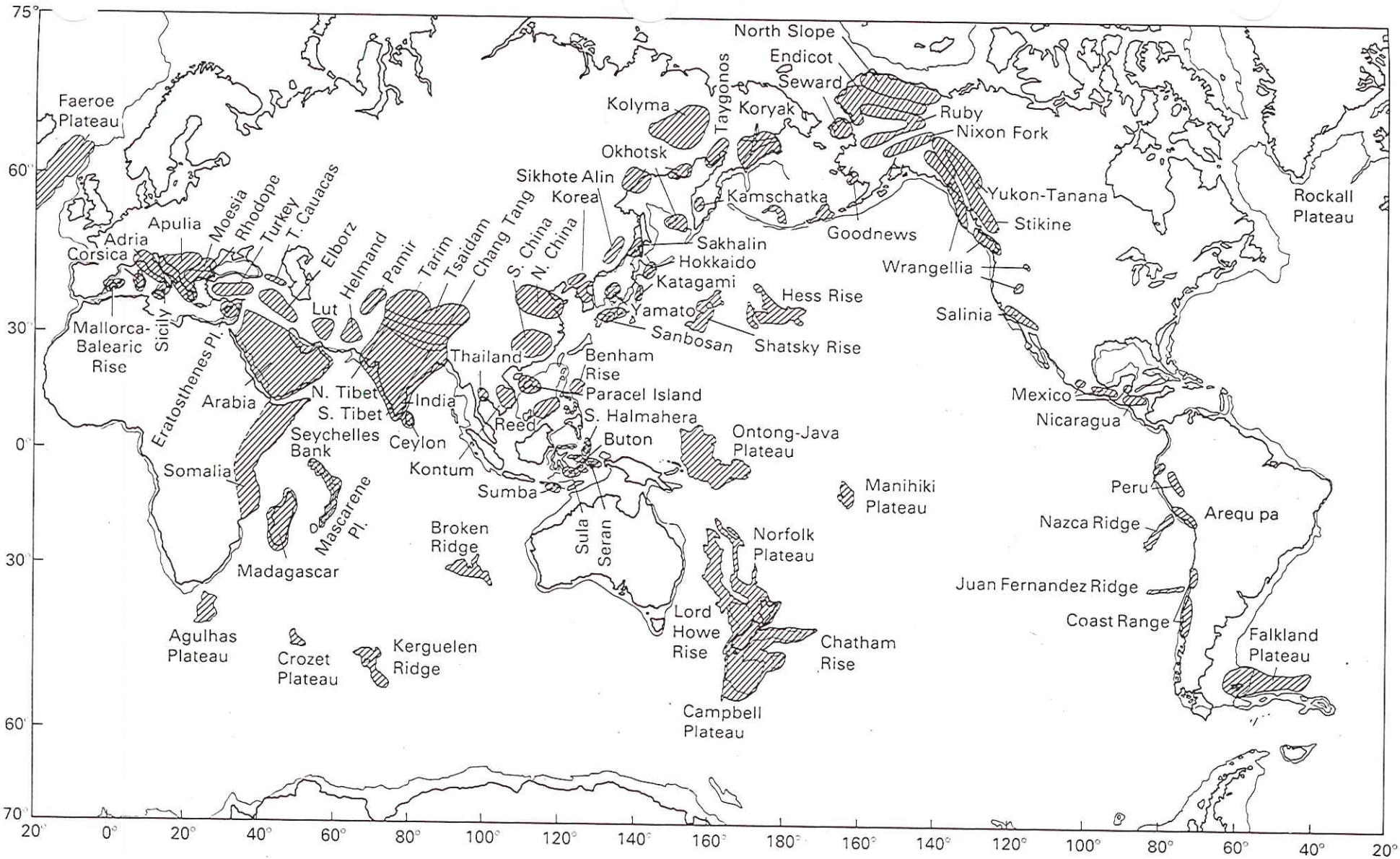

Fig. 9.30 Distribution of past, present and future suspect terrains (redrawn from Nur & Ben-Avraham, 1982, with permission from the American Geophysical Union).

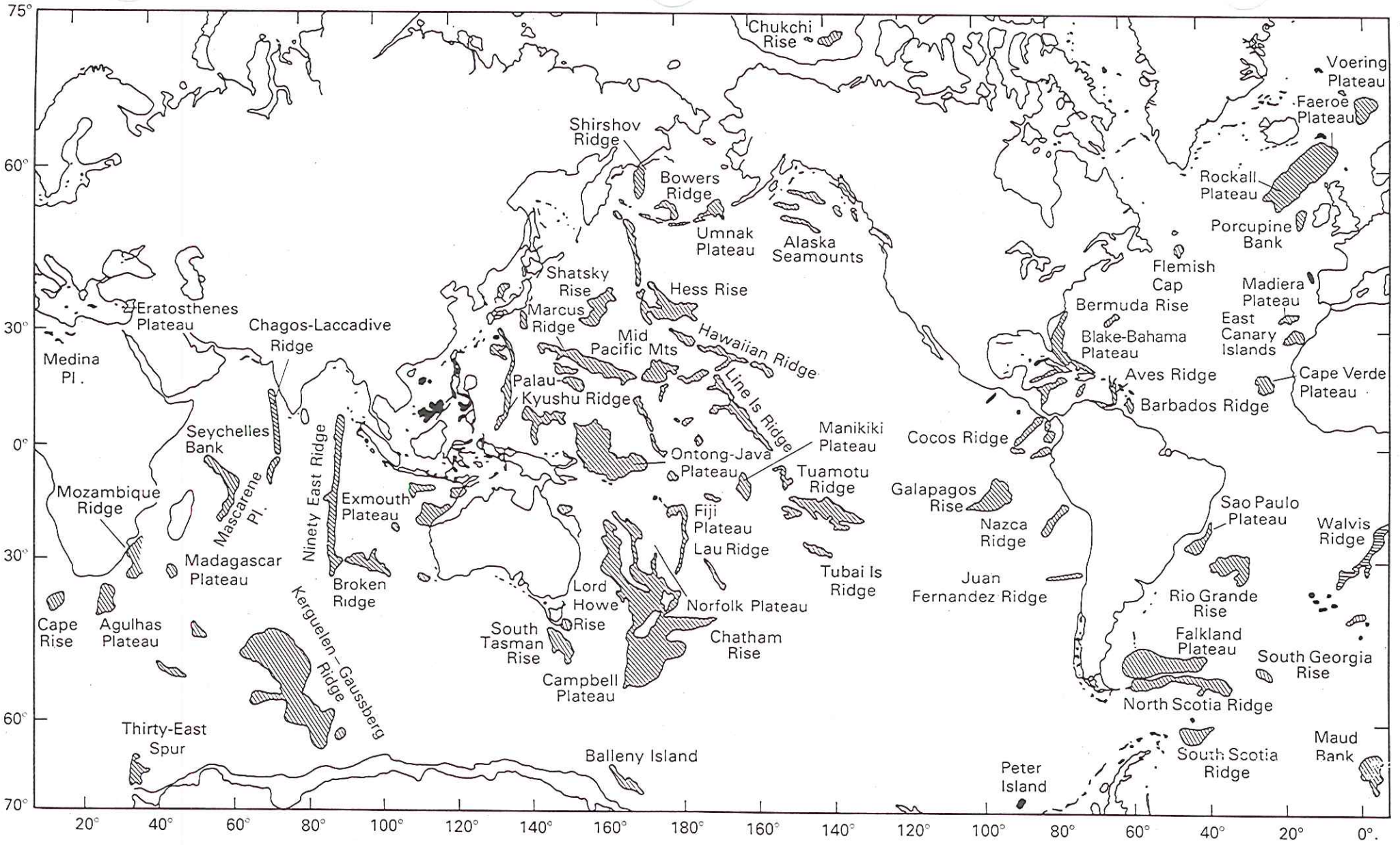

Fig. 9.26. Distribution of present-day oceanic plateau (redrawn from Ben-Avraham *et al.*, 1981, *Science*, **213**, 47–54, with permission from the AAAS. Copyright ©

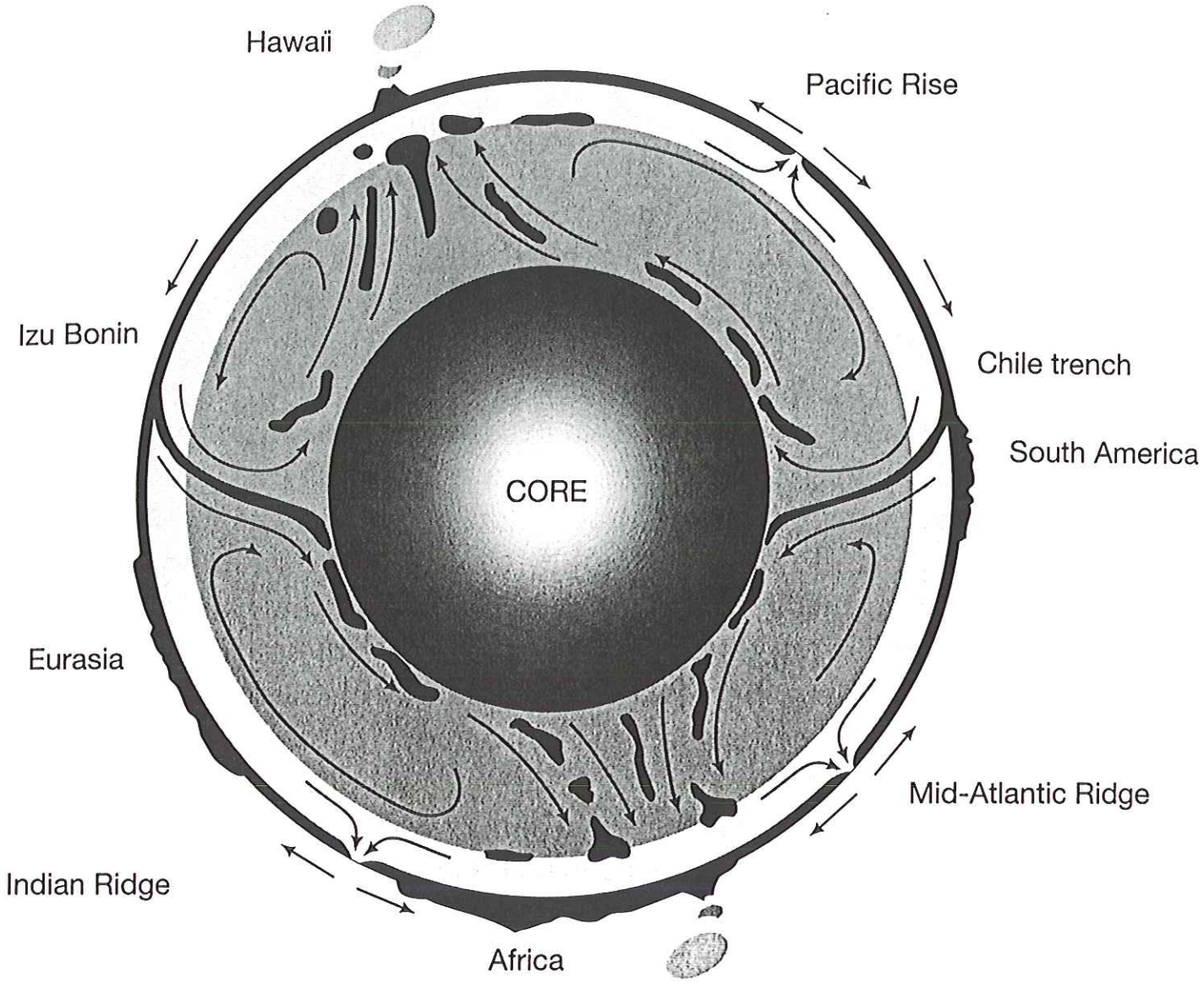

Figure 2.3
Illustration of a possible convective circulation involving the entire mantle. The plates (in *black*) descend along the subduction zones towards the core, traverse the upper mantle (*light grey*) and disperse prior to becoming resorbed in the lower mantle (*dark grey*). Their great longevity (100 Ma) allows them to rise again under the hotspots, contributing eventually to the volcanism at these points. The ridges are fed mainly by material ascending in the upper mantle. (After P. G. Silver and R. W. Carlson 1988. Ann. Rev. Earth Planet. Sci. , 16, 477–541)

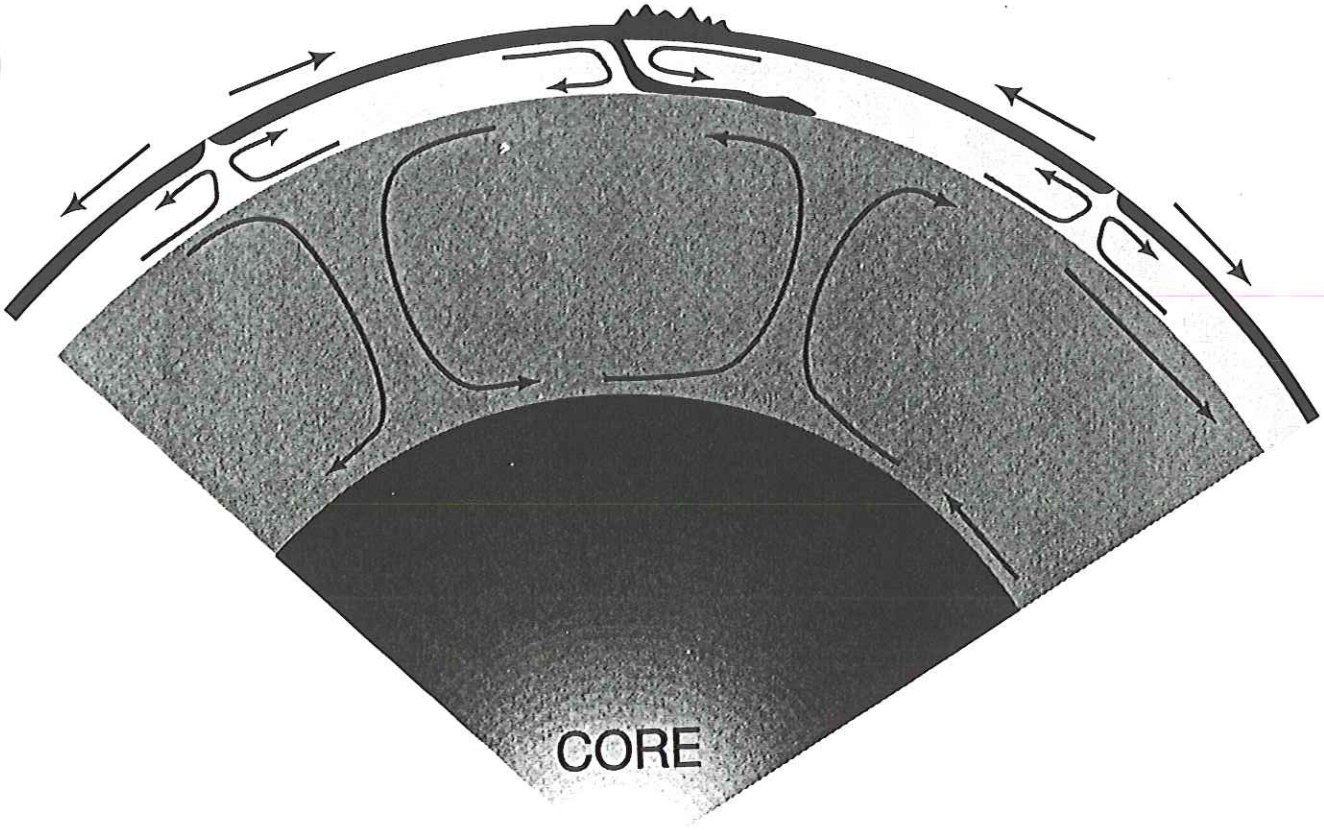

Figure 2.4
Illustration of a convective circulation in two levels in the mantle. The elongated cells of the upper mantle descend along subduction zones and rise below ridges. The circulation in the lower mantle may be mechanically coupled with that of the upper mantle (same direction in horizontal movements, opposite direction in vertical movements), thermally coupled (same sense in vertical movements, opposite sense in horizontal movements) as rather suggested by seismic tomography, or not coupled at all

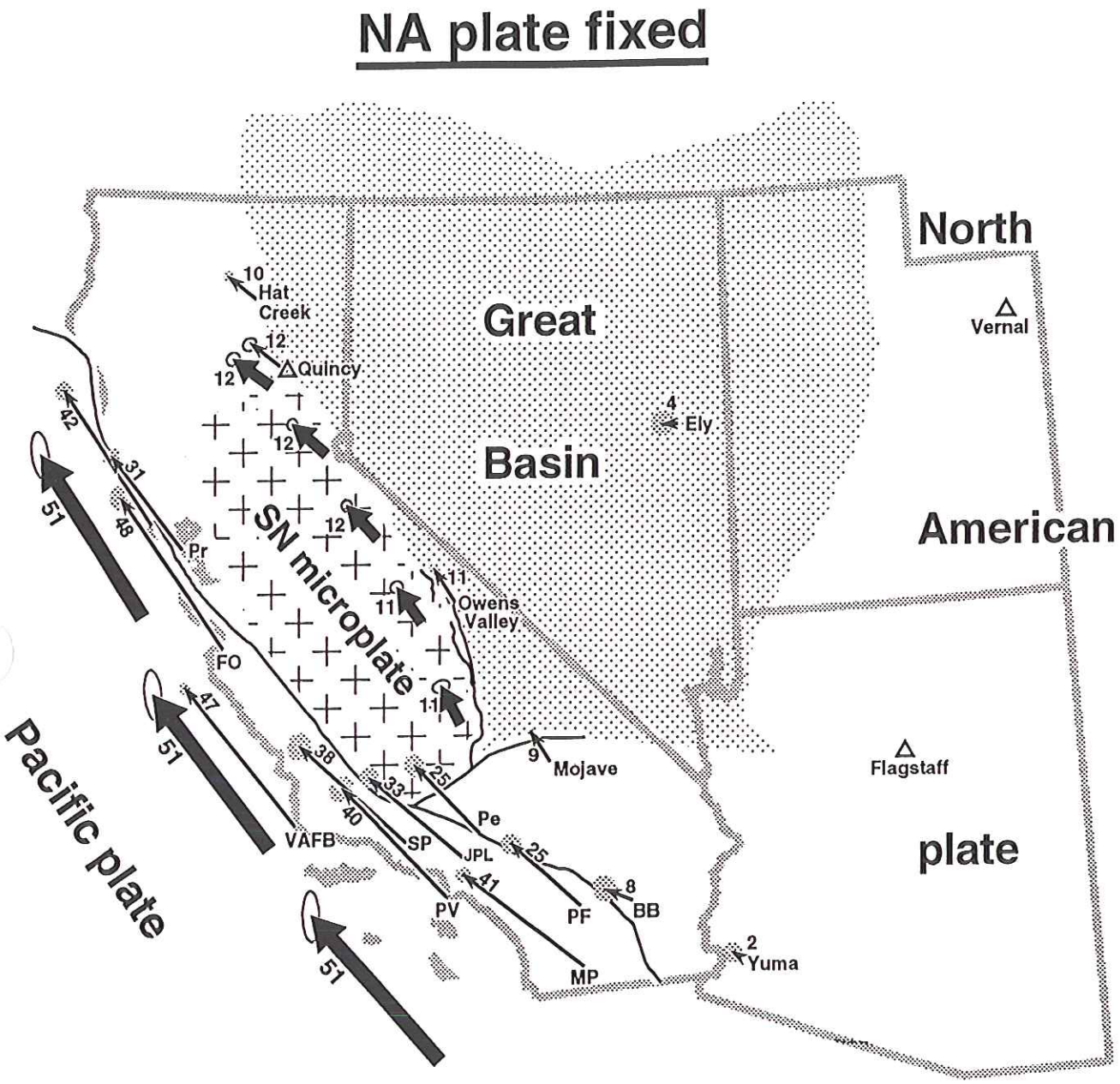

Fig. 4. Plate and site motions relative to North America estimated from VLBI geodetic data. Bold arrows show the motion of the Pacific plate and of the Sierra Nevada-Great Valley microplate relative to North America. Small arrows show the motion of individual radio telescope sites (not constrained to lie on a plate) relative to North America; ellipses centered on the tips of arrowheads are 95% confidence limits. Numerals adjacent to arrows give the velocities in millimeters per year. The lengths the arrows are scaled to show displacements if each velocity was constant for two million years. " is the Sierra Nevada-Great Valley microplate. From D. F. Argus and R. G. Gordon (manuscript in preparation, 1994).

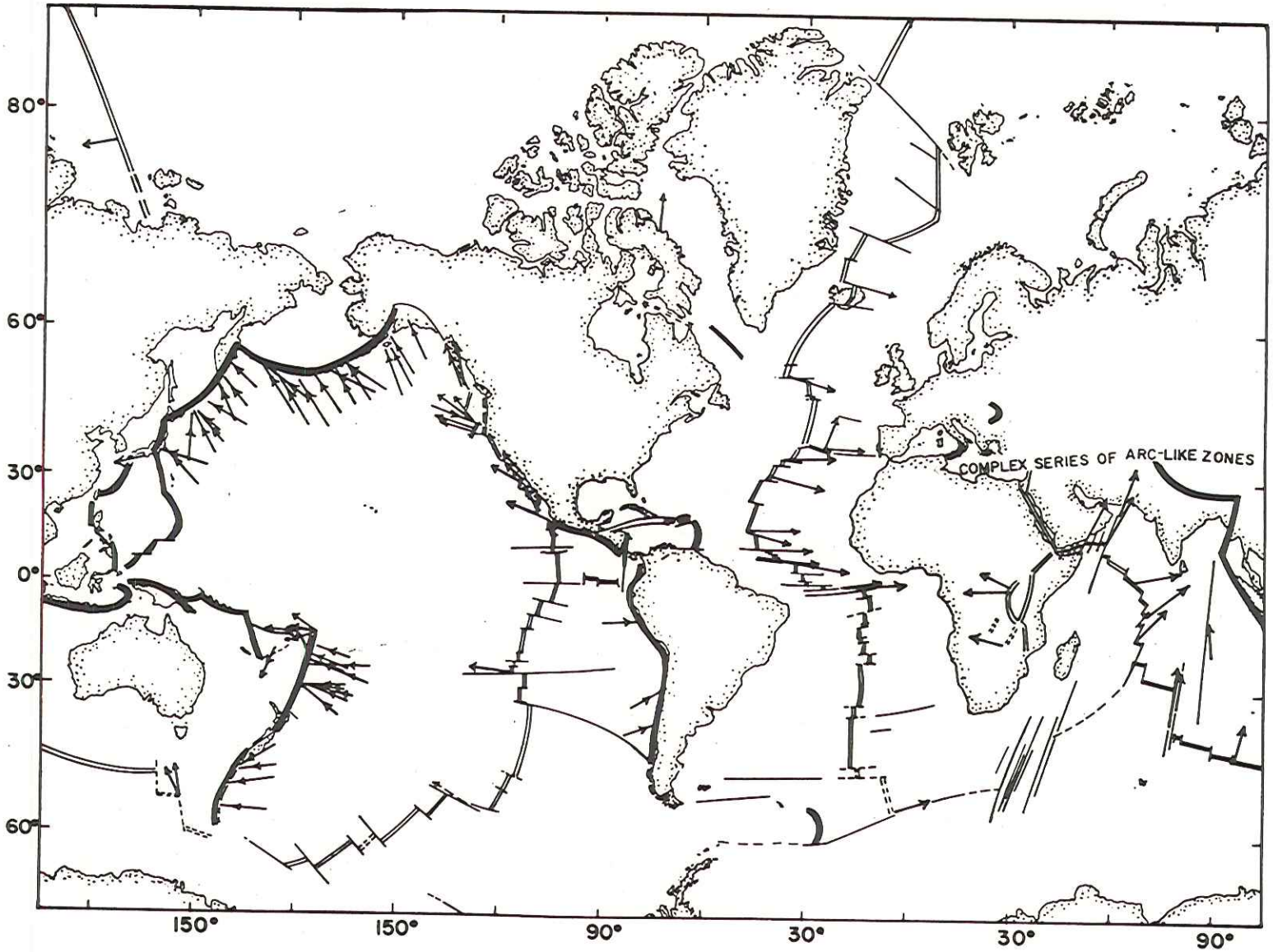
80°
60°
30°
0°
30°
60°
150°
150°
90°
30°
30°
90°
COMPLEX SERIES OF ARC-LIKE ZONES

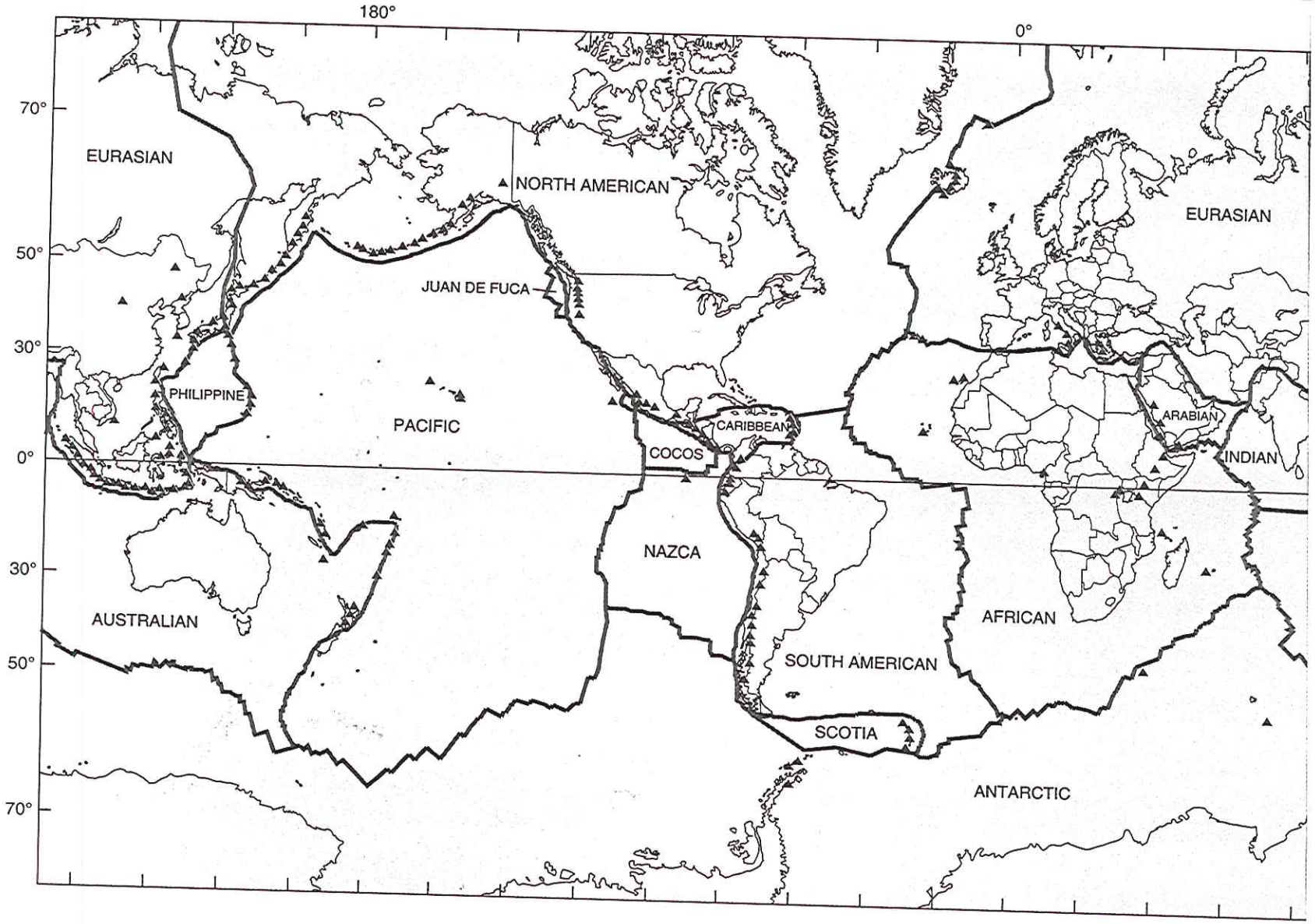
180°
0°
70°
50°
30°
0°
30°
50°
70°
EURASIAN
NORTH AMERICAN
EURASIAN
JUAN DE FUCA
PHILIPPINE
PACIFIC
CARIBBEAN
COCOS
ARABIAN
INDIAN
NAZCA
AUSTRALIAN
AFRICAN
SOUTH AMERICAN
SCOTIA
ANTARCTIC